Towards 3D Covalent Organic Framework Films

MARTIN RATSCH

UNIVERSITY OF GOTHENBURG

Department of Chemistry and Molecular Biology

University of Gothenburg

2022

DOCTORAL THESIS

Submitted for fulfilment of the requirements for the degree of

Doctor of Philosophy in Chemistry

Towards 3D Covalent Organic Framework Films

MARTIN RATSCH

ISBN: 978-91-8009-764-2 (PRINT)

ISBN: 978-91-8009-763-5 (PDF)

Department of Chemistry and Molecular Biology

SE-412 96

Sweden

Printed by Stema Specialtryck AB

Borås

There are people who make things happen, there are people who watch things happen, and there are people who wonder what happened. To be successful, you need to be a person who makes things happen.

Jim Lovell

Inside of every problem lies an opportunity.

Robert Kiyosaki

Abstract

Porous materials are of great scientific interest because they are able to interact with guests, such as ions, atoms and molecules throughout their entire volume. One big subgroup of organic porous materials are covalent organic frameworks (COFs), which are mainly synthesized as powders with an uncontrolled grain size. In order to broaden the application range for those materials towards utilizations, which require mechanical strength, such as membranes and electronics, it would be beneficial to synthesize COFs also as continuous films.

This dissertation aims for developing a method to grow 3D COF films and overcome this powder limitation. The used approach is based on a continuous flow setup and the involvement of a quartz crystal microbalance (QCM), which enables real time monitoring of the film growth by mass deposition. During the performance of these surface reactions, two reactions are kinetically competing with each other. The kinetic promotion of the desired surface reaction over the bulk reaction was achieved by using low concentrations. This led to an increased smoothness of the framework material, compared to its growth under batch conditions. The modular strategy allows full control over the reaction conditions at any time and makes the approach versatile, meaning it can be used for the assembly of different networks. Three different amorphous or crystalline films were synthesized and characterized via EDX-SEM, XPS, GIWAXS, AFM, as well as IR and Raman spectroscopy. The synthesized framework materials use a C-C linkage, making them to one of the first examples for carbon-carbon linked COFs. It could be demonstrated that both networks can be grown on each other, forming a layered COF film. Those findings confirm a successful assembly of a covalently connected layered 3D COF.

The findings presented in this thesis contribute to an increased method variety for the formation of porous materials. This will enable the synthesis of more rigid and stable COF materials, as well as the possibility to introduce a certain functionality only locally into a framework in the future. Additionally, the strategy enables the formation of rigid films on a variety of substrates. Consequently, the results will expand the design and application range for porous materials.

Sammanfattning

Porösa material är av stort vetenskapligt intresse eftersom de kan interagera med gäster, såsom joner, atomer och molekyler genom hela sin volym. En stor undergrupp av organiska porösa material är kovalenta organiska ramverk (COFs), som än så länge huvudsakligen syntetiseras som pulver med en okontrollerad kornstorlek. För att bredda användningsområdet för dessa material mot användningsområden som kräver mekanisk styrka, såsom membran och elektronik, skulle det vara fördelaktigt att syntetisera COFs också som kontinuerliga filmer.

Denna avhandling syftar till att utveckla en metod för att syntetisera 3D COF-filmer och övervinna den här pulverbegränsning. Det använda tillvägagångssättet är baserat på en kontinuerlig flödesmetod och involvering av en kvartskristall mikrobalans (QCM), vilket möjliggör realtidsövervakning av filmtillväxten och dess genomsnittliga tjocklek. Det kinetiska främjandet av ytreaktionen över bulkreaktionen uppnåddes genom att använda låga koncentrationer. Det här ledde till en ökad jämnhet hos rammaterialet, jämfört med dess tillväxt under satsförhållanden. Den modulära strategin tillåter full kontroll över reaktionsförhållandena hela tiden och gör tillvägagångssättet mångsidigt, vilket innebär att det kan användas för sammansättning av olika nätverk. Tre olika amorfa eller kristallina filmer syntetiserades och karakteriserades via EDX-SEM, XPS, GIWAXS, AFM, samt IR- och Raman-spektroskopi. De syntetiserade rammaterial använder en C-C-länkning, vilket gör dem till ett av de första exemplen för kol-kol-kopplade COFs. Det kunde påvisas att båda nätverken kan odlas på varandra och bilda en skiktad COF-film. Dessa fynd bekräftar en framgångsrik montering av en kovalent ansluten skiktad 3D COF.

Fynden som presenteras i denna avhandling bidrar till en ökad metodvariation för bildning av porösa material. Detta kommer att möjliggöra syntesen av styvare och stabilare COF-material, samt möjligheten att introducera en viss funktionalitet endast lokalt i ett ramverk i framtiden. Dessutom möjliggör strategin bildandet av stela filmer på en mängd olika substrat. Följaktligen kommer resultaten att utöka design- och tillämpningsområdet för porösa materialer.

List of Publications

The research results presented in this thesis are based on the findings reported in the following papers. The Author contribution is mentioned for each paper.

Paper I

All-Carbon-Linked Continuous Three-Dimensional Porous Aromatic Framework Films with Nanometer-Precise Controllable Thickness

Martin Ratsch, Chen Ye, Yizhou Yang, Airui Zhang, Austin M. Evans, and Karl Börjesson, *J. Am. Chem. Soc.* **2020**, 142, 14, 6548–6553.

Development of the flow setup, synthesized TBPM and performed experiments and analysis (linkage test reactions, QCM, optical microscope, SEM and EDX-SEM) around the PAF-1 framework. AFM measurements were executed together with Dr. Yizhou Yang. Wrote the paper and the supporting information together with Karl Börjesson.

Paper II

Layered 3D Covalent Organic Framework Films based on carbon-carbon bonds

Martin Ratsch, Yizhou Yang, Austin M. Evans, and Karl Börjesson, Manuscript 2022

Synthesized LTIPB and performed kinetic experiments and analysis (QCM, optical microscope and IR) around the boron- and carbon-COF. Analyzed GIWAXS, ToF-SIMS, XPS and depth XPS data. AFM measurements were done together with Dr. Yizhou Yang. Profilometer experiments were performed with Rahul Bhuyan. Raman measurements were executed in collaboration with Dr. Katarina Logg. Wrote the manuscript draft and the supporting information together with Karl Börjesson.

List of abbreviations

acs	Topology term
AFM	Atomic force microscopy
Ar	Aryl
ATR	Attenuated total reflection
bcu	Topology term, stands for body-centered cubic
BET	Bruauer-Emmet-Teller
bor	Topology term, stands for boracite
BSE	Back scattered electrons
ceq	Topology term
CMP	Conjugated microporous polymers
COD	1,5 Cyclooctadiene
COF	Covalent organic framework
CTF	Covalent triazene framework
ctn	Topology term, stands for carbon nitride
DABCO	1,4-Diazabicyclo[2.2.2]octane
dia	Topology term, stands for diamant
DIPA	Diisopropylamine
DMF	*N*,*N*-Dimethylformamide
EDX / EDS	Energy-dispersive X-ray spectroscopy
ffc	Topology term
fjh	Topology term
FT-IR	Fourier transform infrared
GC	Gas chromatography
GISAXS	Grazing-incidence small-angle x-ray scattering
GIWAXS	Grazing-incidence wide-angle x-ray scattering
hcb	Topology term, stands for honeycomb
HCP	Hyper-crosslinked polymer
HOF	Hydrogen bonded framework
hxl	Topology term, stands for hexagonal lattice
Hz	Hertz
IR	Infrared
IUPAC	International Union of Pure and Applied Chemistry

kgd	Topology term, stands for kagome dual
kgm	Topology term, stands for kagome
ljh	Topology term
lon	Topology term, stands for lonsdaleite
LTIPB	Lithium tetrakis(4-iodophenyl)borate
MOF	Metal organic framework
MOZ	Metal organic zeolite
NMP	N-methyl-2-pyrrolidone
PAF	Porous aromatic framework
PCP	Porous coordination polymer
Ph	Phenyl
PMC	Porous molecular crystal
POP	Porous organic polymer
pts	Topology term, stands for pltinum sulfide.
QCM	Quartz crystal microbalance
QCM-D	Quartz crystal microbalance with dissipation
RCSR	Reticular Chemistry Structure Resource
rra	Topology term
SAM	Self-assembled monolayer
SAXS	Small-angle x-ray scattering
SBU	Secondary building unit
SE	Secondary electrons
SEM	Scanning electron microscope
sql	Topology term, stands for square lattice
srs	Topology term, stands for strontium silicate
STM	Scanning tunnel micrsocopy
stp	Topology term
SXRD	Single-crystal x-ray diffraction
tbo	Topology term
TBPA	1,3,5,7-Tetrakis(4-bromophenyl)-adamantine
TBPM	Tetrakis(4-bromophenyl)methane
TEPA	1,3,5,7-Tetrakis(4-ethynylphenyl)adamantine
TEPM	Tetrakis(4-ethynylphenyl)methane
TFP	Triformylphloroglucinol

THF	Tetrahydrofuran
THF-d_8	Deuterated tetrahydrofuran
TIPM	Tetrakis(4-iodophenyl)methane
ToF-SIMS	Time of flight secondary ion mass spectrometry
WAXS	Wide-angle x-ray scattering
XPS	X-ray photoelectron spectroscopy
XRF	X-ray fluorescence
ZIF	Zeolitic imidazolate framework

Contents

1. Background

Material science covers the design, properties and applications of new materials. An emerging research field within material science is porous materials. Porous materials are of scientific interest because they are able to interact with species such as ions, atoms and molecules. This occurs not only on their surface, but throughout their entire volume. The porosity of a material describes the distribution, shape, uniformity and size of voids, which are formed in between the atoms and molecules, which compose it.[1] The degree of porosity relates to the amount of void ("emptiness") in a specific material volume. According to the International Union of Pure and Applied Chemistry (IUPAC), porous materials are divided into subgroups depending on their pore size: macroporous > 50 nm, mesoporous 50 – 2 nm and microporous < 2 nm.[2] Porous materials surround us in our daily lives. Foam materials, packaging materials, filters, adsorbents, catalyst pellets, bio membranes, minerals or volcano rocks, as shown in **Figure 1**, are just a few examples of this omnipresence.

Figure 1. *An example for a natural porous material, volcano rock.*

Due to their extended surface area and porosity, common applications for porous materials are traditionally ion exchange, catalysis, adsorption, water protective fabrics or insulation. Often those applications require specific pore sizes, shapes, distributions and uniformity to fulfill their desired function. Consequently, the designed assembly of porous materials is a research field of growing interest.

In 1756, the Swedish mineralogist Alex Cronstedt heated the mineral stilbite, he observed that the sample started to release water in the form of steam.[3] Due to his observation he called the material "zeolite", which originates from Greek and means boiling stone. Thus, zeolites are the oldest and one of the first well studied and industrial used class of porous materials. Zeolites can be described as inorganic anionic cages with exchangeable counter ions and they can be divided in those, which occur

naturally and those, which are made synthetically. They belong to the group of aluminosilicates and are microporous solids. The natural frameworks are based on tetrahedral SiO_4 or AlO_4 units, which are connected via their oxygen atoms in a covalent manner. That means that every Si and Al atom is connected to 4 oxygen atoms and the Si and Al atoms are linked with each other via one bridging oxygen atom. Those connected tetrahedra form rings of different sizes and correlated pore sizes. Industrial made zeolites can contain also other framework elements, such as boron, tin, titanium or germanium in exchange for aluminum and silicon. Zeolites have a wide application range from adsorbents, ion exchange via gas separation and gas storage to catalysis.[4]

The example of zeolite shows that in the field of inorganic chemistry, highly symmetric porous framework materials have existed for a long time. They can be made from simple precursors in a single step using thermodynamic control over the reaction. But the use of this thermodynamic control comes together with drawbacks. Disadvantages are the limited design flexibility regarding both the size of the voids and unit cells as well as the shape of the framework.[5] Contrary, synthetic organic chemistry offers a bigger variety of transformations. Nevertheless, the formation of organic or organic-inorganic frameworks seemed to be a much bigger obstacle until the inception of the concept of reticular chemistry in 1995.[6] One of the main problems was, to solve the "crystallization problem", to find reversible reactions while using strong directional bonds, which allowed the crystallization of extended 2D and 3D networks. That prevented the formation of crystalline organic framework structures with covalent bonds. Thus, organic transformations during this time were focused mainly on single molecule transformation and 1D polymers, such as polyethylene, polypropylene or polyvinylchloride used for plastics.[5] Therefore, for a long time it has been challenging to synthesize regular organic porous structures, as it was well summarized in the following statement from Roald Hoffmann in 1993.[7]

"Organic chemists are masterful at exercising control in zero dimensions. […] One subculture of organic chemists has learned to exercise control in one dimension. These are polymer chemists, the chain builders […] But in two or three dimensions, it's a synthetic wasteland. The methodology for exercising control so that one can make unstable but persistent extended structures on demand is nearly absent. Or to put it in a positive way—this is a certain growth point of the chemistry of the future."

1.1. How reticular chemistry opens the door to porous organic framework materials

The formation of strong directional bonds is usually irreversible under mild conditions, making it challenging to obtain the thermodynamic product, which is required to achieve a long range order and

thus crystallinity. In order to overcome this hindrance, the bond formation should be reversible and happen on a time scale which allows self-healing of lattice defects.[5] Reaction conditions, which meet those two criteria, have to be found for the desired linkage formation to overcome its individual crystallization problem. Omar Mwannes Yaghi had a major impact on the inception and development of 2D and 3D porous frameworks with his strategy, called reticular chemistry.[5]

The term reticular chemistry describes the strategy of polynuclear building blocks (secondary building units (SBU)), which combined via directed strong bonds (mainly covalent and dative bonds) form predetermined extended 2 and 3D networks. The usage of shape-persistent building units and the stable bonds gave the resulting frameworks a permanent porosity, enabled large surface areas and allowed control over the structure design. Summarized, reticular chemistry combines the strengths of both fields, the variety of organic synthesis and the inorganic thermodynamic control, in order to open the door for the rise of new porous framework materials. Examples for newly emerged classes of porous materials after the initiation of the reticular chemistry concept are metal organic frameworks (MOFs, also called porous coordination polymers (PCPs)), zeolitic imidazolate frameworks (ZIFs, also called metal organic zeolites, MOZ), porous molecular crystals (PMCs), hydrogen-bonded organic frameworks (HOFs), porous organic polymers (POPs), porous aromatic frameworks (PAFs) and covalent organic frameworks (COFs). Those classes of porous materials will be introduced briefly during the next pages, starting with the metal-containing frameworks, such as MOFs and ZIFs (section 1.2). Afterwards the "metal-free" porous materials, like PMCs, HOFs and POPs and are presented in section 1.3, followed by PAFs (section 1.4) and COFs (section 1.5) in more detail. An overview of the abbreviations used for porous materials in this thesis and their relation is shown in **Figure 2**.

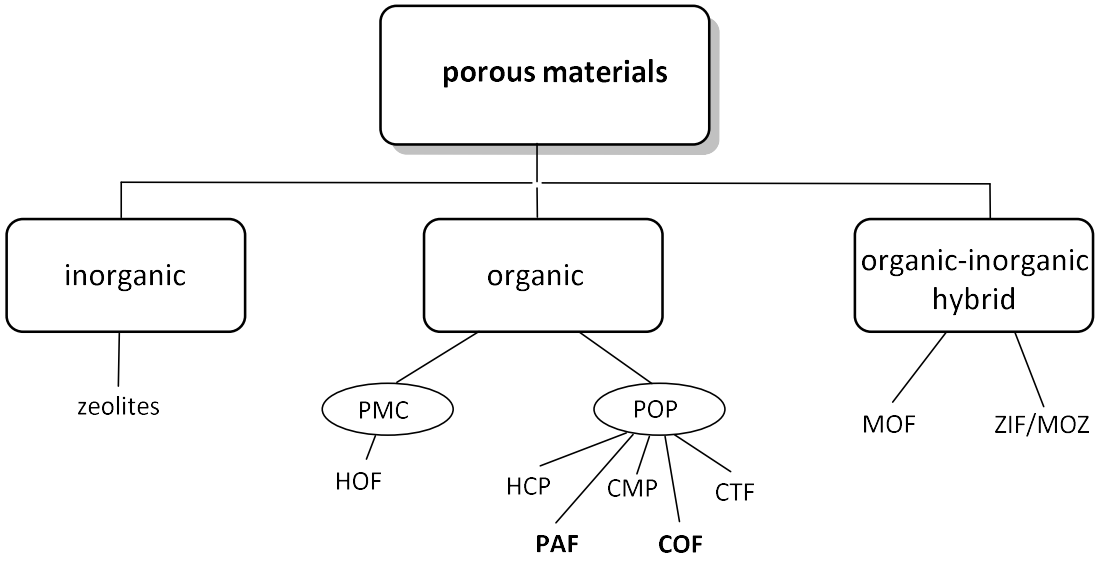

Figure 2. *Overview of the different classes of porous materials discussed in this thesis. Shown in bold are COF and PAF due to their importance in this thesis.*

1.2. Metal-containing porous framework materials

MOFs are one of the most prominent examples of porous framework materials. Their structure is defined by a metal cation or metal cluster connected with polydentate organic linkers via coordination bonds. The framework structure is dependent on the nature of the SBUs. The bond formation between the SBUs during the synthesis is reversible, which allows a self-healing mechanism of defects during the framework formation. This leads to a high crystallinity of the gained materials. Depending on the amount of binding sites in the SBUs, many different network topologies are possible, leading to more than 20,000 reported structures so far.[8] MOFs have a wide application range, such as gas capture and storage, removal of toxic chemicals, catalysis, drug delivery and as coatings on textiles, to mention a few.[8-12] Metal organic frameworks often show a high porosity, connected to large BET (Brunauer-Emmet-Teller) surface areas, which can be up to 6240 m^2/g in the case of MOF-210.[13] Other prominent examples for MOFs, which are produced on a ton scale by BASF for gas adsorption and separation,[9] are for example HKUST-1,[14-15] MIL-53[16] and MOF-5,[17] which is shown in **Figure 3**.

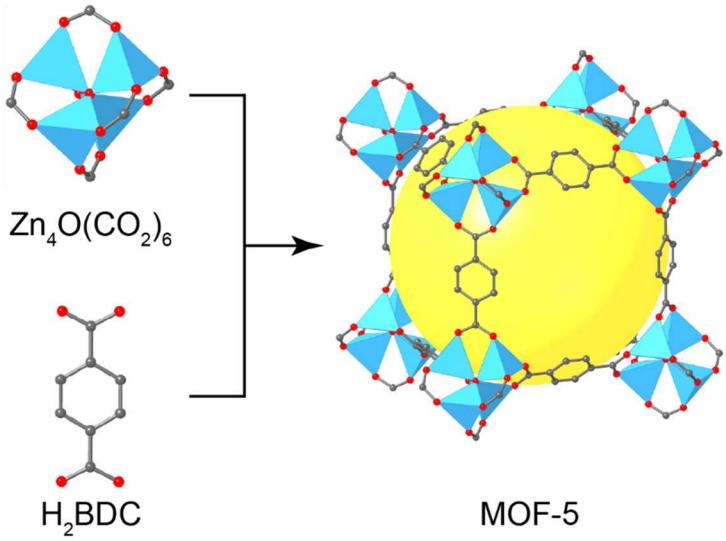

Figure 3. *SBUs and structure of the industrial produced metal organic frameworks, MOF-5. The yellow sphere represent the void in the framework. (Reproduced from reference [9] with permission from The Royal Society of Chemistry)*

Numerous MOFs are unstable under ambient conditions. One explanation for that lies in the nature of the coordinative bonds between e.g. carboxyl linkers and the metal ion. This oxygen-metal bond can be hydrolyzed in contact with water. ZIFs however, show a much higher water stability.[18] They usually consist of tetrahedral transition metal ions, such as Fe^{2+}-, Zn^{2+}- or Co^{2+} ions and are connected to each other via imidazole linkers. The imidazole-metal ion bond is not as prone to hydrolysis as the carboxylic dative bond. Due to their stable zeolite topology, ZIFs have higher thermal and chemical stability than MOFs.[18] Their network topology is isomorph to zeolites, when tetrahedral metal ions are used. Thus, ZIFs can be seen as a hybrid of zeolites and MOFs. Zeolitic imidazolate frameworks show

in general high surface areas, good crystallinity and a really good thermal and chemical stability.[19-20] Those properties make zeolites, especially the intensely studied ZIF-8,[21-23]outstanding materials for separation,[24-25] catalysis[26-27] and sensing.[28-29] ZIFs and MOFs have in common that they use metal ions in their framework structure. On the contrary, there exist also different classes of porous materials, which don't contain transition metals in their structure, but only elements such as C, N, O, H or B.

1.3. Organic porous materials & organic porous framework materials

Two subgroups of organic porous materials, which don't contain transition metals are PMCs, as well as POPs. Both can be further divided into subgroups, as shown in **Figure 2**. Porous molecular crystals are not framework materials in a traditional way, since they are not made via polymerization. This makes them unique in the family of porous materials and means they don't form extended dative or covalently linked lattices in between the molecules. Instead, their discrete molecules organize themselves via weak interactions in a way that they form voids in between each other. That gives them the advantage that they can be dissolved in common organic solvents, whereas this is not possible for most frameworks materials without decomposition.[30] Their voids are usually occupied by solvent molecules in liquid phase. A common problem in the beginning was that the hollow spaces collapsed, when those guest molecule were removed, but this obstacle could be overtaken by stabilizing them with intramolecular interactions, resulting in stable solid PMCs with empty voids. The voids can be isolated from each other or form 1D and 3D channels.[31] PMCs are much more flexible in their structure than most other framework materials and can change their void sizes, since the molecules are connected via weak interactions. That makes them very suitable for sensing applications[32-33] and as molecular switches.[34] Porous molecular crystals can be divided in two categories, intrinsically and extrinsically porous.[35] Intrinsically porous describes the property that the single molecules are already porous and bring their own shape-persistent voids into the organized structure. Macrocycles and molecular cages are examples for this category. On the other side are molecules, which form extrinsically PMCs, not porous on their own, but their packing is so inefficient that they generate voids in their solid states.

PMCs, which are based on hydrogen bonds to form frameworks are called HOFs. They show a good solution processability, ability to restore crystallinity and they can be easily grown as single crystals.[36-38] The development of HOFs was limited in the beginning, similar to PMCs, by structural collapse when the solvent molecules were removed from the voids. This disruption is caused by the insufficient strength of the hydrogen bonds to stabilize the framework. Later, additional Van der Waals forces or

π-π-interactions between the building blocks were used to increase the stability of HOF structures. This led to the synthesis of the first HOF with permanent porosity in 2011[39] and thus, HOFs could show their full application potential. They are for example used for gas storage,[40-41] carbon dioxide capture[42-44] and gas separation.[39, 44-46] Common functional groups and binding moieties for HOFs are shown in **Figure 4**.

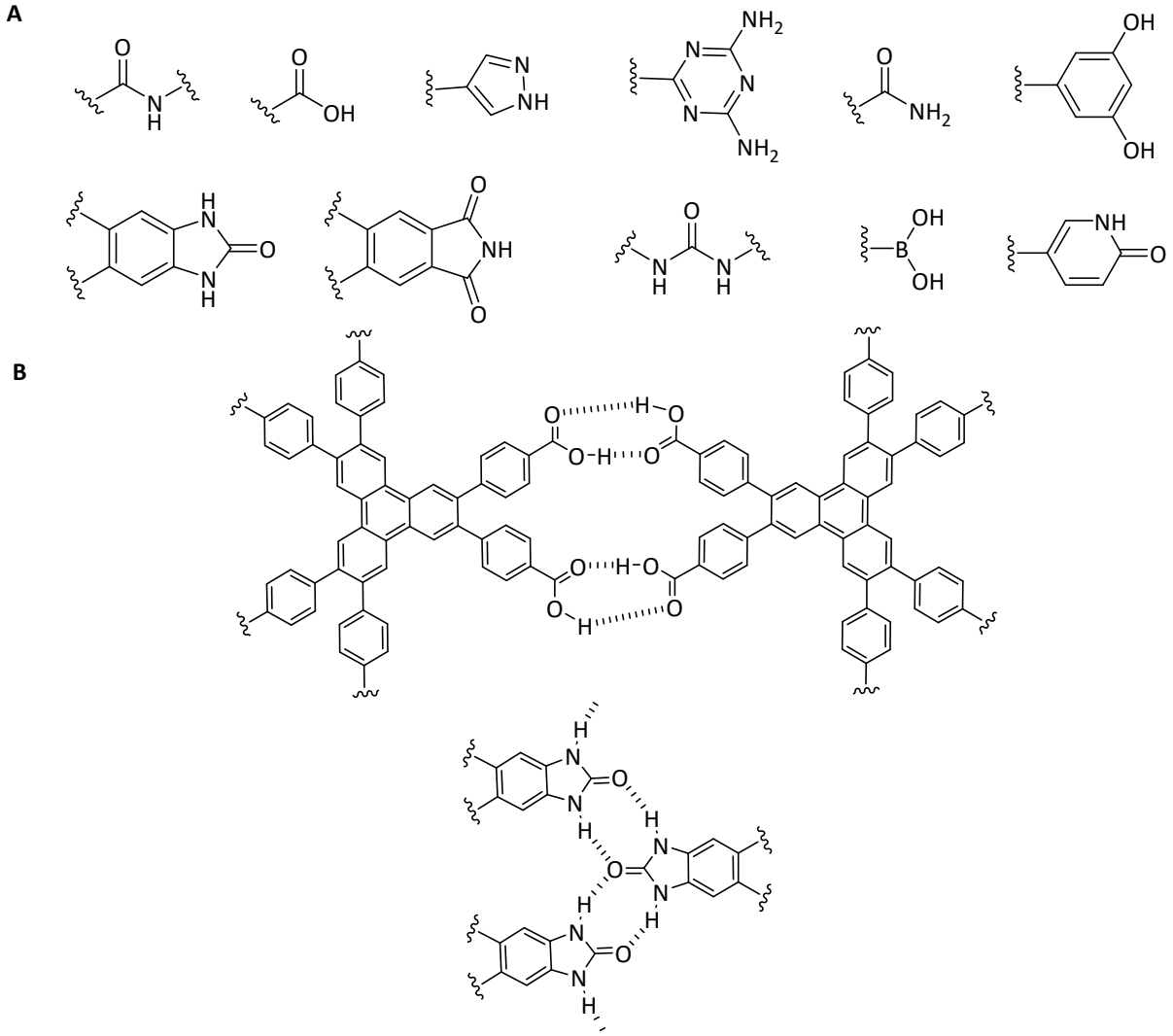

Figure 4. *Common binding moieties in HOFs. A) Shown are functional groups used to connect building blocks via hydrogen bonds. B) Illustrated are two examples of how building blocks in HOFs are connected via hydrogen bonds (dashed lines).*

The term porous organic polymers describes a rather diverse group of 2D and 3D polymers. POPs are synthesized through the cross-linking of their building blocks and are often amorphous due to a missing long range order. Even though those polymers can be divided according to their synthesis and structure into different sub groups (see **Figure 2**), they still share certain characteristic properties. They are in general highly porous, contain only lighter main group elements (unless further

functionalized) and they are connected via strong covalent bonds, giving them a more rigid structure, which show a high thermal and chemical stability.[47] Since those networks can be functionalized through the incorporation of active sites,[48] metals ions[49] or even nanoparticles,[50-51] POPs are used in metal-catalyzed reactions,[52] metal-free catalysis[53] and as nanoreactors.[47] Besides catalysis other applications for porous polymers are CO_2 capture,[54-55] gas separation[54, 56] and flue gas conversion[52, 57] or organic electronics.[58]

As earlier mentioned, the term POP serves also as an umbrella term of different subgroups, e.g. hyper-crosslinked polymers (HCPs), conjugated microporous polymers (CMPs), porous aromatic frameworks (PAFs), covalent triazine frameworks (CTFs) and covalent organic frameworks (COFs). The building blocks in HCPs are randomly connected with each other, as a consequence of their non-directed bond formation, e.g. Friedel-Crafts polycondensation.[59-61] This leads to an amorphous network without any long- or short-range order, which means there is no common unit cell in the framework. Apart from that, CMPs use directed cross-coupling reactions for the linkage of the building blocks, leading to a network with short-range order.[62-63] Since the used coupling reaction is kinetically controlled, the material doesn't have a long-range order and is amorphous. Nevertheless the precise control over pore size and surface area is given through the choice of the building blocks.[62] CPMs and HCPs won't play a further role in this thesis and were just mentioned here for the sake of completeness and for giving an overview of the different porous materials, which were explored during the last decades. CTFs have a lot in common with COFs, that's why they will be described in section 1.5.1. With that I would like to change the focus towards the two subgroups of POPs that will have an outstanding importance for this thesis, PAFs and COFs.

1.4. PAFs

The term porous aromatic framework, was formed by Ben et al. in 2009.[64] PAFs are usually synthesized via cross-coupling reactions and their aromatic building blocks are connected via covalent bonds, as shown in **Scheme 1**, the homo-coupling of tetrakis(4-bromophenyl)methane (**1,** TBPM) to form PAF-1.

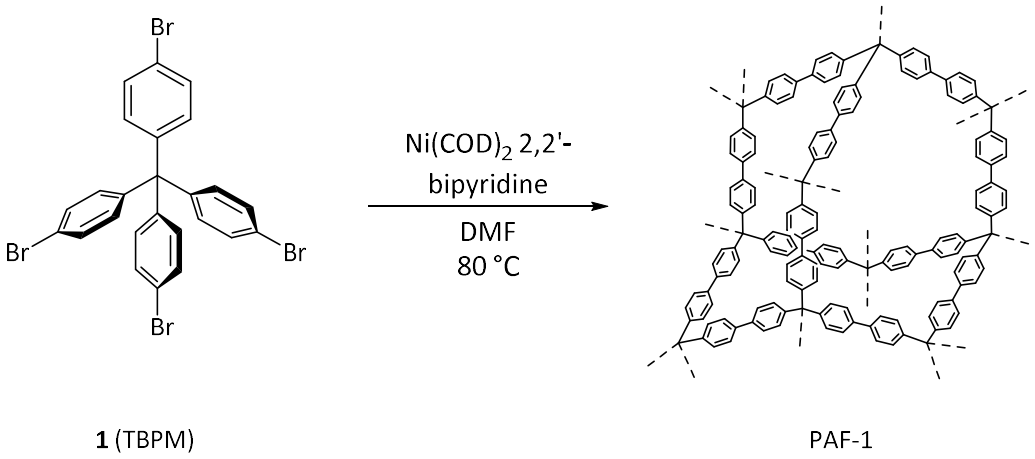

Scheme 1. *Cross-coupling of tetrakis(4-bromophenyl)methane (TBPM) to yield PAF-1.*

Due to the nature of their strong covalent bonds, the resulting materials demonstrate a high thermal and chemical stability. The topology of the frameworks can be controlled by the number of binding sites on the used building block. 3D PAFs have been synthesized by using cubic,[65] triangular prismatic[66] and tetrahedral[67-68] building units, whereas square (porphyrin[69] or pyrene[70] based) and triangular[71-72] starting materials lead to 2D networks. The tetrahedral building units around TBPM allow more synthetic versatility in making the frameworks, because of the possibility to exchange their central carbon atom. To change the framework properties, it is for example possible to exchange the carbon atom in the center with a hetero atom, such as silicon or germanium.[73-74] Silicon and germanium are from the same group as carbon in the periodic system, therefore they have the same valency. But it is also possible to use atoms from group 13 (boron)[75-76] and 15 (phosphorous)[77] and change the valency of the central atom. Exchanging the carbon atom with boron or phosphorous leads to the conversion into a charged building block with tetrahedral geometry and introducing coordinately bound counter ions into the framework. The introduction of exchangeable counter ions is advantageous, since it increases the functionalization and application range. The exchange of the counter ion can for example be used to modulate the available pore size in the framework. Even though those materials are amorphous, it could be shown that it is possible to design unit cell size, volume and surface area by the choice of building units. Computational calculations[78-79] and the synthesis of PAFs from differently sized building blocks,[72] confirmed the hypothesis, that with an increase of building block and/or linker size the pores increases as well. But surprisingly increasing the size of the building units does not always increase the porosity. The bigger the voids become, the higher the chance for interpenetration of the framework.

Interpenetration

Interpenetration describes the phenomena of overlapping networks within the unit cell. A framework can be interpenetrated once or even several times, defined as the degree of interpenetration. A consequence of this phenomena is a dramatic decrease of the porosity, because the voids are now filled with frameworks. There exist strategies to avoid an interpenetrating framework. One strategy is to increase the steric demand of the building units. That approach was tested with the tetrahedral building unit tetrakis(4-ethynylphenyl)methane (TEPM) and its more bulky analogs where the carbon center was exchanged for an adamantane moiety (1,3,5,7-tetrakis(4-ethynylphenyl)adamantine, TEPA and 1,3,5,7-tetrakis(4-bromophenyl)-adamantine, TBPA).[80] The calculated surface areas for all three resulting networks are comparable under the condition that the frameworks are not interpenetrated. This finding couldn't get confirmed when measuring the sorption isotherms and calculating from those the surface area for the three materials. Lu et al. could show that the usage of the smallest building unit, TEPM, resulted in a framework with a much smaller surface area compared to the materials gained from TEPA or TBPA.[80] The authors explain this behavior with the fact that the carbon center in TEPM supports a more efficient packing of the building blocks and with that a higher degree of interpenetration of the resulting network. With those finding it was confirmed that an increased steric demand of the building blocks can decrease the chance of interpenetration. Since an increased steric demand of the network also decreases the pore size, Totten at al. used the idea of using labile bulky ligands on their Sn-porphyrin building units.[81] The bulkiness of the porphyrin linkers suppressed interpenetration during the framework synthesis. After the synthesis the bulky labile ligands on the tin ions could be easily removed to gain a non-interpenetrated framework with big pore size.

Linkage formation

For the carbon-carbon bond formation during the PAF assembly traditionally reactions, such as Yamamoto type Ullmann coupling reaction,[64, 66, 73] Suzuki–Miyaura cross-coupling,[72] Sonogashira cross-coupling,[82] Heck reaction,[83-84] 1,3-diyne formation[85] or Stille coupling[84] are used. Yamamoto type Ullmann reactions usually result in frameworks with high surface areas, caused by the high yield of the coupling reaction. On the contrary, due the nature of the homo-coupling, the design possibilities are more limited compared to the presented hetero-couplings. All those reactions also have the drawback that they are oxygen sensitive, and the palladium complexes are costly, which makes an industrial upscaling less favorable. That is why reactions, such as nucleophilic substitutions of cyanuric chloride with amines,[86-87] azo formation reactions[88-89] or click reactions[90-91] for the linkage formation were also explored. Friedel–Crafts alkylation reactions were also reported to produce PAFs.[92-93] But to

call the resulting polymeric structures without a clear unit cell PAFs, is debatable, since it could be also seen as a HCP.

Functionalization

Even though all those discussed reactions and different building blocks lead to a quite diverse library of possible PAF structures, it is possible to increase the variety even more by functionalization of the framework. The robust structure of PAFs make them suitable, also for treatments under harsher conditions. There are three possible strategies to functionalize frameworks: Via direct synthesis, post-synthetic modification or a hybrid form, in which directly included motifs get transformed after the framework assembly, as illustrated in **Figure 5**. Direct synthesis describes the functionalization of the building units. This method allows a good control over the equal distribution of the functional sites. Common motifs to introduce in the monomers are for example hydroxyl,[94-95] carboxyl,[95-96] amine[95] and nitro groups.[97] A drawback can be the needed compatibility between the functional groups and the used coupling reagents or conditions during the assembly. For example, the commonly used Yamamoto type Ullmann coupling reaction is incompatible with nitro groups. In that case, it was shown that an alternative version of the Ullmann reaction with copper instead of nickel works.[97] The

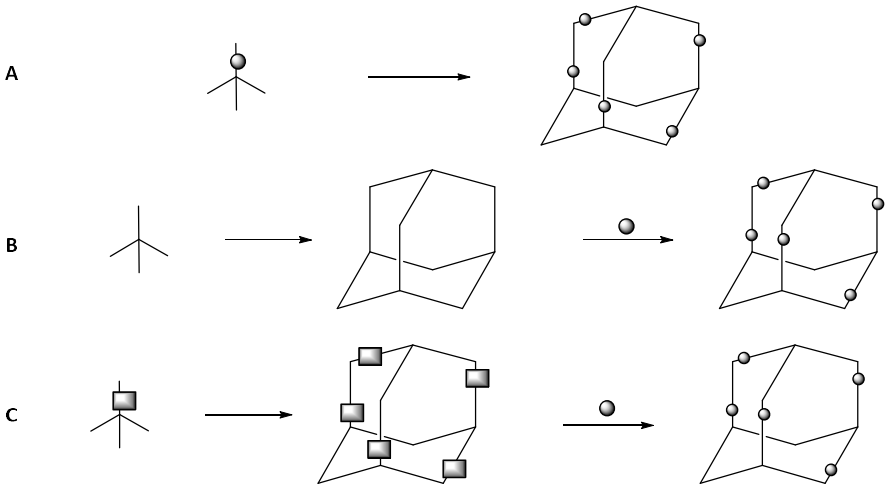

Figure 5. *Illustration of the tree possible modification option for PAFs. The three strategies are A: Direct synthesis, B: post-synthetic modification and C: post-synthetic conversion of directly included functional sites.*

post-synthetic modification approach is the opposite of the direct synthesis. It describes the strategy to include functional groups after the formation of the framework. Consequently, there are no considerations about the compatibility of functional groups and synthetic conditions necessary, but depending on the reaction type and the resulting porosity, their equal distribution might be hard to control. An example for those post-synthetic modifications are the introduction of sulfonate groups into the framework and increasing its acidity through the treatment with chlorosulfonic acid.[98-99] Other groups, which can be introduced after the assembly, are amino groups[99-100] or benzyl chloride, which

can be used for a variety of further transformations.[101-102] The third strategy, the post-synthetic transformation of directly included functional sites, represents a combination of the advantages of both previously described strategies. It allows a good compatibility with the coupling reagents and also control over the distribution in the framework. An example for this approach was presented by Yang et al., where they introduced alkylamines into PPN-200 in order to increase the CO_2 adsorption of the material.[102]

Applications

Potential applications for PAFs are numerous. Due to their high porosity and big internal surface area, they can be used as adsorbents for gas molecules, specifically hydrogen,[74, 103] methane[73, 104] or CO_2.[92, 105] Since the frameworks do not adsorb all gases in the same amount, PAFs are also used for gas separation, for example for separation of hydrocarbons.[106-107] But they can even be used for the adsorption of organic solvents,[108-109] antibiotics,[110] mercury,[111] lead[112] and copper.[113] Besides adsorption, porous aromatic frameworks can also be used in many different kind of catalytic reactions, such as cascade catalysis,[99, 114] asymmetric catalysis,[115] photocatalysis[116] and redox catalysis.[117] Other application fields are sensing, for example of explosives,[118] Fe^{3+} ions[119] or iodine vapor[120] and drug release.[86] An example for the application of ionic frameworks is the capturing of radioactive elements.[76] Furthermore, it was shown that PAFs can be used as nanoreactors for polymerization of acrylonitrile[121] or the dehydrogenation of ammonia boran.[122] PAFs also have been reported as responsive materials, which are able to react on different stimuli. Those stimuli can be light radiation, triggering metal capture and release or a pH change, resulting also in a color change.[123] Another azobenzene PAF showed an increase of its surface area under UV radiation due to photoisomerization.[124] Besides porous aromatic frameworks, one of the biggest subgroups of POPs and organic porous framework materials in general are COFs, which will be discussed next.

1.5. COFs

The synthesis of the first COF in 2005 was a breakthrough, since it demonstrated for the first time that it is possible to create crystalline 2D networks with only covalent bonds and without incorporating transition metals.[125] Simultaneously it delivered a first solution for the long existing crystallization problem. Covalent organic frameworks are in many aspects similar to PAFs. According to their name, they are constructed from building units, which only contain organic elements and are connected via covalent bonds. They have in general very low densities, permanent porosity, a high surface area, tunable topologies, high thermal stability and diverse functionalities.[126] With regard to reticular

chemistry, their framework topology is designable through the choice of the geometry of the building units, similar to PAFs. The big differences between both classes is by definition that COFs are crystalline, so they show the long range order that PAFs are lacking. From that perspective, PAFs and COFs can be seen as siblings, coming of their parents, POPs. COFs are just the slightly more known and more organized sibling of the two.

Linkage formation

For achieving a long-range order and consequently crystallinity in COFs, usually reversible reactions for the connection of the building blocks, as shown in **Scheme 2** are used.[126] In those reactions the product formation happens in equilibrium with the back reaction if specific conditions are fulfilled. That leads to the useful consequence that the framework can self-heal errors occurring during the assembly and thermodynamic control over the product will be achieved. To overcome the crystallization problem and promote the equilibrium character of the shown linkage forming reactions in **Scheme 2** different strategies are used. The first reaction in the scheme shows the formation of a boronate ester, but similarly can boronic acids also self-condensate and form boroxines. For those reactions it is crucial that the water, which is formed as a side product remains in the reaction flask to

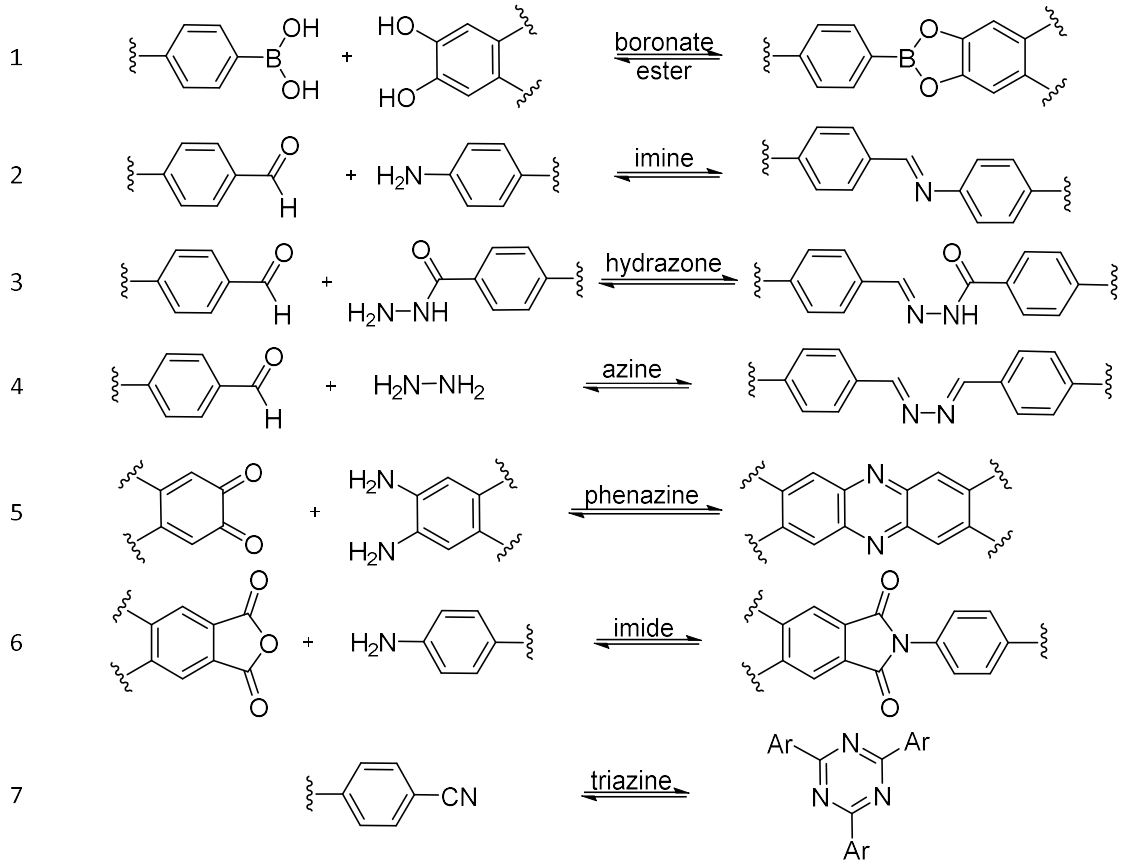

Scheme 2. *Common reversible reactions to form linkages in between building units.*

support the back reaction. This can be achieved by using a closed and pressure tight system. Additionally a solvent mixture has to be chosen, which limits the solubility of the building blocks, to slow down the reaction. The next reactions, number 2-5 shown in **Scheme 2**, describe different Schiff-Base reactions. Schiff-Base reactions are the most common reactions to assemble COFs. Those reactions require an acid catalyst, which consequently makes the final frameworks also more stable at neutral pH even in aqueous media. Similar to the condensation of the boronic acids, the water that is formed throughout the reaction with elevated temperatures, has to be kept in the closed system to support the reverse reaction and the self-healing of lattice errors. The assembly of imine COFs is often done in a two-solvent systems, such as mesitylene/dioxane between 85-120 °C.[127] It is believed that the more polar solvent is increasing the reversibility of the reaction, whereas the more aromatic one solubilize the aromatic parts of the building units and disrupting their π-π-stacking. The formation of imides, as shown in reaction 6 is reversibly done under basic conditions at high temperatures between 200-250 °C in *N*-methyl-2-pyrrolidone (NMP) and mesitylene.[128] Imine and imide COFs are mainly made using solvothermal synthesis, which is the most common synthetical approach.[126] Even harsher conditions, than for imides, are needed for the condensation of cyano groups into covalent triazine frameworks (reaction 7 in **Scheme 2**).[129] The required nitriles are dissolved at 400°C in molten $ZnCl_2$. This approach is called ionothermal synthesis and is quite rare in COF constructions, since not many building blocks can withstand those high temperatures without decomposition.[126]

Stabilization of imine COFs

Imine COFs have due to their reversible imine bond formation a reduced stability compared to e.g. triazene COFs. There are different possibilities to increase the stability of imine bonds and with that of the entire framework. They can for example be stabilized via hydrogen bonding[130] or resonance with electron donating groups (e.g. methoxy groups)[131] as shown in **Scheme 3**.

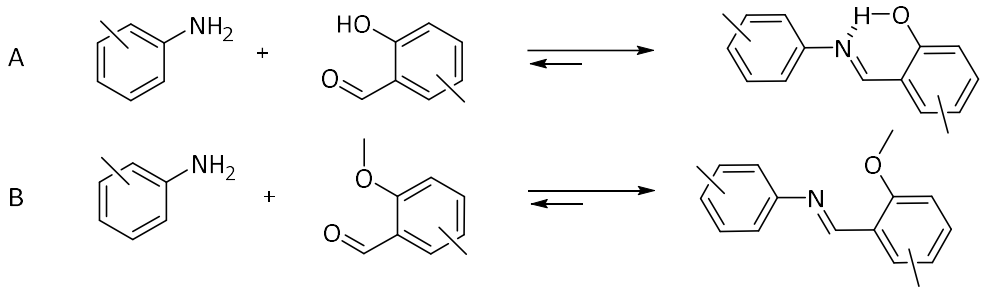

Scheme 3. *Examples for stabilization of imine COFs, via A) hydrogen bonds or B) electron donating groups.*

Another strategy describes the reversible formation of the linkage, which is then in its final conformation irreversibly locked. This can be observed during the formation of phenazine moieties (see **Scheme 2**, reaction 5), since the resulting aromaticity, makes the second step of the condensation

irreversible and locking the framework in the final configuration.[132] A similar example for the combination of reversible steps followed by an irreversible step to enhance the stability is the formation of β-ketoenamines. They can be synthesized under the usage of triformylphloroglucinol (TFP, **2**) via keto-enol-tautomerism as illustrated in **Scheme 4**.[133]

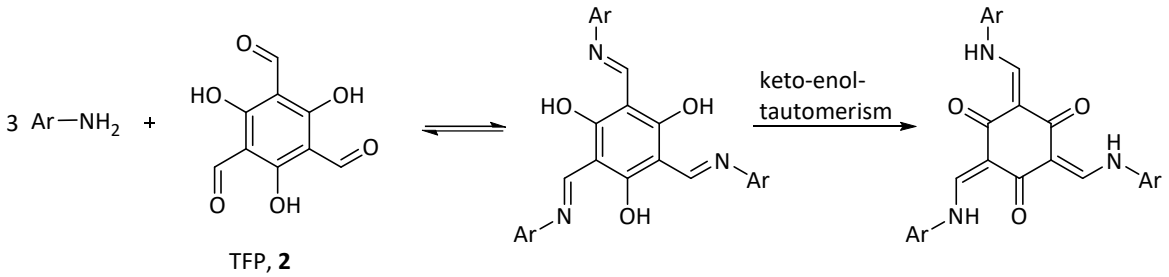

Scheme 4. *Increased stability through the combination of reversible steps (imine formation) between an amine and TFP (**2**) followed by an irreversible step (keto-enol-tautomerism).*

Alternative synthesis possibilities

Besides solvothermal and ionothermal synthesis, microwave synthesis is another option to build up COFs. It was demonstrated by Campbell et al. that it is possible to make boronate ester COFs in only 20 min, much faster than with the usual solvothermal approach.[134] Furthermore, it was shown that the boron-based COF-5 can be made with ultrasonic in a sonochemical synthesis.[135] Using the ultrasonic approach has several advantages, for example shorter reaction times, less energy consumption and increased crystal domain size, compared to the normal solvothermal approach. Other, more unusual approaches are via electron beam irradiation,[136] photochemical[137-138] and mechanochemical synthesis.[139-141] All those more uncommon strategies try to tackle the problems of upscaling solvothermal synthesis for industrial use, such as required high pressure, high temperatures and long reaction times. Another improvement regarding faster reaction, better crystallinity and lower reaction temperature can be achieved by using metal triflates, especially scandium triflate in imine COF synthesis instead of acetic acid.[142-143]

Functionalization

It is possible to functionalize COFs with the same three strategies as earlier described for PAFs (see **Figure 5**). Those are pre- and post-synthetic modifications as well as a fusion of both, post-synthetic conversion of directly included functional sites. A diverse field for functionalization are covalent modification, which transform existing functional groups in the framework or create new ones. Important is that those transformations need to have a high yield and don't compromise the framework integrity. Frequently used reactions under those circumstances are copper(I)-catalyzed click reactions,[144-145] succinic anhydride ring openings[146] as well as nitro reduction and amide

formation.[147] Linkers in an existing framework can be exchanged, without decreasing crystallinity.[148-149] In both cases a nucleophilic substitution was used to exchange the already existing linker in the imine framework. Another approach is to convert the reversible linkages post-synthetically to more stable linkages. Those more stable bonds can't be used directly for the framework formation, because of their insufficient reversibility and thus, lack of thermodynamic control. One example for this functionalization is the oxidation from an imine to an amide COF.[150] A common possibility to metalate covalent organic frameworks pre-synthetically is with the help of porphyrins.[151] The functionalization of the resulting COF-366-Co was further investigated with different substitutions on the framework backbone, through a pre-synthetic modification of the linker.[152] Post synthetic trapping of guest molecules is another option to change the functionality of a framework. If the framework is sufficiently porous, it can trap small functional molecules, such as triazole and imidazole and increase through that the proton conductivity of the material.[153] The nitrogen heterocycles function as proton carriers and let the protons hop in between them following a Grotthuss mechanism. Additionally, it was shown that even bigger nanoparticles, which are exceeding the pore size of the framework can be embed in COFs. Due to the size of those nanoparticles, it is often difficult to incorporate them after the framework assembly. Nevertheless, it could be demonstrated that it is possible to coat the nanoparticles first with an amorphous imine polymer of defined thickness. Afterwards the acid catalyst is added, which initiates the self-healing and the crystallization of the polymer into its respective COF around the nanoparticles.[154]

Applications

COFs have, depending on their functional groups, their topology and their linkages a quite wide range of specific properties, which makes them suitable for various applications. One of the most common application fields for covalent organic frameworks due to their high porosity and low density are gas storage of hydrogen,[155-156] methane,[155, 157] carbon dioxide[155, 158] and amonia[159-160] as well as gas separation.[106, 161] Furthermore they are excellent heterogeneous catalysts, since the nature and distribution of their catalytic sites in the framework and their pore size is tunable. Explored catalytic areas are photocatalytic reactions,[162-164] electro-,[152, 165-166] cascade-,[167] size selective-[168] and organic catalysis, such as coupling reactions,[169-170] oxidations,[171] reductions,[172] condensations[168, 173] and additions.[131, 174] Other useful applications are in electroactive materials,[175-178] water purification,[179] proton conductors,[153] sensing of copper ions,[180] mercury ions[181] or explosives[182] and drug delivery.[183-185] Furthermore their porosity can be used to capture for example enzymes,[185] metal nanoparticles,[186] fullerenes[132] or metal ions.[170, 187-189]

Dimensionality

Conventionally COF materials are divided regarding their topology into two and three dimensional frameworks. 2D COFs consist of sheets, which have covalent bonds along the x-y plane and which are connected to each other through non-covalent interactions, mostly π-π interactions in z-direction. Contrary, 3D frameworks have covalent bonds in all three dimensions. More recently a new class of sometimes called 1D COFs has been added to the COF family as well.[190-191] They consist of one dimensional polymer chains, which are woven into each other, resulting in a more flexible framework, than previous 2D and 3D frameworks.[192] The term 1D might be a bit misleading, since it refers to the used one dimensional polymer chains, but the resulting woven framework is actually a 3D structure. Weaving can be seen as a wanted form of entanglement of 1D chains. As already discussed, 2D and 3D structures can also show entanglement, which is called interpenetration.[193] Special features of two and three dimensional COFs will be described in the following two sections.

1.5.1. 2D COFs

The first studied 2D COFs were described by Cote at al in 2005.[125] The frameworks were assembled via the self-condensation of diboronic acid (COF-1) or the condensation of diboronic acid with hexahydroxy triphenylene (COF-5). Both COFs crystallize in a honeycomb (**hcb**) topology. The topology of each COF is depending on how many points of extensions (binding sites, "n-topic") their polygonal building units (vertex) have and which angle they have in between them. Common building blocks are di-, tri-, tetra- or hexatopic. 2D COFs can have five different topologies. Besides the already mentioned **hcb** exist square lattice (**sql**), kagome (**kgm**), hexagonal lattice (**hxl**) and kagome dual (**kgd**), as illustrated in **Figure 6**.[126] Four out of those five (**hcb**, **sql**, **hxl** and **kgm**) topologies result from the re-

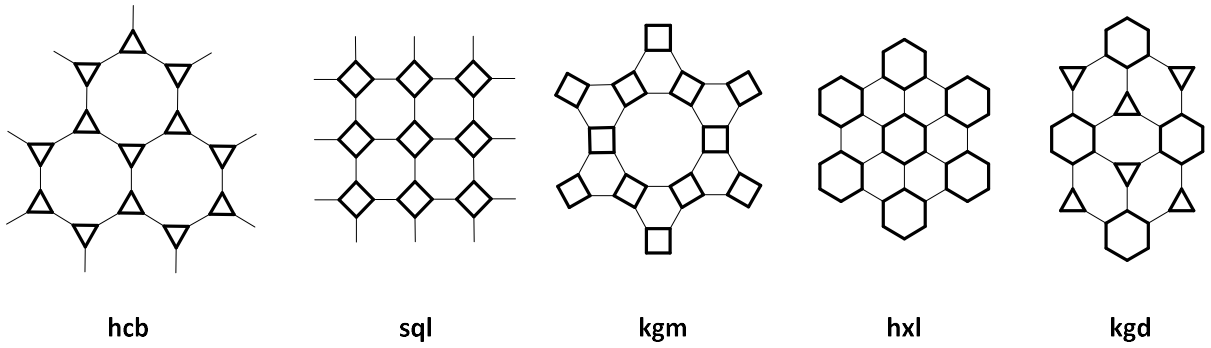

Figure 6. *Overview of the different topologies in 2D COFs (building units are shown bold). The resulting network topology is depending on the amount of the available binding sites of the building unit and their angle to each other. Tritopic building block lead to an* ***hcb*** *topology, whereas the use of tetratopic vertices results in a* ***sql*** *or* ***kgm*** *topology (depending on the angle between the linear linkers). Planar starting materials with six binding sites form* ***hxl*** *networks. The* ***kgd*** *framework is the only known topology for 2D COFs which requires 2 different vertices, a tri- and a hexatopic one.*

action of one building unit (vertex) with a linear linker, whereas the combination of two vertices (a tri- and a hexatopic one) lead to the assembly of a **kgd** framework.

Crystallization mechanisms

2D COFs not only have different topology frameworks, they also undergo different mechanisms during their assembly, depending on the used linkage. Crystallization studies performed by Dichtel and coworkers for boronate ester COF-5 and for an imine COF revealed that the formation process of those frameworks is entirely different.[194-196] In case of boronate ester COFs, the monomers start within minutes to form oligomers in a reversible manner, which then grow and form sheets. The formed oligomers have already the final crystalline form. Then the growing sheets start to stack and crystallites are forming, which precipitate out from the solution. At this point they are not available anymore to participate in the formation equilibrium, unless they are forced, e.g. through water addition. It could be shown that the amount of added monomer to the formed oligomers influences the average particle size.[197] Fast addition of monomers leads to formation of new oligomers and thus new nucleation seeds, resulting in a smaller particle size. If the rate of monomer addition is reduced, the available new building blocks rather connect to the already existing nucleation seeds, then forming new ones. That means that a lower concentration of building units supports in average bigger crystals. The formation of imine frameworks works differently. The building units for imine COFs react in presence of catalyst within seconds to amorphous polymers, which then during an extended amount of time slowly change into the final form and crystallize. Surprisingly, this conversion from the kinetic to the thermodynamic product occurs automatically, even if no new monomers are added. That means, precipitated amorphous polyimine networks can still undergo self-healing mechanisms, whereas boronate ester COFs precipitate directly in their final crystalline form.

Covalent triazine frameworks

CTFs can form crystalline and amorphous structures, depending on the used monomers and the reaction conditions.[198] That makes them special regarding their taxonomical classification. The few known crystalline CTFs are often seen as a part of the (2D) COF family, whereas the majority part of them, the amorphous structures, form their own subgroup of POPs. After the inception of the CTF material field in 2008,[129] several synthesis methods apart the initially used ionothermal synthesis were described. Triazene frameworks show some unique characteristics, such as the aromatric C=N linkage and consequently an increased nitrogen content. They show also an enhanced chemical stability compared with many other COFs. Therefore, they have an increased shelf-lifetime against other framework materials using more reversible bond formation, such as imines, boronate esters, boroxine and hydrazones.[198] The combination of the increased nitrogen content and the enhanced stability

makes CTFs a suitable material for gas separation and storage,[199-201] photocatalysis,[202-204] energy storage[205-207] and catalysis.[208-210]

Stacking Offsets

COFs are usually assembled from aromatic building blocks, which support the mechanical and architectural stability of the network. Consequently, many building units have extended conjugated areas, which tend to interact in an intermolecular manner via π-π interactions with each other. Thus, 2D COFs crystallize as layered structures with laminare pores along the z-axis. But even though they are often illustrated as perfectly eclipsed stacked sheets, the reality shows often a different picture of this interlayer stacking. Often the layers are serrated, inclined or staggered towards each other. This leads to decreasing pore sizes and in general difficulties in pore size engineering. It is rather difficult to measure this stacking offset, since problems arise from the polycrystallinity and the small grain size gained through solvothermal synthesis.[211] However, theoretical calculations have been performed and confirmed the offset in between the layers.[212-214] One reason for the described offset is the repulsion of the more polar regimes (e.g. the imine bond) in between the sheets.[126] Nonetheless, Ascherl et al. could show that it is possible through targeted building block design to enforce an eclipsed stacking of the sheets.[215] They used screw- or propeller shaped monomers which lock the resulting framework into the desired stacking mode.

Another approach to avoid stacking errors, increase the rigidity of COFs and gaining full control over the framework in all three dimensions would be to form directed covalent bonds in between the sheets. This can be achieved by using polyhedral instead of planar building units. This strategy leads to 3D COFs.

1.5.2. 3D COFs

So far most of the reported COF structures are 2D COFs, even though there exist more theoretical possible 3D framework topologies. The first three dimensional COFs (COF-102, -103, 105 and -108) were reported by El-Kaderi et al. in 2007.[216] The linkage chemistry was, similar to the first 2D COF, based on boroxines and boronate esters. But this time polyhedral, rather than polygonal building units were used. The combination of a tetrahedral and a trigonal building units resulted in a carbon nitride (**ctn**) (for COF 102, -103 and -105) and a boracite (**bor**) topology (for COF-108). Besides **ctn** and **bor** inititally only two more were known, which have been found in 3D COFs. Diamant (**dia**) topology is usually the result of the combination of a tetrahedral and a linear building unit and platinumsulfide (**pts**) is the product from a tetrahedral and a square planar monomer. **Dia** and **pts** frameworks have a

high tendency to form *N*-fold interpenetrations. With an increase of the degree of interpenetration, the pore size decreases and for high interpenetration degrees just 1D channels persist in the materials.[183] Fang et al. could show that the use of a bulky building block, based on adamantane prevents interpenetration in **dia** networks and leads to larger pore sizes, similar for PAFs.[183] While the available topology library has been rather small for the first decade of 3D COF research, more recently, structures with **rra**,[217] strontium silicate (**srs**),[218] **ffc**,[219] lonsdaleite (**lon**),[220] Luojia Hill (**ljh**),[221] **ceq**,[222] **stp**,[223] **acs**,[224] **tbo**,[225] **fjh**[226] and body-centered cubic (**bcu**)[227] could be synthesized as well. Illustrations of these and other possible network topologies can be found in the Reticular Chemistry Structure Resource (RCSR) databank, which was established and is hosted by Michael O'Keeffe.[228] Remarkable is that the **ffc**-COF was constructed without the usage of polygonal building units. Instead, Lan et al. used only tri- and tetratopic polygonal building blocks.[219] Gropp et al. expanded the scope of so far mainly tri- and tetratopic building blocks further to octatopic (cube shaped) building blocks.[227] They presented also a strategy to use boron-oxygen-phosphorous rods to create building blocks with a theoretical infinite amount of binding sites.

Single crystal crystallization

There have been a few attempts in order to grow single crystal 3D COFs. In 2013 could Beaudoin et al. show for the first time that they could grow sufficient big COF single crystals for single-crystal x-ray diffraction (SXRD).[229] In the same year the attempt from Yaghi's group to crystallize an imine COF resulted in too small crystals for SXRD.[230] Instead they used rotation electron diffraction to confirm the crystal structure. It took another 5 years until in 2018 the first SXRD of an imine 3D COF could be measured.[220] Ma et al. used aniline as a modulator in the synthesis of COF-300 to slow down the assembly. Aniline could be removed from the framework through a slow imine exchange. SXRD analysis is unique, since it offers information about the degree of interpenetration, arrangement of guest molecules, linker disorder and uncommon topology features, which would be otherwise hard to reveal.

Linkage formation

3D COFs use so far a much smaller variety of linkages as two dimensional covalent organic frameworks. Most of the studied 3D frameworks are based on boronate esters or imines. Besides those two main groups, there are just a few more studied examples, such as borosilicate cages,[231] *trans*-azodioxide,[229] amides,[232] spiroborates[217]or silicates.[218] But none of them has been presented in the literature more than once. Even a COF with carbon-carbon linkages was synthesized recently.[176] But it shows a rather low crystallinity compared to most other COFs, likely attributed to the lack of reversibility in the

carbon-carbon bond formation. Similar to the used linkage variety is the selection for used tetrahedral and planar building blocks rather limited.[233]

The limitation for building units and linkage chemistry shows the need for further investigation and development, especially towards new synthetic methods. Another limiting hindrance for the new applications is the fact that COFs are commonly made via solvothermal synthesis, which results in powdery COFs with uncontrolled grain size. Powders are sufficient for several applications like gas storage, but they are limiting for applications, which require mechanical strength and connectivity, such as membranes and electronics.

1.5.3. COF films

Crystallinity is important to get an understanding of the material structure on an atomic level. This is fundamental in order to draw conclusions about structure-property relations of a framework and to target-design a material with specific characteristics. While crystallinity leads to information about the long-range order on atomic scale, it doesn't result necessarily in conclusions about the morphology. But there are cases where the material morphology has a big influence on the performance. Therefore, various attempts to grow thin films have been explored during the last years. They can be divided into top down and bottom up approaches.

Top down approaches

Top down approaches target usually already synthesized 2D frameworks and try to break the interlayer forces (mainly π-π interactions) in order to separate the sheets from each other and gain thin films. The required energy can be applied through sonication[234-235] or mechanically through grinding.[236] The thickness of the exfoliated films is different. Grinding leaded to stacks of 10-30 layers,[236] whereas sonication resulted in thicknesses between three and five[235] or 10-25 layers[234] for the presented examples. Another top down strategy is chemical exfoliation. In that case the intention is to separate the layers from each other by introducing bulky substituents, which then overcome the interlayer interactions through their steric repulsion. Khayum et al. could show that this can lead to single layered sheets in solution.[237] Researchers from the same group could also show in the same year the development of a self-exfoliating 2D cationic COF, which had halogen counter ions located in between the sheets.[238] Grinding and sonication have the advantage that they are applicable to a wide range of different 2D COFs, but the thickness of the resulted films is difficult to control. The thickness after chemical exfoliation and self-exfoliation are easier to tune, but those methods have structural

requirements towards the COF and are not universally applicable. Another drawback is also that chemical exfoliation changes the COF structure permanently.

Bottom up approaches

Contrary, bottom up approaches allow theoretically a better control over the size and the thickness of the film. Another advantage is, that it is possible to grow materials in different morphologies than thin films. Additionally it is an option to grow films in interfacial contact on specific surfaces, such as conductive substrates for electrodes. Colson et al. reported in 2011 a method to grow 2D boronate ester-linked COF thin films on single-layer graphene, by immersing the substrate into the solution during the solvothermal synthesis.[239] With the help of scanning electron microscopy (SEM) measurements of the film's cross-section a thickness of around 200 nm could be confirmed. Another method, called vapor-assisted conversion, was shown in 2015.[240] Medina et al. dissolved the building blocks for their boronate ester COF synthesis in polar solvents. Then they dropcasted this solution on a glass plate as a substrate and placed the substrate together with a vessel containing mesitylene and dioxane in a desiccator. After three days at room temperature they could confirm the film formation of a porous, crystalline COF film. The big advantage of this approach is the ability to produce films of any shape, since it is tunable via the morphology of the substrate. Additionally the film thickness could be controlled via the initial concentration of the drop casted solution.

A third option is the use of liquid-liquid interfaces to control the polymerization and form thin 2D films.[241] The idea is to separate the required compounds for the framework formation from each other and just let them react with each other in a defined area, e.g. a liquid-liquid interface. Imine COFs are preferred for this strategy, since they require a catalyst, which can be separated due its polarity. The building units are soluble in the organic phase, whereas the catalyst is soluble in the aqueous phase. Thus, it is possible to separate the catalyst and the building blocks through dissolving them in different solvents, which form the required liquid-liquid interface. The commonly used imine-COF catalyst (acetic acid) is not suitable for this approach, because it is soluble in both phases. Additionally the acetic acid catalyzed reaction requires elevated temperature, which would disturb the formation of a smooth interlayer. The substitution of acetic acid by metal triflates offers a solution for both problems. The salts are insoluble in most organic solvents and they catalyze the transformation already at room temperature. Dey et al. showed that this strategy works as well, when the chosen monomers have a different polarity and can be dissolved in different phases.[242] The film thickness can be controlled in both approaches via the used monomer concentration and the reaction time. The strategy to grow films on an interlayers is limited by the requirement that the compounds have different solubility. The

proof of concept of limiting the reaction to take place at an intersection could also be shown by using a solid-vapor interface which leads to single layered 2D COFs.[243]

Even though there exist even more methods to build up COF films, such as electrophoretic deposition[244] and knife-casting,[245] all so far presented approaches have a major drawback. They suffer from the missing possibility to monitor the film growth in real time. This shows, that the precise control over the film thickness is one of the biggest challenges while synthesizing COF films. This limitation could be overcome by forming the film in continuous flow on a quartz crystal microbalance (QCM) sensor.[246] Bisbey et al. grew different 2D boronate ester COFs on titanium coated QCM sensors. Via the increase in motional resistance of the quartz crystal they could calculate the deposited mass on the sensor. They confirmed the crystallinity via x-ray diffraction measurements and concluded as well that films grown under continuous flow conditions are smoother, than those obtained from bulk. Additionally they pointed out that this general strategy allows to grow films in a nearly constant rate over time, which allows precise thickness control for the first time.

3D COF films

Apart from electrophoretic deposition lead all previously described strategies to 2D COF films. During the last years only a few 3D COF films have been made. The few described 3D COF films or membranes are e.g. synthesized via continuous flow[176] electrophoretic deposition[244] and interfacial synthesis.[247-249] The continuous flow synthesis from Yang et al. can be seen as a further development of the approach from Bisbey et al. making 2D COF films.[246] Using electrophoretic deposition has the advantage, that films can be grown on conductive templates of various shapes. Rotter et al showed that the intrinsic electric surface charge of COF particles immerged in a non-conductive solvent can be used to grow 2D and 3D COF films on the electrode of the opposite charge, when an electric field is applied.[244] The thickness of the gained films of imine and boronate ester COFs could be tuned via deposition times, particle concentrations and electrode potentials. The fabricated 3D film was the first example for a 3D COF film on a conducting substrate.

After gaining control over the targeted synthesis of continuous porous films during the last years, the next logical step would be to explore the possibility to grow different films on each other. This would allow a different local composition of functional sites within the same framework and therefore broaden the application range for framework materials even further. The next section will give an overview over the different layered framework structures, which have been explored so far.

1.6. Layered framework materials

Besides the described methods to grow COF films in the previous sections, there exist also methods to produce films of other porous materials, such as MOFs[250-251] and ZIFs.[252] But so far the library of porous film synthesis approaches was mainly used to grow homogenous films. In order to develop porous films further, it would be useful to explore general methods, which lead to layered multifunctional films. It could broaden the application range of porous films tremendously, if strategies can be found to introduce specific functional sites just in certain areas of a framework. That could lead for example to catalytic membranes, which have a size selective outer layer that sieves the entering molecules before the catalytic reaction. Another option would be to catalyze a cascade reaction in flow, where the entering molecule gets first converted into an intermediate product, which then gets further converted in the next layer of the framework. The development of those kind of sandwich-structures is for MOFs already more sophisticated.[253-256] Layered MOFs can be used among others as cascade-selective catalysts for cyclopentene oxidation.[254] Furthermore there are studies of MOF-COF composites, which have been used for example for gas separation, water capture and energy storage.[257-259] However, COF-COF bilayered materials have been very rarely described in the literature so far. Fan et al. synthesized a 2D-2D COF bilayer, consisting of two different imine COFs stacked on each other. They observed also an increased separation selectivity H_2/CO_2, H_2/N_2, and H_2/CH_4 for the bilayered material compared to the individual frameworks on their own. Stacked 2D bilayered COFs have, similar to normal 2D COFs, the disadvantage that the different layers are just connected via non-covalent bonds, mainly π-π-interactions. Thus, there is only limited control over the way how both layers are oriented towards each other (eclipsed, inclined or staggered). More certainty in this regard would layered 3D COFs provide. But so far this stacking challenge remains unsolved for 3D COFs and thus, preventing reticular chemistry to continue its fascinating evolution towards future materials.

2. Thesis aim and scientific objectives

The overall aim of this work was to develop a method of growing 3D COF films on surfaces. The intention was to transfer the known advantages of powdery COFs into films, and with that expand their application range to those, which require mechanical strength, such as electro catalysis, membranes and organic electronics.

The specific objectives of this thesis were:

- The development of a continuous flow bottom up strategy, incorporating a QCM for real time monitoring of the film formation, to assemble smooth and continuous porous 3D films;
- Establishing a correlation between the QCM signal and the film thickness;
- Exploring the possibility of promoting the surface reaction over the bulk reaction and therefore increase the smoothness of the obtained films;
- The design, synthesis and evaluation of two different frameworks, which have the same unit cell dimensions and can be covalently stacked on each other in a layered film;
- Investigation if by using a hetero-coupling, a single layer by single layer growth can be monitored with the QCM and consequently, if this approach leads to a promotion of the thermodynamic product and therefore to an increased crystallinity.

3. Analytical methods

The following chapter will give an overview of the techniques which were used to obtain the data presented in this thesis. Additionally, deviations from commonly followed procedures are mentioned, particularly where common methodologies were not successful. The techniques covered are the use of a quartz crystal microbalance (QCM), atomic force microscopy (AFM), depth X-ray photoelectron spectroscopy (depth XPS), energy-dispersive x-ray spectroscopy (EDX) in combination with scanning electron microscope (SEM), grazing incidence wide angle x-ray scattering (GIWAXS), time of flight secondary ion mass spectroscopy (ToF-SIMS) as well as Raman and Infrared (IR) spectroscopy.

3.1. QCM(-D)

The quartz crystal microbalance (QCM) was initially invented by Günter Hans Sauerbrey during his PhD studies at the TU Berlin in the 1950s. He showed that there is a proportional correlation between the observed change of the resonance frequency of a quartz crystal and the mass deposited on it as illustrated in **Figure 7**.

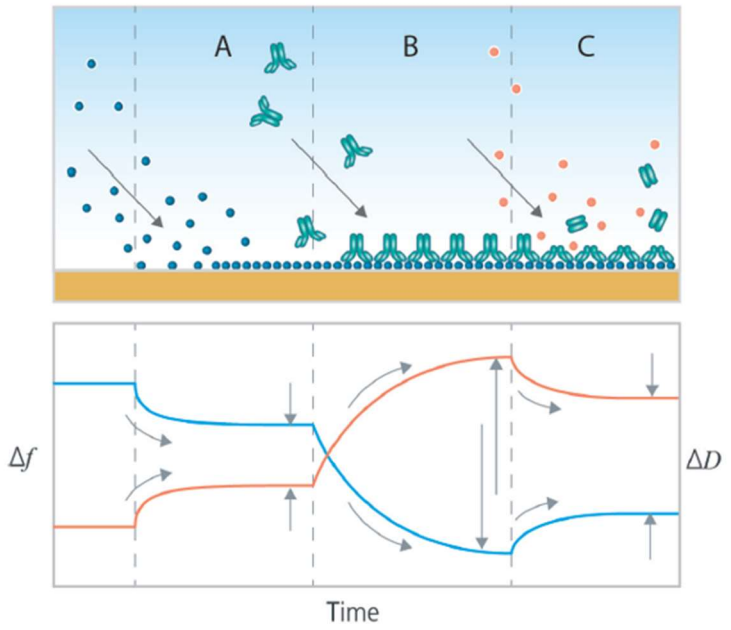

Figure 7. *Schematic surface reaction and the expected resulting frequency (blue) and dissipation (orange) change of the resonance frequency of the quartz crystal. (Image is owned and provided by Biolin Scientific)*

This phenomena allowed him to weigh thin layers with an accuracy down to 10^{-10} g.[260] The QCM was used initially only in gas phase and in vacuum, but later in liquid media as well.[261] The main working principle of the QCM technique is based on the use of the piezoelectric quartz crystal in the sensor. A

material is piezoelectric if it accumulates electric charge under mechanical stress.[262] Known examples include certain ceramics, crystals or biomolecules, such as bone[263] and DNA.[264] The creation of electric charge is usually depending on the mechanical stress in certain orientations. This means that the piezoelectric material undergoes a predictable movement under the influence of an electrical field. This phenomena is called the inverse piezoelectric effect and is used for the QCM measurements. The good thermodynamic stability together with a high natural abundance and easy processability makes quartz a very suitable piezoelectric material for QCM sensors. Sensors are cut from the bulk quartz crystal in a specific orientation (e.g. 35° 10' for AT-cut) regarding their crystallographic axis, in order to gain a product in which both surfaces always oscillate with a phase difference of 180°. After cutting, a pair of electrodes (commonly gold) are evaporated on both sides of the sensor. By applying a driving voltage the crystal will oscillate at its resonance frequency, which depends on the thickness of the quartz chip. Commonly used are 330 µm thick sensors, which have a resonance frequency of 5 MHz. The resonance frequency is temperature dependent and differs by a couple of Hz/°C, depending on the surrounding media (liquid or gas) and the cut orientation of the sensor. This means that a stable temperature during the experiment is essential for high quality data collection. We note that, depending on the planned use, sensors can be purchased with a huge variety of coatings on their front side.[265] For the experiments in this thesis only bare gold coated QCM chips were used, but for other applications silicon dioxide, stainless steel, aluminum oxide and many more are available.

Besides the measurement, Sauerbrey also developed the so-called Sauerbrey equation[260] (**Equation 1**), which is used to describe the dependence of the resonance frequency shift on the deposited mass for a quartz crystal:

$$\Delta f = \frac{2f_0^2}{A_a\sqrt{\rho_q \mu_q}}\Delta m \qquad (1)$$

Where, Δf is the normalized frequency change, f_0 the resonance frequency of the fundamental, A_a is the active area in cm^2, ρ_q is the quartz density (2.65 g/cm^3), μ_q represents the shear modulus of quartz ($2.95 \cdot 10^{11}$ $g \cdot cm^{-1} \cdot s^{-2}$) and Δm the mass change. To use the Sauerbrey equation and to calculate the mass (or via the density and the surface area the thickness) of a film, the attached film needs to fulfill the following criteria. The measured film has to be firmly connected to the surface of the quartz crystal, rigid and be relatively thin, otherwise the calculated mass will be underestimated. Sauerbrey also showed that the vibration of the crystal is limited to the area in between the electrodes, which is called active area of the crystal. This leads to another limitation of the Sauerbrey equation, the deposited film has to be evenly distributed over the surface in order to gain information over thickness and mass of the film. If the information about the density of the investigated material and the surface area are available, it is relatively easy to calculate the average thickness of the film via the volume as

well. Those mentioned requirements are usually given for films which are deposited in vacuum or gas phase. However, if films are observed in a liquid media, the system often becomes more complicated since soft or viscoelastic films are formed. Viscoelastic materials are materials, which show to some extend characteristics from a liquid and a solid.[266] Viscoelastic films are films where solvent molecules are adsorbed on the surface of the quartz crystal and/or can be entrapped in the framework, which prevents the film from completely coupling with the crystal. This results into an energy loss of the oscillation which is called damping. In that case the Sauerbrey equation cannot be used and in order to calculate or model the film thickness more information is needed. One useful tool can be the measurement of the dissipation (D), which is the energy loss due to damping. If both, ΔD and Δf are measured simultaneously the method is called quartz crystal microbalance with dissipation (QCM-D). QCM-D is a powerful technique, which gives access to real time information of the absorbed viscoelastic film, such as viscosity, elasticity and density. The technique was discovered at Chalmers in Gothenburg, Sweden[267] and led later on to the foundation of Q-Sense, a developer of QCM-D instruments. The dissipation *D* in a QCM is defined as the inverse quality factor *Q* of the sensor, using **Equation 2**.

$$D = \frac{1}{Q} = \frac{E_{dissipation}}{2\pi \cdot E_{stored}} \tag{2}$$

Where, $E_{dissipation}$ is the energy lost within one oscillation cycle and E_{stored} is the energy contained in the oscillating system. There are different QCM approaches available, such as QCM-A, QCM-R, QCM-I and QCM-Z, but in this thesis the focus will be exclusively on the QCM-D approach. In this approach an adequate driving voltage is applied to the sensor in order to excite it to its resonance frequency for a short time. Afterwards the electric field is switched off and the voltage produced by the (damped) oscillating sensor is measured. The decay of the voltage over time (t) can be described by **Equation 3**.

$$A(t) = A_0 \cdot e^{\frac{t}{T}} \cdot \sin(2\pi f t + \varphi) \tag{3}$$

Where, *A* represents the amplitude of the oscillation, A_0 the oscillation amplitude in the beginning, *T* the decay time constant, *f* the frequency and φ the phase angle. The higher the loading on the sensor and/or the interaction within a viscoelastic film or the solvent molecules the higher the exponential damping/ dissipation. If the decay curve is fitted to **Equation 3**, it is possible to obtain the frequency and the dissipation simultaneously. Afterwards, the values for the normalized frequency shift and the dissipation are shown in the software and the quartz crystal gets excited again. The whole cycle happens within milliseconds, which allows data collection in real time during the reaction on the surface. During the QCM-D experiments discussed in this thesis, seven different overtones of the resonance frequency shift were recorded. The first one f1, is the fundamental, with the lowest

resonance frequency (5 MHz). The other ones are integral multiples of the fundamental. Those integral multiples have to be odd, since for even overtones the amplitude A_0 in **Equation 3** equals zero and the function can't be fitted. The next usable overtone is then f3 with a resonance frequency around 15 MHz and so on for f5-f13. Those overtones can provide data for the calculation of unknown material properties, such as adsorbed mass, film thickness, film density, shear modulus, viscosity and kinetics of the viscoelastic film.[268] However, the obtained QCM-D data for this thesis were mainly used to monitor the progress of the surface reaction and to correlate them to the film thickness. Therefore the focus lay on the observation of one overtone (f3) in order to keep the data comparable between each other. In all QCM-D plots in this thesis is for that reason just the 3rd overtone (f3) showed, even though the others were initially recorded as well. The same applies to the measured dissipation, it was recorded but not used for the data analysis and is not shown in figures in this thesis to increase the intelligibility. In general different overtones can give an insight in different layers of the film since with an increasing overtone the penetration depth decreases (δ) using **Equation 4**.[269]

$$\delta = \sqrt{\frac{\eta_m}{\pi \cdot n \cdot f_0 \cdot \rho_m}} \tag{4}$$

Where η_m is viscosity of deposited material, n the used overtone, ρ_m is the density of the film. It was observed as well that higher overtones tend to fail throughout the buildup of thicker films. This can be explained as damping of the growing viscoelastic film above the measured layer reduces the signal to zero. With regard to **Equation 4**, it seems logical that for thicker films the signal for higher overtones is lost first. The measured frequency shift in the experiments presented in this thesis was usually used as an indicator for the kinetics of growth of the film. That means that there is no particular difference if for example the 3rd or the 5th overtone in all experiments would have been used for the analysis. To decide if a film can be considered as "quartz like", a condition to use the Sauerbrey equation, can usually be taken just by looking at the recorded data for the frequency shift and the dissipation of different overtones during one experiment. If the film is sufficiently rigid, all overtones overlap for both frequency shift and dissipation. Additionally the dissipation throughout the experiment stays at 0 ppm. If this behavior is observed, the film thickness and the deposited mass can be calculated with **Equation 1**. On the other hand, if there is a spread between the different overtones and the dissipation increases, viscoelastic models have to be used in order to obtain the film thickness and other properties. During the QCM-D experiments for this thesis, the dissipation was unequal to zero and the overtones clearly didn't overlap. That means that the produced films are in the viscoelastic regime and the Sauerbrey equation couldn't be used. Therefore, another way had to be found to correlate the resonance frequency shift to the film thickness. Instead of using a model, the film thickness was determined via SEM measurements on the cross sections of the QCM sensors or via the depth

measurements of scratches, using a profilometer. The maximum detectable film thickness via QCM depends on the rigidity of the attached film and varies in between several hundred nanometers up to a few micrometers.

To conclude, a broad background to the QCM-D technique and its use in COF film preparation have been given. The high mass sensitivity, the real time measurements and the versatility of QCM-D explain why this technique can be used to solve a wide array of scientific questions. Examples are molecule-surface interactions, kinetics of molecular interactions, such as protein-protein interactions, build up and study of polymer films (e.g. MOFs and COFs), like in this thesis or the study of coating behavior under the influence of different surfactants.[270-272]

3.2. AFM

Despite its name atomic force microscopy (AFM) is not a microscopy technique in the common sense, since its function is not based on light interacting with a sample surface. The first AFM was built by Binning in 1985 and used for the first measurements from Binning, Quate and Gerber in 1986.[273] AFM is a type of scanning probe microscopy and its function is based on mapping a surface with a small tip, as illustrated in **Figure 8**.

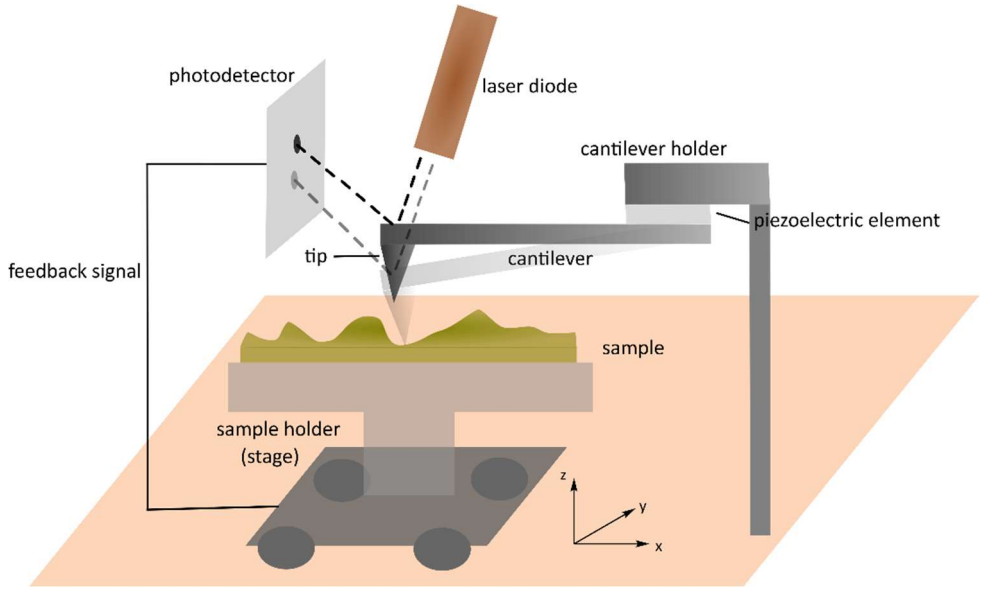

Figure 8. *Illustration of an AFM set up. Shown here is the used set up which has a moveable stage and a fixed cantilever. There are other systems, where both are mobile or the cantilever is adjustable and the stage in a fixed position.*

The tip is attached to a cantilever (see **Figure 8**) and the sample is slowly moved on the sample holder underneath the tip in a fashion that the tip can raster scan the surface line by line. Motions of the cantilever are visible through the changes of the reflected laser beam, generated in a laser diode and

are detected by a photodetector. The movement of the cantilever while moving over the surface leads to the information of the z coordinate while x and y are given through the movement of the stage. With those three coordinates the software generates a topological map of the surface. AFM offers an insight to the basic morphology of the surface, such as shape, size and distribution of particles, surface roughness and uniformity. The spatial resolution of AFMs is below one nanometer, allowing it to even investigate nanoparticles[274] and offering an atomic resolution.[275] Besides the already described topographic imaging of surfaces, AFM can be also used for force measurements[276] and surface manipulation, such as lithography.[277]

If the tip approaches the surface, it is first in the attractive sample-tip regime, where the attractive forces (e.g. Van der Waals interactions) become stronger, pulling the tip closer to the surface. With further increasing proximity, the repulsive interaction (Pauli repulsion between the electron clouds) increases, pushing the tip away from the surface. At the point when the atoms from the tip "touch" the atoms from the surface the repulsive forces become stronger than the attractive forces and the net force becomes positive, repulsive. The combination of both forces is described in the Lennard-Jones-Potential as shown in **Figure 9**.

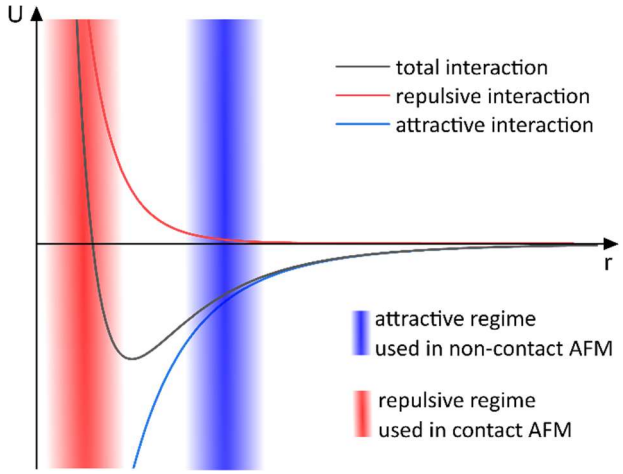

Figure 9. *Repulsive and attractive sample-tip regimes and the resulting Lennard-Jones potential (black).*

AFM measurements can be done in different modes. The most common ones are contact, tapping and non-contact mode. The names of the modes relate to the tip movement. In contact mode the tip "scratches" over the surface and is constantly in the repulsive regime (blue area in **Figure 9**), which means it is in contact with the sample the whole time. The cantilevers for this mode have in general a low spring constant to avoid damage to the sample. Changes of the cantilever position or bending depending on the sample-tip distance can be detected on the photodetector. Usually for all modes a feedback signal is generated, which is needed to keep the tip constantly in the same proximity to the surface (see **Figure 8**). One disadvantage of this mode is that it can result in damages to the sample

and cantilever tip. When the wear increases, the tip diameter becomes bigger, and the resolution and preciseness of the measurement decreases. The contact mode is also called static mode, whereas the tapping and the non-contact mode are dynamic modes. This terminology relates to the oscillating movement of the cantilever in the tapping and non-contact mode. In non-contact mode the cantilever oscillates in its resonance frequency only in the attractive sample-tip regime (yellow area in **Figure 9**), so it never comes in contact with the surface. The oscillation of the cantilever origins from a piezoelectric element (see **Figure 8**). When the tip moves closer to the surface the attractive forces will decrease the resonance frequency of the cantilever. If the applied frequency from the piezoelectric element stays the same, the amplitude of the oscillation on the photodetector changes. Then the height of the stage will be automatically adjusted in order to reestablish to the original amplitude. If the measuring conditions are sufficient, there won't be any wear effects on sample nor tip. Tapping mode is the most common mode and works similar, but the tip oscillates also in the repulsive sample-tip regime and touches the surface. The risk for damages on tip and surface are smaller compared to the contact mode, so this method is better for softer samples.

3.3. (depth)XPS

X-ray photoelectron spectroscopy (XPS) is an analysis method for surface investigations. It gives information on the atomic composition of a sample surface. All elements besides hydrogen and helium can be detected with XPS because hydrogen and helium have too low a probability to emit a photoelectron. This technique is very versatile, as almost every material, e.g. soils, plastics, semiconductor and textiles can be investigated.[278] The method is based on the photoelectric effect, which was first observed by Heinrich Hertz in 1887,[279] but for the first time more excessively described by Albert Einstein in 1905.[280] Einstein was later also rewarded with the Nobel Prize in 1921 for his discoveries around the photoelectric effect. The development of x-ray photoelectron spectroscopy goes back to the Kai Siegbahn in Uppsala, Sweden in the 50s and 60s of the last century.[281] Siegbahn received for his work the Nobel Prize in Physics in 1981.

When a sample surface gets hit by a soft x-ray beam (usually up to 6 keV), the sample atoms will start to emit photoelectrons, Auger-electrons and x-ray photons as illustrated in **Figure 10**.

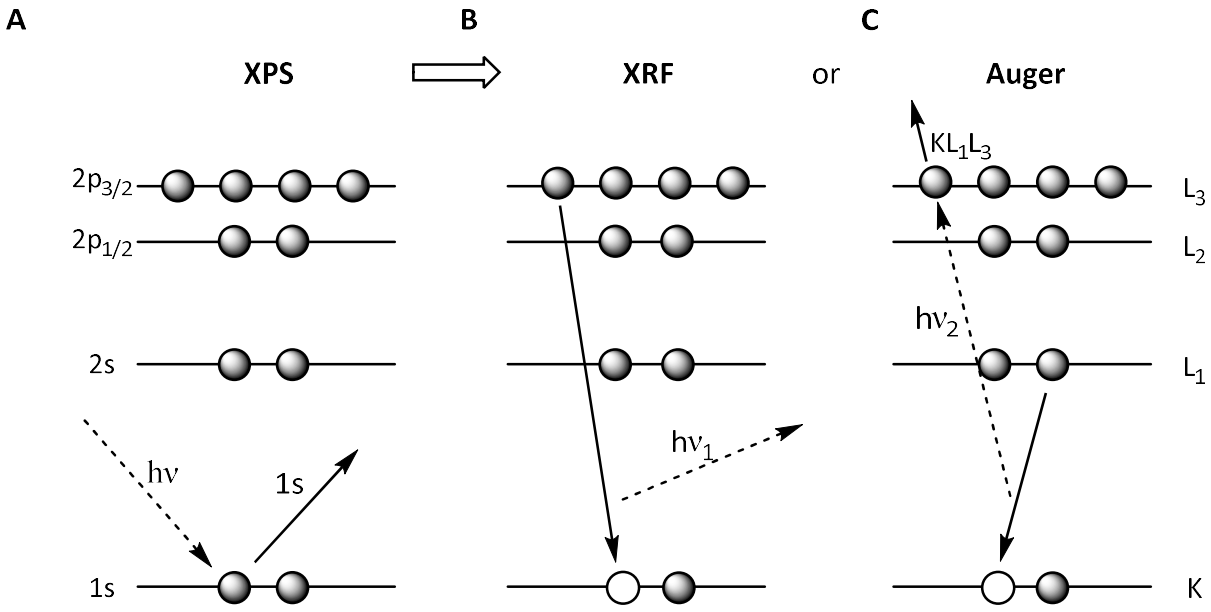

Figure 10. *Possible light-matter interactions on the sample surface during XPS measurements resulting in A the emission of a photoelectron, followed by B the emission of an x-ray photon (XRF: x-ray fluorescence) or C the release of an Auger electron. Dashed arrows represent electromagnetic radiation and normal arrows show electron movements. The orbital annotation is shown on the left side, the electron shells are defined on the right side.*

An important condition for a shell electron to leave its atom, is that it gets excited by an x-ray, which is equal or greater than the electron's binding energy. The exceeding energy is converted into kinetic energy of the leaving photoelectron. The photoelectrons are then detected and analyzed according to their energy and their quantity, which results in a XPS spectra. After removal of an inner shell electron two competing pathways are possible. One electron from the valence shell can fill the hole (see **Figure 10B**) with emission of a photon with the energy equal to the binding energy difference of the two shells. The other option is that an electron from a closer shell will refill the hole. In that case the redundant energy is not released in the form of photon, rather in form of a released electron from the valence band (the so-called Auger electron; see **Figure 10C**). The discrete energies of Auger electrons detected are used to add additional information about the atom characteristics such as spin and binding environment to the spectrum. Furthermore, the integration of the individual peaks of detected photo electrons allows conclusions about the element ratio in the sample. Thus, the photoelectrons carry both qualitative and quantitative information about the sample composition, making XPS to a very versatile analysis method.

As the generation depth of photoelectrons is increased, the probability of inelastic collisions with other electrons in the sample increases. This reduces their kinetic energy and means they cannot be measured above background noise. The surface sensitivity is an advantage and disadvantage at the same time, since it results in detailed surface information of the sample, but prevents any insight into deeper layers of the material. But there are variations of the XPS technique available that overcome

this limitation. In order to perform an XPS measurement with depth profiling, the system used must be equipped with a sputter gun. After the initial surface measurement the sputter gun shoots particles, commonly Ar^+, at the surface and removes with those ions sample atoms and larger fragments from the surface and etches into the material. After a defined amount of time the gun switches off and the XPS spectrum of the new surface can be measured. Then the cycle is repeated and the gained data reveal the elemental composition from deeper layers. The use of Ar^+ in the sputter gun has some drawbacks. It can for example change the oxidation state of some metals, leading to misinterpretations. Additionally the removal of sample material is uncontrolled and some atoms are easier to remove than others. That can lead to difference of the measured element ratio compared to the actual one. For that reason in newer setups C_{60} fullerenes or argon clusters are used. They are gentler, because for example they don't change the oxidation state of the metal atoms.

3.4. (EDX-) SEM

Common optical microscopes have a resolution limit, they can't show objects which are smaller than half of the used wavelength. Since they work with visible light (around 400-800 nm), objects smaller than 200 nm can't be seen. If one wants to observe objects smaller than that, it is necessary to go away from visual light and towards radiation with a smaller wavelength. Electron beams in electron microscopes have a wavelength below 0.1 nm, which makes them useful to study nano sized objects. A scanning electron microscope (SEM) maps the surface in a similar fashion to AFM, line by line. But instead of a mechanical tip, the surface is scanned with a focused electron beam, which has an acceleration voltage between 0.5 and 40 keV. The spatial resolution of a SEM is depending on size of the electron beam spot and on the interaction volume. The interaction volume is defined as the teardrop-shaped volume of the sample material, which interacts with the electron beam as shown in **Figure 11**. When the electron beam hits a sample surface, different interactions between the electrons and the sample atoms are possible. Every one of those different interactions reveals different information about the sample. Commonly detected are for example Auger electrons, secondary electrons, backscattered electrons and characteristic X-rays. They originate from the electron-matter interaction in different depths of the penetration volume of the specimen material.

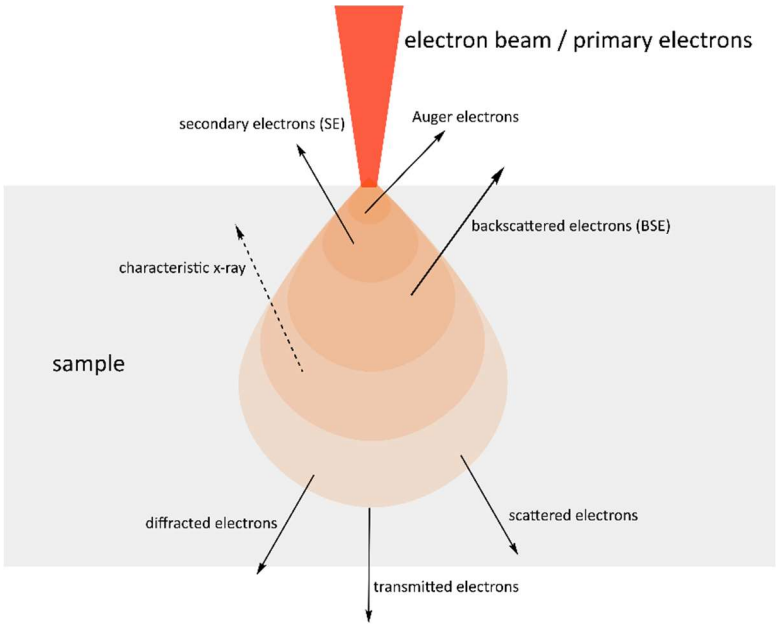

Figure 11. *Observed electron-matter interactions in the interactive volume (selection).*

A secondary electron (SE) is an electron, which was originally part of the outer shell of a sample atom and gets removed through inelastic scattering of the primary electrons from the electron beam. They have a much lower energy than primary electrons, usually in the order of 50 eV, which makes it impossible for them to travel far through solids. That means that all the detected SEs originate from the first surface layers of the sample, where the electron beams hits. They are carrying structure information about the surface and their detection leads to a high resolution image of the surface morphology. Back scattered electrons (BSEs) are electrons from the electron beam which are reflected from sample atoms through inelastic scattering. They have a much higher energy compared to the SEs, hence they can also originate from deeper parts of the sample. Their intensity increases with heavier elements in the sample, because the primary electrons have a higher chance to hit a nucleus and get reflected. Because of that, BSEs can give information about the distribution of lighter and heavier elements in the sample, but not about their elemental identity. Characteristic x-rays can be used to analyze a sample qualitatively and depending on the sample also quantitative. The characteristic x-ray radiation is created in a similar way as shown for XPS in **Figure 10B**. The main difference is that for XPS x-ray radiation is used to eject an inner shell electron, while it is the electron beam for AFM. The measuring technique for the x-ray detection and its evaluation is called energy-dispersive x-ray spectroscopy (EDX or EDS). Important to know is that the spatial resolution for the BSE and the characteristic x-rays is lower than for the SE, since they can pass longer distances through the sample. The release mechanism of Auger electrons is the same as in SEM measurements, shown in **Figure 10C**. The emission of them is more likely for lighter elements. Auger electrons have similar to the SEs a very small detectable range and thereby only Auger electrons from the surface layers can

be detected. They contain topographical and also qualitative information, because their energy is also discrete. Since the small electron beam scans constantly over the surface, the local elemental composition can be revealed. If this is done for many points in an area, the technique is called elemental mapping.

A particular limitation in the measurement of PAF and COF samples presented in this thesis was that the charge carried by the electron beam, especially using higher acceleration voltages couldn't conduct fast enough through the sample. This led to charging effects and decreased the quality of the images, because the background noise increased in a way that it was not possible anymore to see the structural details of the surface. To weaken this effect a lower acceleration voltage was used and copper tape was applied close to the measured area of the surface. The copper tape is highly conductive and could transport the accumulating charge to the metallic sample holder.

3.5. GIWAXS

Grazing-incidence wide-angle x-ray scattering (GIWAXS) is a surface analysis method, which uses the interference pattern of a diffracted x-ray beam created on a sample surface or in the sample in order to gain structural information of a crystalline specimen. Diffraction describes the phenomena when a wave hits an opening or, like in the case of GIWAXS, a diffracting object, like a sample. Due to interaction of the incident wave with the particles in the specimen, the particles themselves become a source of a spherical electromagnetic waves. Those spherical waves interfere with each other in the form of interference. The sum of all spherical waves and their interference results in the diffracted beam with characteristic patterns. Those patterns contain information about the structure of the sample, such as particle size and shape.[282] The working principle for x-ray diffraction experiments is based on Bragg's law and the interaction between the inner shell (high energetic) electrons from the sample and the incoming x-ray photons. When an x-ray photon hits one of those electrons, it transfers its energy to the electron (elastic scattering), which starts to oscillate and emit radiation according to that oscillation. If a sample doesn't have any crystalline structure the incoming x-ray beam gets scattered on the sample electrons, causing a diffuse diffraction spectrum without any peaks. But if the atoms and electrons are aligned in a crystalline lattice at certain incidence angles θ_i (angle between the ray and the surface plane) the scattered beam will show constructive interferences. In order to result in constructive interference, the incidence angle have to fulfill the Bragg condition, given by **Equation 5**.

$$n_D \cdot \lambda = 2d \sin \theta_i \tag{5}$$

Where n_D is the diffraction order, λ the wavelength of the x-ray beam used and d the distance in between the lattice planes. Another important parameter for x-ray diffraction experiments is the critical angle of the interface between two different media. The critical angle is defined as the angle below which a surface becomes reflective. Consequently, if a light beam hits a surface with an incidence angle below the critical angle of that interface, it will get completely internally reflected. That means that it gets completely reflected back into the first medium, instead of getting refracted into the second medium. By changing the incidence angle above or below the critical angle, it is possible to gain structural information from inside the sample or from its surface respectively.

There is a number of similar x-ray scattering techniques which have different names, correlating to the used incidence angle θ_i and the angle of the observed scattered beam. Small-angle x-ray scattering (SAXS) and wide-angle x-ray scattering (WAXS) use an incidence angle far above the critical angle of the sample and the substrate. Thus, the beam will penetrate through the entire material and the analysis of the elastic scattering leads to structural information averaged through the entire thickness. For grazing-incidence small-angle x-ray scattering (GISAXS) and GIWAXS the incidence angle is much smaller, usually lower than the critical angle of the sample-air-interface to avoid a penetration of the beam into the material. When the beam gets totally internal reflected, the gained structural information origin just from the sample surface and the first few layers as illustrated in **Figure 12**.

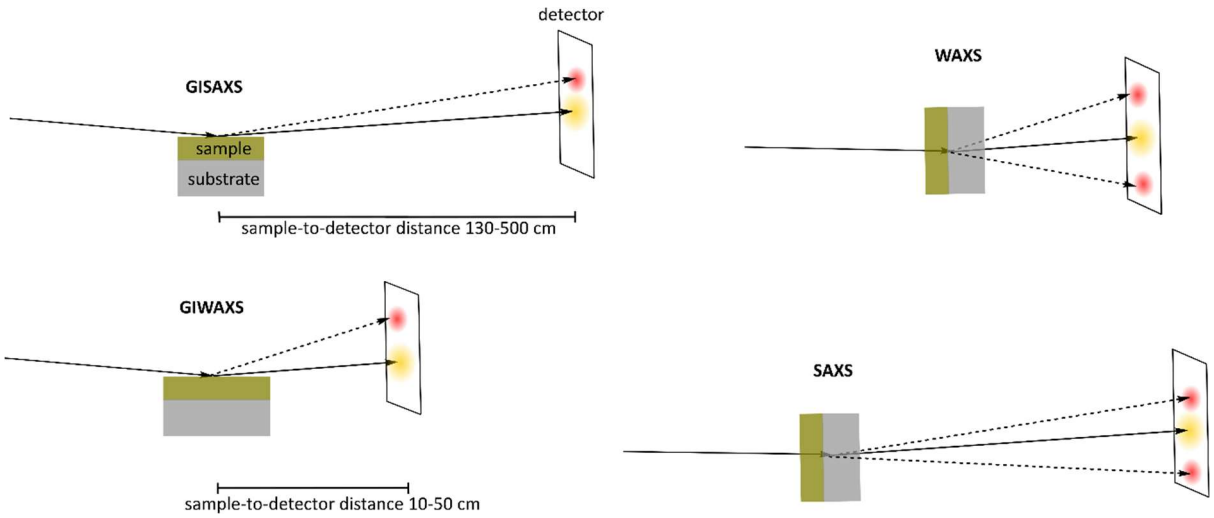

Figure 12. *Overview of the measuring set up for GIWAXS, WAXS, GIWAXS and SAXS experiments. The dashed arrows show the light path of the scattered beam resulting in red spots on the detector, whereas the normal arrows show the reflected beam for GIWAXS and GISAXS (with a yellow dot on the detector, which is usually hidden by a beam stop). For SAXS and WAXS the normal arrow represents the transmitted beam (with a yellow dot on the detector, which is usually hidden by the beam stop). The fact that the WAXS and SAXS show two red spots on the detector is supposed to visualize the conical shape of the scattered light, where as in GIWAXS and GISAXS the scattered beam is just half conical.*

If the incidence angle is increased above the critical angle, the x-ray beam will start to penetrate into the sample. Consequently, the resulting diffracted beam will contain average information from deeper layers of the sample. Another method is also to use an incidence angle in between the critical angle

for the sample-air and the sample-substrate-interlayer. In that case, average information from the whole sample depth are obtained with an enhanced signal, since the beam has a longer pathway through the sample. Small angle and wide angle in the terminology for GIWAXS, GISAXS, WAXS and SAXS defers to observation and analysis of small angle scattering (the scattering angle θ_S is around 0.1 – 1 °) or wide angle scattering (θ_S around 5 – 60 °). The sample-to-detector distance for small angle observations has to be longer than for wide angle detection (see **Figure 12**). That means that observation of different scattering angles is depending on the sample-to-detector distance. Another method to gain information about interfaces, thickness, surface roughness and electron densities in layered films is x-ray reflectometry.[283] In this case the inference patterns of the reflected, rather than the diffracted beam, are analyzed.

In the GIWAXS/GISAXS set up the sample is mounted on a sample-tilt stage to change the incidence angle of the x-ray beam on the surface. The constructive interferences produce scattering features (e.g. dots, rings or rods depending on the lattice structure and the nanoscale order), which are recorded with a detector. The much more intense reflected beam is usually blocked with a beam stop, in order to not damage the detector. Afterwards the information from the detector are compiled into a spectrum that shows the scattering features. The detected peaks can be analyzed and contain information about the structure of the crystalline sample, such as the orientation of the regular features, their shape or their size. The question if small- or wide-angle scattering is more beneficial for the analysis depends on the size of the crystalline features of interest. There exists a reciprocal correlation in between momentum transfer *q* and feature size. Smaller regular features show at higher q-values, bigger structures at smaller q-values, expressed by **Equation 6**.

$$d = \frac{2\pi}{q} \tag{6}$$

That means conversely that the momentum transfer of a specific peak correlates to a real space distance of the crystalline features. In a typical GIWAXS spectra the signal intensity is not plotted against the scattering angle θ_S and the azimuth angle ϕ, rather q is used, which can be calculated with **Equation 7**.

$$q = \frac{4\pi}{\lambda} \cdot \sin(\theta_S) \tag{7}$$

This convention makes it possible to compare spectra independently from the used x-ray wavelength. The GIWAXS experiments included in this thesis were conducted, in order to prove the crystallinity of the frameworks. For the grown COFs the expected scattering features look like half circles. The sharper they are, the better is their crystallinity. Their position on the q-axis should reflect the inter lattice distance in the framework. Since the framework is polycrystalline, thus contains many different

crystalline domains with random orientation, the spectrum shows half circles. Perfectly layered thin films, which consist of large domains show either parallel or perpendicular lines in the spectrum, depending on their orientation with respect to the beam. Contrary, single crystals show only their characteristic dot-shaped peaks.

3.6. ToF-SIMS

Time of flight secondary ion mass spectroscopy (ToF-SIMS) is a method for surface analysis, which leads to information about the elements and their distribution in a sample. Similar to XPS, ToF-SIMS is very surface sensitive, but its working principle is not based on light-matter interactions. In contrast, a primary ion gun fires Ga^+, Ar^+, gold cluster or bismuth clusters, with a highly focused ion beam on a small surface area. Even though the method is per definition destructive, the amount of primary ions shot on the surface and the incidence area are comparably small. When those high energetic ions hit the surface, they will ionize and fragment the surface. The emitted ions from the surface are called secondary ions and are accelerated in a “flight tube” towards a detector. All ions enter the tube simultaneously, but they need a different amount of time to travel through it to reach the detector, depending on their charge and their mass. The heavier ions will need more time to reach the detector than the lighter ones. The same applies for ions with different amount of charges. An ion, which has more charges will always be accelerated faster in the electric field then than an ion with the same mass and fewer charges. That means that the ratio between m/z (mass over charge) will decide when an ion hits the detector. With the gained information about the time of flight (ToF) from the detector, it is possible to achieve information about the nature of the ion and with that about the surface composition. When the beam is scanned over the surface and the measurement is repeated in different areas it is possible to build an elemental composition map of the surface.

Similar to depth XPS measurements it is also possible to perform depth profiling with ToF-SIMS. For this a second ion gun is needed, which shoots additional ions (usually C_{60} fullerenes, Cs^+, argon cluster or Cs^+) on the surface. This happens when the first gun is not active and the measurement is paused. The second gun will start etching through the sample and when stopped, the first gun is activated to desorb fragments from the surface. Those contain then information about the elementals contained in the deeper layer. When this cycle is repeated, it is possible to get a depth profile about the elementals contained in the sample. However, the gained abundancy information of different elements cannot be compared with each other, since they might ionize differently well. The type of material that is supposed to get analyzed usually decides about the used ions for the first ion gun. For

low-mass areas (e.g. elements) single metal ions are better, whereas cluster ions work usually better for in high-mass regimes (e.g. molecule fragments). The same considerations apply for the sputter ion gun.

3.7. Infrared & Raman spectroscopy

Atoms and molecules always move in space. Each atom has three degrees of freedom (in x-, y- and z-direction), which means that every molecule containing N atoms has 3N degrees of freedom. There are different types of movements which they can undergo: translation, rotation and vibrations. Translation describes the movement of the entire molecule through space while the position of each atom in the molecule relative to each other doesn't change. Molecules are also able to perform rotational transitions, in which the distance in between all atoms stays the same. But the whole molecule rotates along three perpendicular axes, which pass through the center of mass. Polyatomic molecules, which are not linear have in that regard three degrees of rotational freedom. Linear molecules are an exception since they only have two different rotations which they can undergo.

All other movements are part of the group vibrations and are investigated in infrared (IR) and Raman spectroscopy. That means that every N-atomic molecule has 3N-6 or 3N-5 (for linear molecules) vibrations. During molecular vibrations, the position of atoms relative to each other is changing but the orientation of the entire molecule in space stays the same. There are two groups of vibrations, stretching and bending. The most important examples for bending vibrations of organic molecules are scissoring, rocking, wagging and twisting, illustrated in **Figure 13**.[284]

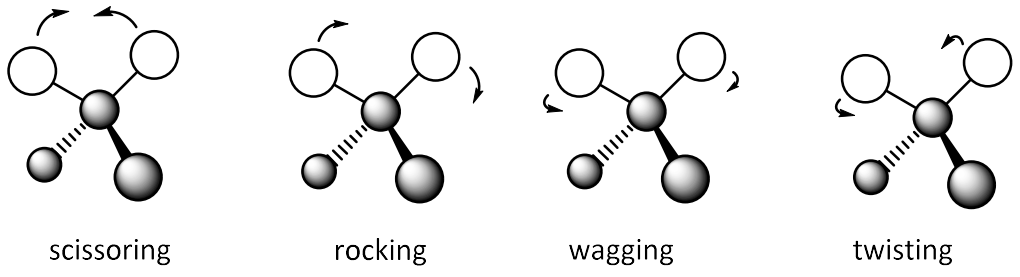

Figure 13. *Common vibrational modes in organic molecules used in IR and Raman spectroscopy.*

While it is reasonable to calculate the energy of a molecular vibration for a simple molecule like a diatomic one using the equation of a harmonic oscillator, shown in **Equation 8**.

$$\nu = \frac{1}{2\pi \cdot c}\sqrt{\frac{K}{\mu_R}} \tag{8}$$

Where *v* is the wavenumber of the vibrational band, *c* the speed of light, *K* the force constant of the band and μ_R represents the reduced mass of the involved atoms, by **Equation 9**:

$$\mu_R = \frac{m_1 \cdot m_2}{m_1 + m_2} \tag{9}$$

Where m_1 is the mass of atom 1 and m_2 the mass of atom 2. It becomes inefficient to do those calculations for every group of atoms in bigger molecules. In those cases tables with group frequencies are used to give a good estimation about the expectable vibrational energies. An additional tool for distinct identification offers the comparison of the fingerprint region (400-1500 cm^{-1}) of the sample molecule with a database. Infrared and Raman spectroscopy are in many aspects very similar, as they both provide information about molecular structure and molecular vibrations (for gases also molecular rotations). The samples can be in all three states, solid, liquid and gaseous. The structure as well as the distribution of the electrons in the molecule influence the intensity of the vibrational transitions. But both techniques are also fundamentally different in the way the sample molecule is interacting with the radiation. An IR spectrum arises from absorption of photons with a particular wavelength, whereas Raman spectroscopy is based on inelastic scattering of photons by sample molecules. That is the reason why many consider both techniques as complementary to each other.[284] Inelastic scattering means, that a photon after colliding with a molecule loses some its energy. This energy is absorbed by the molecule and used to excite it to a virtual state. When the molecule relaxes back, it emits a photon with a higher (anti Stokes line) or lower energy (Stokes line) or the same energy (Rayleigh line) compared to the initial photon as shown in **Figure 14**.[284]

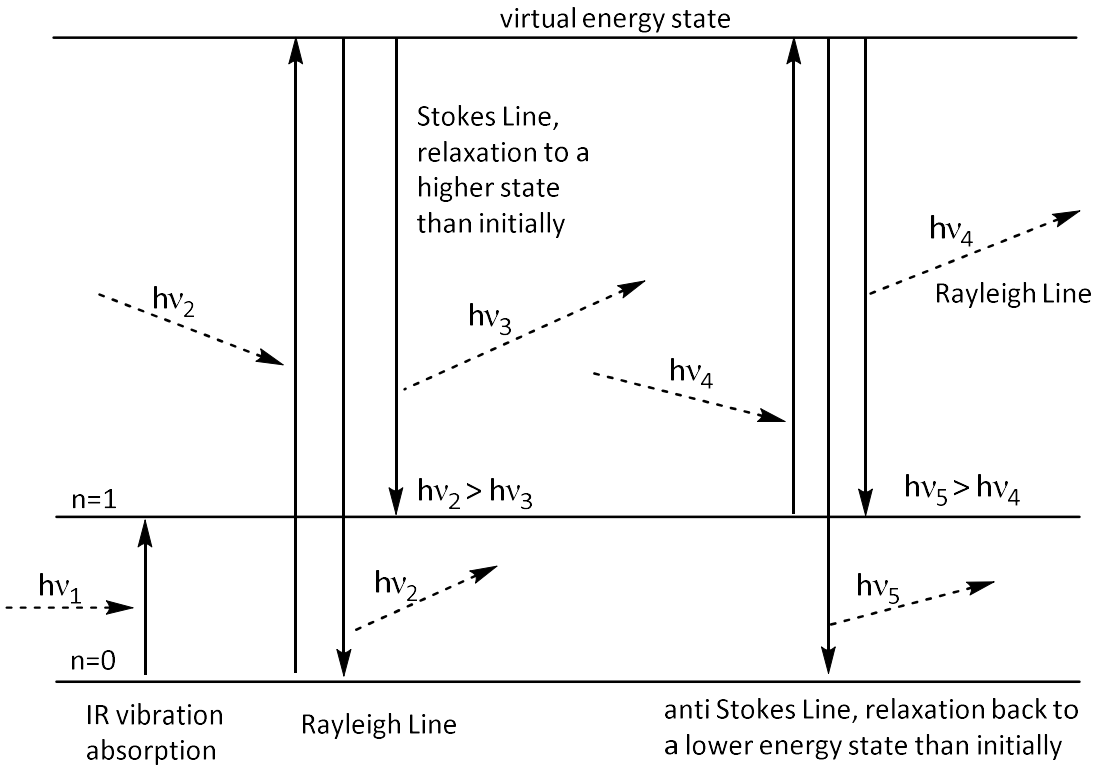

Figure 14. *Origin of Stokes, anti-Stokes Raman and Rayleigh lines after a molecule collides with a photon and gets excited to the virtual energy state. Dashed arrows represent radiation, the normal arrows illustrate changes in the molecular energy state. The virtual state describe a new state for an infinitesimal small amount of time in to which the molecule and the photon constitute after interacting with each other.*

A vibration is IR active if the dipole moment during the vibration changes. On the contrary, a change in the polarizability of a vibration is required to make it Raman active. This can be illustrated with two stretching modes in the symmetric carbon dioxide molecule:

Figure 15: Different stretching modes of CO_2. *The arrows show the direction of the atom motion during one half cycle of the vibration.*

During the symmetric stretching vibration the net dipole moment of the molecule stays the same, whereas the polarizability changes due to the simultaneously changing bond length of both C=O bonds. That explains why the symmetric stretch is IR inactive but Raman active. The antisymmetric stretch results in the opposite effect. The net polarizability doesn't change since one C=O bond gets extended by the same length, which the other one is losing during one half cycle of the vibration and then vice versa in the second one. That means that this vibration can't be seen in any Raman spectrum. Nevertheless, because the net dipole moment changes always twice its orientation during one vibration cycle, the vibration is IR active.

Both techniques were used in this work to identify the transformations of the functional groups in the building blocks, when they are reacting with each other to form the 3D framework. Especially the change from the monosubstituted alkyne (in diethynylbenzene) to the disubstituted alkyne (in the framework) was examined. For this the previously mentioned group frequency tables were used.[285]

The powdery building blocks were measured in an attenuated total reflection (ATR) set up, while the thin film was measured in reflection mode. The signal for the film is very weak compared to the powdery building blocks due to the smaller sample mass. To suppress background noise and increase the signal to noise ratio for the thin film measurement, the detector was cooled down with liquid nitrogen. The ATR set up has one big advantage against the normal transmission mode, no sample preparation has to be done. Thus, the sample could be measured directly and didn't have to get pressed into a KBr tablet. Because the penetration depth in this mode is independent from the thickness of the sample, just a small sample area in which evanescent waves can penetrate will be measured. That makes ATR measurements especially useful to analyze strongly adsorbing samples. Evanescent waves arise at interfaces, where total reflection occurs. While the light beam stays in the optical denser medium, evanescent waves propagate with a small range through the optical less dense medium. The used Fourier transform infrared (FTIR) spectroscopy has the advantage over a conventional IR which measures, wavelength after wavelength, that the FTIR measures them all at the same time, resulting shorter measuring times and higher throughput.

4. Towards 3D COF films

At the outset of this work, synthetic methodologies to produce 3D COF films were considerably more limited than their 2D analogues. As discussed in section 1.5.3 a majority of all so far known COF films are of a 2D nature. The topology of a framework has a fundamental influence on its material properties. For the targeted design of 2D frameworks this can be seen as a weakness, since the stacking of its sheets is rather difficult to predict and define.[211] Even though, presented framework structures show often the perfect eclipsed conformation, in reality most of those networks are rather serrated, inclined or staggered.[212-214] One possibility to lock the framework also in the third dimension into a specific orientation is the usage of directed covalent bonds in between the 2D sheets. This is usually done by using polyhedral instead of polygonal building units. The resulting 3D framework can also be seen as more rigid, since it requires more energy to break covalent bonds than π-π-interactions in 2D networks. To broaden the application range for COFs and also other framework materials, it is in my opinion essential to explore new strategies to produce porous 3D films, which was the motivation for this project.

4.1. Increasing control, continuous flow vs batch

In order to design any kind of films, it has to be decided first, is if a bottom up or top down approach is more suitable for the synthesis. The aim was to develop a strategy, which is as versatile as possible and results in films with defined thicknesses. To obtain films with a designated thickness, the top down approach can be unreliable, since it usually leads to a range of thicknesses, which is difficult to change and influence.[234-236] Another problem is that a theoretical top down approach in our case would start with an existing 3D film, without answering the question of its origin. Furthermore, a bottom up approach allows more flexibility regarding the temporary change of the reaction conditions during the framework assembly. It is also easier to obtain information about the framework formation kinetics if this approach is applied. Therefore, this argumentation led us to the use of a bottom up approach, since it allows more control over the obtained films.

As summarized in section 1.5.3 there are several different approaches described in the literature how one can make 2D COF films in a bottom up approach. Most strategies follow a typical batch synthesis, which makes the control and the monitoring of the films growth difficult if not even impossible. Even if for the described immersion of a substrate[239] or interlayer synthesis[241] the building block concentration and the reaction time can be used to stir the film thickness to some extent, the precise

control leading to a predictable thickness remained unachieved. Furthermore, another problem is that the reaction conditions during the reaction process are difficult to control. For example the decreasing concentration of building blocks in bulk as the reaction proceeds will slow down the film growth. The same is likely to happen when the building blocks have to pass through the extending network in order to react on the film surface during an interlayer synthesis. Another problem can be the competition between the oligomer formation in bulk and the desired reaction on the film surface. Bulk oligomers binding to the surface could lead to an increased film roughness and a decreased crystallinity, depending on the reversibility of the linkage formation reaction.

Most of those problems can be addressed by using a continuous flow setup. Flowing the building blocks over the surface guarantees a constant concentration of monomers. This leads to a full control over the reaction conditions throughout the entire film formation. Additionally, eventual created bulk oligomers will get transported away constantly which should lead to an increased smoothness and crystallinity of the film. Another advantage of a continuous flow approach is that it is possible to change reaction parameters, such as concentrations, flow speed or starting materials at any time during the film formation. This results in an extended synthetic flexibility compared to bulk synthesis. This increased control and flexibility of the film growth is responsible for our decision to explore film synthesis in a continuous flow setup.

4.2. Linkage, substrate connection and flow setup

In order to grow 3D films in a continuous flow approach, three elemental questions have to be answered first:

- Which linkages should be used to connect the building units with each other?
- How will the film be connected to its substrate?
- How can the flow setup be realized?

Those three question will be answered in this section.

I) The linkage chemistry

A look at the commonly used COF linkages in **Scheme 2** reveals that their reversible formation results often in decreased chemical stability of the framework. Boronate and boroxine linkages are prone to hydrolysis under aqueous conditions and many imines tend to hydrolyze under strong acidic or basic conditions. Carbon-carbon bonds on the other hand have traditionally an increased chemical stability, since they are stronger (C-C: 347-376 kJ/mol vs. C-N 288-313 kJ/mol).[286] Additionally, a C-C bond is less polar than a C-N or B-O bond, making it less prone to nucleophilic attacks. But this stability also limits the ability of C-C bond forming groups to perform reversible reactions. For that reason they

haven't been explored much in COF synthesis so far, rather in PAFs. Due to the increased chemical stability it was decided to choose a C-C linkage for this project. However, we anticipated as well to increase the crystallinity when applying suitable reaction conditions during the flow synthesis, e.g. slowing down the reaction or via the flexibility of the used self-assembled monolayer (SAM).

Ben et al. showed that the homo-coupling of tetrakis(4-bromophenyl)methane (TBPM) leads to PAF-1, a highly porous 3D network, based on C-C linkages (see **Scheme 1**).[64] They used a Yamamoto cross-coupling reaction to connect the building blocks with each other and form the C-C linkage as illustrated in **Scheme 5**.[287]

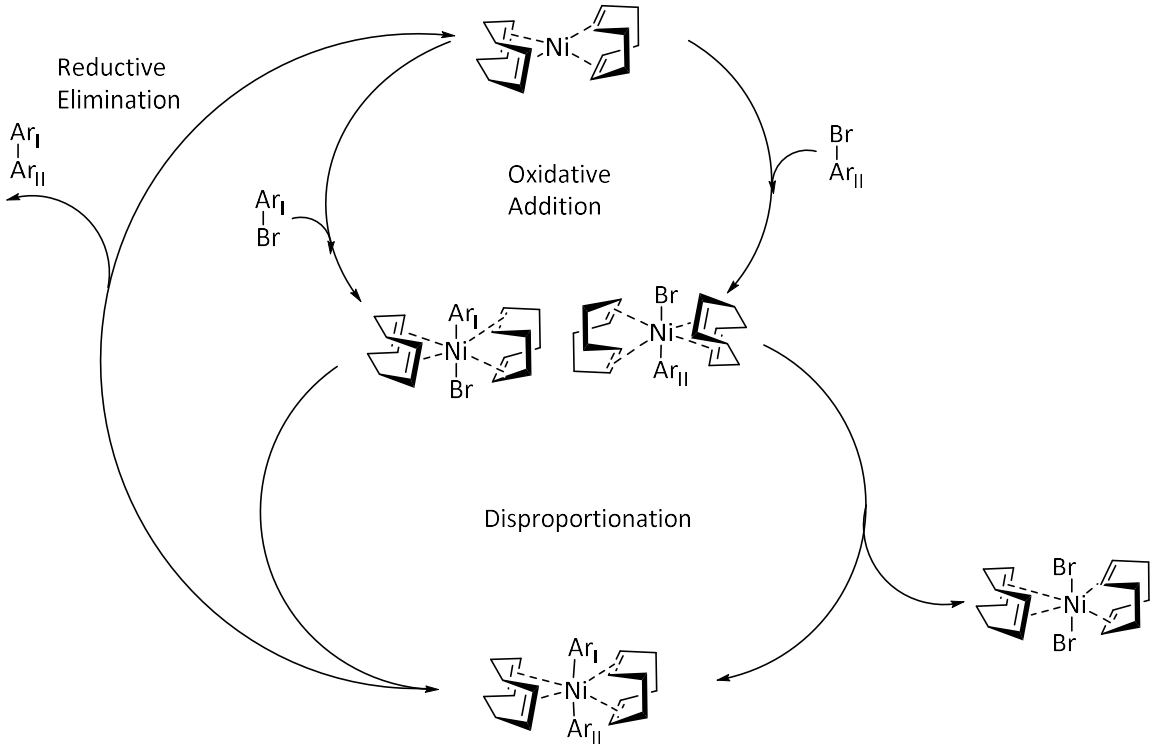

Scheme 5. *Mechanism of the Yamamoto coupling.*

They reported a reaction temperature of 80° C to form the insoluble PAF-1 framework.[64] For our film synthesis we aimed for room temperature conditions, therefore it was investigated if the reaction also works at lower temperatures. Instead of TBMP, bromobenzene was used as a model compound, since the homo-coupling product, biphenyl, is soluble in organic solvents and thus detectable by e.g. gas chromatography (GC) as shown in **Figure 16**.

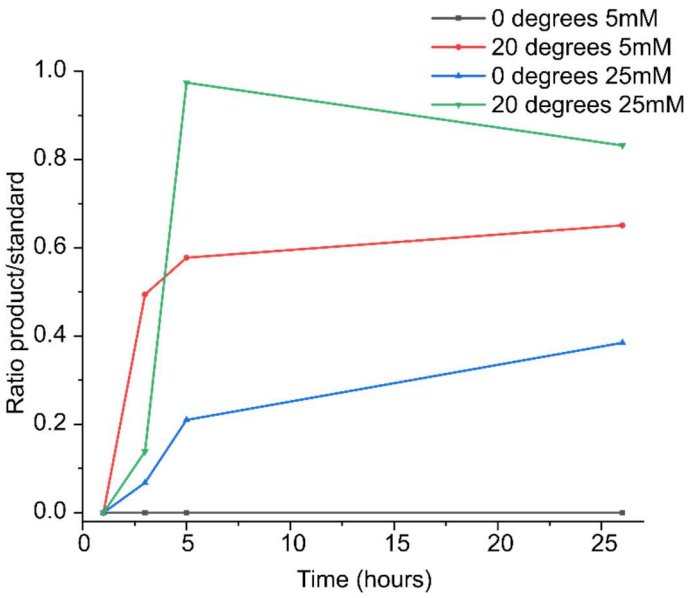

Figure 16. *Measured product/standard ratios (via GC) for the homo-coupling reaction of bromobenzene to biphenyl under different temperatures and concentrations.*

The results show that the formation of biphenyl takes place places at room temperature as well as at 0 °C. That indicates that it should be possible to use the Yamamoto coupling also at those temperatures. The slower reaction rate at 0 °C was considered as advantageous to prevent or slow down a potential polymerization in the vessel before the building blocks reach the substrate surface. After those initial considerations TBPM (***1***) was chosen as the building block for the first synthesis of porous films in this project. Building block ***1*** was synthesized following a literature procedure, as shown in **Scheme 6** starting from triphenylchloromethane (***3***) and aniline (***4***) in a two-step synthesis via tetraphenylmethane (***5***).[288]

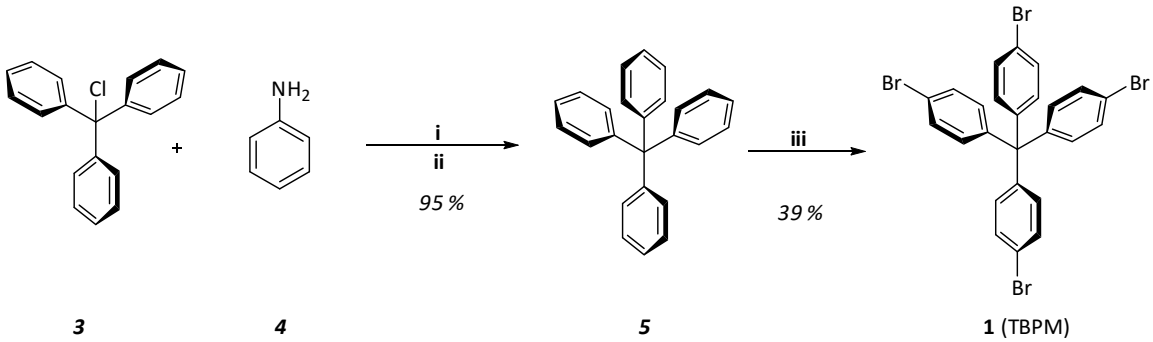

Scheme 6. *Synthesis route to form TBPM from triphenylchloromethane. Reaction conditions:* ***i)*** *190 °C, 15 min, HCl (2M), MeOH, 80 °C, 0.5 h;* ***ii)*** *H_2SO_4, DMF, -15 °C, isoamyl nitrite, 1 h, then hypophosphorous acid, 50 °C, 0.5 h;* ***iii)*** *-78 °C, bromine, overnight room temperature.*

II) Connection to the substrate

Many different materials such as graphene,[239] glas,[240] indium tin oxide,[289] silicon dioxide,[176, 290] graphene,[291] graphene oxide[291] or gold[289] were already tested as substrates for frameworks. If

frameworks are grown on surfaces, it can be beneficial if the structure has a rigid attachment to substrate. This offers a certain degree of control over the network growth similar to epitaxial growth of crystals. Epitaxy means that the growing material has at least one well-defined orientation in regard to its underlying substrate. One possible strategy to connect the framework with the substrate is with the help of a SAM. The idea is that the molecules, which form the SAM, have two moieties. One, which binds selectively to the substrate surface and one on the other side, which can be seen like an anchor point for the formation of the first film layer. Becker et al. presented in 2015 a strategy to grow a PAF-1 framework on a SAM templated gold surface in a batch reaction.[292] They used 4-bromothiophenol to form a SAM on the gold surface. Thiols have a strong binding affinity to gold and the easy preparation of thiol SAMs in gas phase or from solution making them very suitable candidates for surface functionalization.[293] On the other hand, the bromine in *para* position to the thiol group, acts as a binding site for the first layer of TBPM building blocks. Another reason for the decision to use a gold substrate with this thiol SAM is the confirmed mobility of thiols on gold surfaces.[294] The movability would allow to a certain extend a flexibility during the formation of the first layer of the film. This well-organized monolayer should serve then as a template for the further growth.

Thiol SAMs on the golden QCM sensors were formed through dipping of a freshly cleaned QCM chip in a 1 mmol/L ethanoic solution of 4-bromothiophenol overnight. Water contact angle measurements were performed to confirm the formation of the SAM. The measured contact angles for the templated gold surface during ten measurements were consistently between 90 and 99 degrees with an average of 95 degrees. The average contact angle for water on a clean gold surface is according to the literature 60-65 degrees and thus much lower.[295] That confirms the existence of the SAM on the gold surface.

III) The continuous flow setup

The realization of the flow setup was one of the biggest challenges in the beginning of this project. The involvement of a quartz crystal microbalance (QCM) to monitor the film growth in situ seemed highly beneficial after the already described study performed by Bisbey et al, in which they investigated growing boronate ester COFs on QCM sensors in real time.[246]

The data from the kinetic study in **Figure 16** showed no product formation after one hour reaction time. Based on this observation, it was decided to grow a PAF-1 framework using a flask containing a premixed solution with TBPM, cyclooctadiene (COD), $Ni(COD)_2$ and 2,2-bipyridine in DMF/THF (1:1) under nitrogen. The initial monomer concentration was the same as used by Becker et al. in their batch reaction (around 5 mmol/L).[292] The resulting mixture was transferred via a peristaltic pump into the QCM chamber, to the templated surface of the QCM sensor. The assumption that the formation of the framework in the vessel can be suppressed or at least sufficiently slowed down by cooling it

until it reaches the QCM chamber could not be confirmed. Instead, a few minutes after adding the last reagent to the solution, precipitation of a dark solid could be observed in the flask. The solid could also be observed in the tubing to the pump and the QCM cell. Optical microscopy of the gold surfaces after the reaction revealed that flowing those particles over the sensor surface, led to an unequal distribution of aggregates on the surface, rather than a film formation. Those observations let us consider the role of the used monomer concentration.

The reaction on the surface competes in the investigated system with a homo-coupling of TBPM in the bulk phase. Under the assumption that the amount of binding sites on the surface stays constant during the film growth, the reaction rate of the surface reaction is only influenced by the amount of monomers in bulk that arrive at the surface. Thus the transformation can be described as a reaction with first-order kinetics. However, the bulk reaction follows a second-order kinetics, because the reaction rate is dependent on two monomer molecules reacting with each other and both can be influenced by the used concentration. Therefore, both reactions rates r can be described as shown in **Equation 10** and **Equation 11**.

$$r_{bulk} = k_{bulk} * [monomer]^2 \tag{10}$$

$$r_{surface} = k_{surface} * [monomer] \tag{11}$$

Where *k* is the relevant reduced rate constant (including the concentration of non-monomeric coupling reagents, catalysts, etc.). This leads to the conclusion that a decreasing concentration will slow down the bulk reaction more than the surface reaction. Furthermore, under a specific threshold is the surface reaction even faster than the bulk reaction, which should lead to an improved smoothness of the surface. Consequently, the monomer concentration was stepwise reduced until at 0.05 mmol/L (1 % of the initially used concentration) no particle formation in the tubing was observed anymore. The optical microscopy images taken from the sensors after the reaction also showed an increased smoothness of the surface using lower concentrations. The hypothesis of an improved smoothness while using lower monomer concentrations could be also confirmed while measuring the surface roughness with an AFM. A monomer concentration around 0.05 mmol/L resulted in the lowest observed surface roughness for the used system. Additional improvement regarding the macroscopic smoothness could be achieved by dissolving monomer and the nickel catalyst separately from each other and mixing them shortly before they get flown over the sensor surface. Finding a working mixing unit was difficult in the beginning since the used machines did not tolerate the used organic solvents or the microfluidic device used got clogged by the formed framework. In the end, a self-built system of individual programmable syringe pumps together with common HPLC tubing and junctions gave the best results. The final system showed a much higher reproducibility of results and an increased air

tightness. **Figure 17** gives an overview over the final system, including the linkage chemistry (A), the connection to the substrate (B) and the continuous flow setup (C).

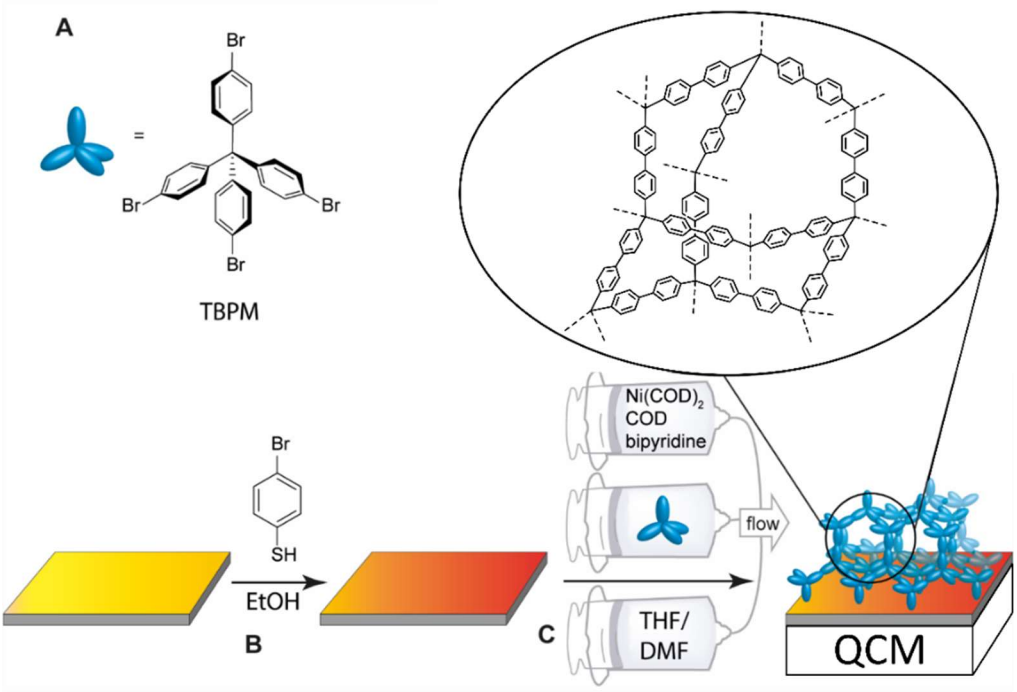

Figure 17. *The general reaction setup. A-C represent the previously discussed bullet points, linkage, connection and flow set up. A: chosen C-C linkage for building up the framework; B: SAM formation to connect the film to the substrate; C: continuous flow set up, using individual programmable syringe pumps for the different reagents.*

Additional tests confirmed that the described conditions, such as a low concentration of the TBPM, the use of a brominated SAM and continuous flow conditions are required to form smooth films. As shown in **Figure 18**, deviations from those conditions resulted in non-uniform surface topologies. Those observations are matching with previous reported results. Becker et al. observed after their batch reaction in their SEM cross section images a similar surface topology caused by aggregates as shown in **Figure 18A**.[292] Interestingly, Medina et al. observed also cracks in their 2D COF films, which they grew under solvothermal conditions on ITO glass plates, without a SAM.[289] But those cracks were only observed in the beginning of the synthesis and were not visible anymore in the end of the 12 h synthesis. The authors argue that their formation is caused by an initial island formation mechanism. That means that the COF starts growing from small initial starting points (islands) which then get bigger and grow into each other. The investigated COF contains boronic ester linkages, so presumably the cracks get removed due to self-healing at later stages during the reaction. However, the comparably much straighter shape of the cracks, which we observed makes it probably more unlikely that their origin is an island formation mechanism. Another fact, which confirms this assumption, is also that the cracks shown in **Figure 18A** do not vanish during longer reaction times, as they do for COFs showed

by Medina et al.[289] After being able to produce continuous films, the focus shifted towards the investigation of their thickness.

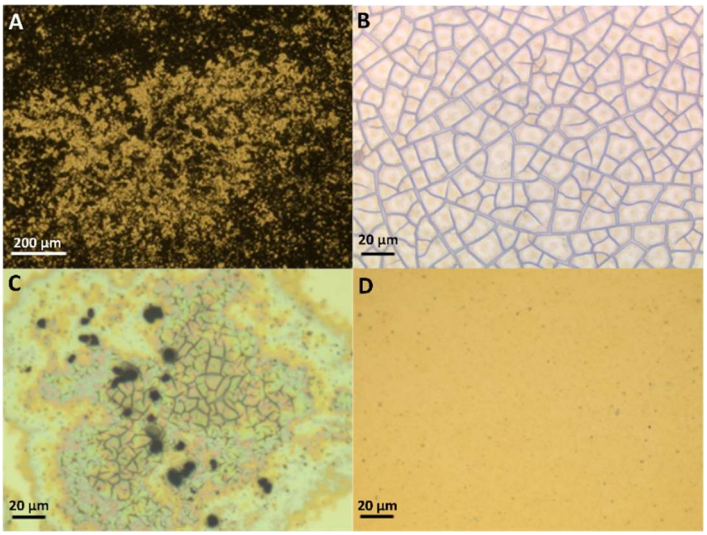

Figure 18. *Optical microscope photographs of samples made under different conditions. A shows the observed aggregation on the surface if the film is produced in batch. The sample presented in B was made using a non-brominated SAM. Similar cracks and additional aggregate formation were observed if the monomer concentration is too high as illustrated under C. D represents a framework surface without visible damages, built under continuous flow, low monomer concentration and with a brominated SAM.*

4.3. Correlation between frequency shift and film thickness.

In the first attempts to gain information about the film thickness a profilometer was used. Unfortunately, this did not result in reliable information about the framework thickness. One reason for this is the fact that it was unclear, where the baseline of the measured profile was. Accordingly, it was tried to make films with defects (holes), which reach through the entire depth of the film. That would allow to find a baseline using the profilometer and gaining information about the film thickness. Therefore, during different attempts small parts of the sensor surface during the SAM formation were covered with polystyrene. The assumption was to locally prohibit a SAM formation and thus later prevent framework formation in this region. The polystyrene was removed before the QCM sensor was inserted into the QCM chamber and the reaction was started. Unfortunately, this strategy didn't lead to the desired defects in the grown films. Furthermore, optical microscopy images didn't reveal obvious differences between the SAM and the polystyrene templated areas. As previously described in section 3.1., the Sauerbrey equation cannot be used to achieve information about the film thickness either, since the film is viscoelastic. But we expected a correlation between the resonance frequency shift of the QCM sensor and the thickness of its connected film. Hence, it was decided to make six samples, which have different frequency shifts, break them and look with a SEM at their cross sections

in order to measure their film thickness. The average thickness of each sample was plotted against its correlating frequency shift. The resulting plotted data points shown in **Figure 19** confirmed the expected linear correlation between film thickness and the frequency shift. The slope of the fit (0.057 nm·Hz^{-1}) can be seen as the conversion factor in between resonance frequency and thickness for this PAF-1 system. This assumption is valid for smooth and equally distributed films. With this information it was finally possible to monitor the film thickness during its growth in real time.

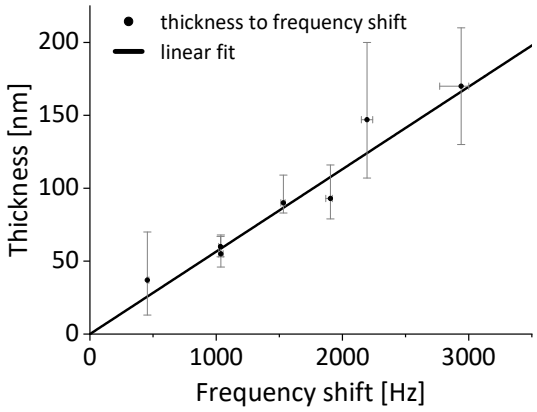

Figure 19. *Correlation between the resonance frequency shift measured with the QCM and the film thickness.*

The linear correlation also confirmed that the rate of surface reaction is steady when the monomer flow and its concentration is constant. Additionally, it could be shown that the growth rate under a stable monomer concentration is depending on the used flow speed. A lower flow rate results in a bigger boundary layer through which the monomers and the nickel complex have to diffuse and thus a lower reaction rate. The boundary layer is the fluidic region close to the surface. The fluid velocity in this layer decreases towards 0 in direction to the surface. Contrary, an increased flow rate reduces the thickness of the boundary layer and thus increases the mass transport via diffusion to the framework surface and accelerating the film growth.

Knowing that the film growth can be described with a viscoelastic model, it was investigated if encaged solvent molecules influence the frequency shift. To evaluate this hypothesis experiments with a solvent change from THF to the heavier deuterated THF-d_8 were performed. It was expected to see a frequency drop while switching from THF to the heavier THF-d_8 and an increase while changing back to normal THF. This frequency change should be stronger for a sample with a framework than for a clean sample, in case that the solvent molecules have an influence on the frequency shift. The observed frequency changes are shown in **Figure 20**. It could be shown that the expected frequency shifts take place when the solvent was changed. The absolute frequency change for the framework sample was bigger, which consequently indicates that caged solvent molecules do have an influence

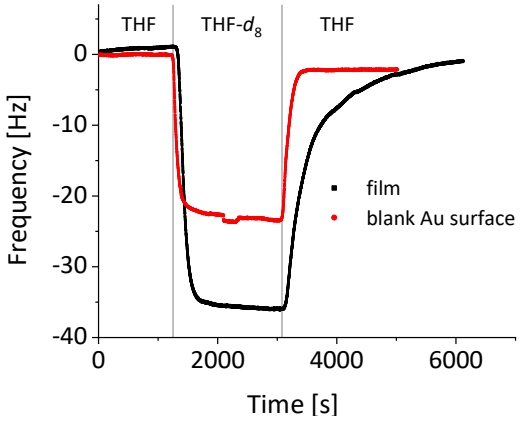

Figure 20. *The solvent influence on the frequency shift.*

on the frequency shift. This observation leads to the important conclusion that the obtained conversion factor of 0.057 nm·Hz^{-1} is solvent dependent. Furthermore, the assumption of a viscoelastic model for the film growth could be confirmed. After achieving control over the continuous nature of the films and understanding of their thickness, the focus was moved towards the analysis of the produced films. The findings are summarized in the next section.

4.4. Material analysis

In order to gain information about the elemental composition and the distribution, techniques such as SEM-EDX and (depth) XPS were used. SEM-EDX was performed on a film surface as well as on a cross section from a broken sensor. Detected elements were as expected, Au and Si from the substrate and C from the framework. Additionally Cr, Ni, S, O were observed. It could be confirmed by the manufacturer, Biolin Scientific, that chromium is used as an adhesive layer between the quartz crystal and the gold layer. Nickel origins presumably from entrapped $Ni(COD)_2$, sulfur from the thiol SAM and oxygen from entrapped solvent molecules. Interestingly, bromine from free binding sites (lattice errors) couldn't be detected. This observation matches with previous findings that frameworks constructed via Yamamoto couplings usually don't contain residual halogens inside the material because the reaction is efficient in eliminating halogen atoms.[296] The XPS spectra, which were taken from the surface confirmed the elemental composition detected using SEM-EDX. Additionally, depth XPS was performed, confirming the expected elemental distribution as shown in **Figure 21**. Etching into the material, the first layers mainly contain carbon and nickel. When the signals for those two elements become weaker, around layer 5-6, the signal for the gold layer becomes more prominent. This indicates that the ion beam from the sputter gun etched through entire framework and reached the gold layer of the substrate.

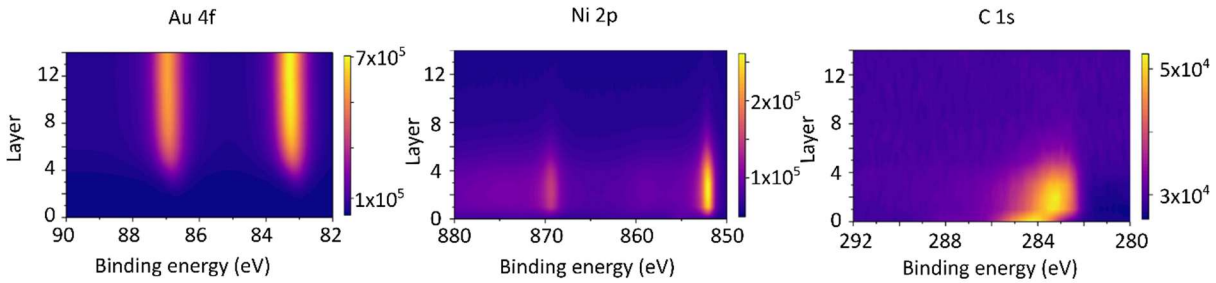

Figure 21. *Depth XPS spectra of gold, nickel and carbon for the PAF-1 film. The dual peaks for the 4f and the 2p signal occur because of spin-orbit splitting.*

The porosity of the material was confirmed via x-ray reflection spectroscopy. Compared to the idealized structure, the increased electron density origins probably from an interpenetration of the framework as well as residual solvent and catalyst. However, non-ideal PAF-1 materials with a similar electron density have shown high surface areas,[297] which led to the indirect conclusion that the here synthesized PAF-1 is also porous. The crystallinity of the porous films was tested using GIWAXS measurements. Unfortunately, the results showed that the material is amorphous, similar to their powder analogue. Therefore, it was confirmed that even with a 100 times lower monomer concentration, compared to the bulk approach from Becker an al.[292] and the flexibility of the SAM molecules for the formation of the first framework layer, the produced films remain without any long range order.

4.5. Conclusions from **Paper I**

Even though the synthesized films were missing the anticipated long range order and therefore do not qualify to belong to the group of COF materials, the developed method leads to several other advantages. The approach can be used to synthesize smooth and continuous porous 3D films. It could be shown that it is possible to kinetically promote the surface reaction over the bulk reaction by reducing the monomer concentration. Furthermore, all molecules, which didn't bind to the surface are removed constantly. This leads to an increased smoothness of the framework material, compared its growth under batch conditions. The continuous flow setup allows a constant transport of new building blocks to the surface and therefore keeping their concentration steady over the entire reaction time. This allows a full control of the reaction conditions during the entire reaction time and the possibility to adjust or change them at any time. The involvement of a QCM enables the real time monitoring of the film growth and its average thickness. This gives a major advantage over most other film growing strategies, where the film thickness can only be determined after the assembly. Most importantly, the modular strategy is versatile, as it was shown in initial experiments for the formation of films using a Sonogashira hetero-coupling. Further experimental information can be found in the

Supplementary Material, figure S8 in **Paper I.** Thus, the developed method is suitable to grow a wide range of porous films, which require a defined thickness. Additionally, the strategy enables the formation of rigid films on a variety of substrates, which is important for the future development of for example electrode materials or organic electronics. Therefore it is expected that the developed method can be used to grow numerous different porous framework materials in the future. The explored synthetic approach could be used to assemble hetero-structured materials. Those findings will therefore pave the road towards the development of layered porous film materials. This development will be part of the second project.

4.6. The next level: hetero-couplings, hetero atoms and layered materials

As described in section 1.6, known strategies for the synthesis of layered porous materials are limited. If strategies can be found to introduce specific functional sites just in certain areas of a framework, it could broaden the application range of porous films tremendously, e.g. for cascade catalysis. The usage of hetero-couplings is in this regard advantageous, since it allows a bigger diversity for potential framework structures than homo-couplings. Additionally a sequential material build-up would be enabled. Since the initial trials to make films with a Sonogashira coupling gave promising results in the first project, it was decided to continue with this system. Aryl iodides react faster in Sonogashira reactions then aryl bromides,[298] thus the tetrahedral building **1** unit was exchanged to tetrakis(4-iodoophenyl)methane (TIPM, **6**). Besides the carbon centered tetrahedral building unit **6**, lithium tetrakis(4-iodoophenyl)borate (LTIPB, **7**) with a boron center was selected as well. TIPM (**6**) and LTIPB (**7**) share the same geometry and have almost the same size, hence their particular resulting framework (boron-COF/carbon-COF) are expected to have very similar unit cells. This unity in their lattice parameters is important when growing them on each other as layered films. As a linear linker, diethynylbenzene (**8**) was chosen as shown in **Scheme 7**.

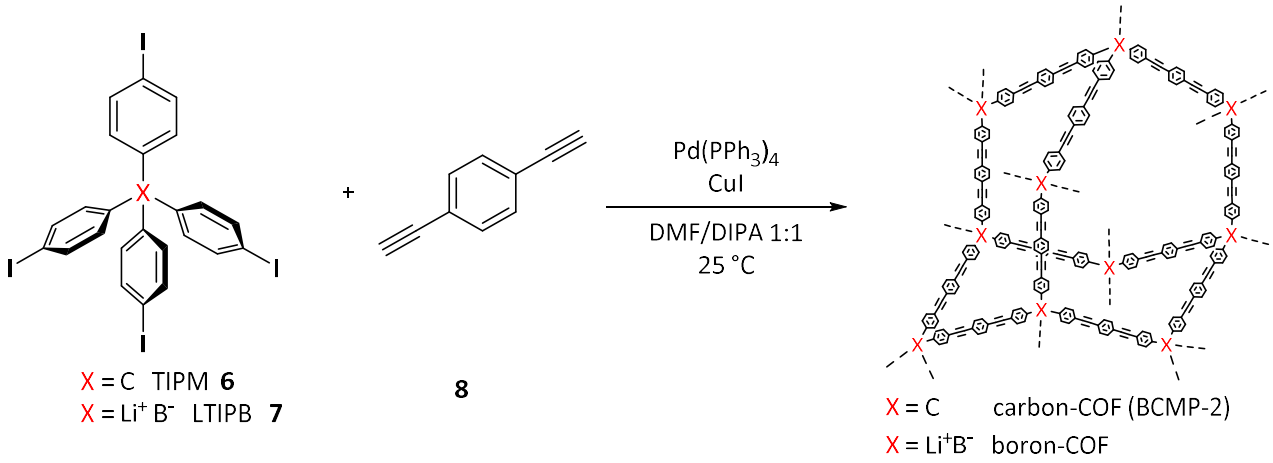

Scheme 7. *Formation of the carbon-COF and boron-COF via a Sonogashira coupling.*

Previous studies could show that films synthesized using a homo-coupling of ionic building block, e.g. **7** are not stable and tend to partial decomposition.[77] Furthermore, by including a neutral co-polymer, such as diethynylbenzene, into the synthesis, the disintegration can be avoided. Building unit **6** and alkyne **8** were commercially available, whereas **7** was synthesized following a literature procedure as illustrated in **Scheme 8** starting from 1,4-diiodobenzene (**9**).[288]

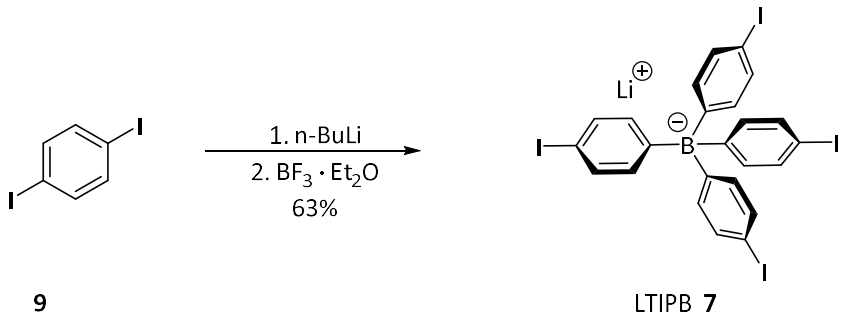

Scheme 8. *Synthesis of the boron centered building block LTIPB.*

The carbon- and the boron-COF films were produced in flow in a similar way than the previously discussed PAF-1 films. A possible way to obtain information about the Sonogashira coupling efficiency during the framework assembly is to look at the transformation of the triple bonds. During each linkage formation a terminal alkyne of the diethynylbenzene gets converted into a disubstituted alkyne, as shown in the mechanism of a Sonogashira coupling, illustrated in **Scheme 9**.

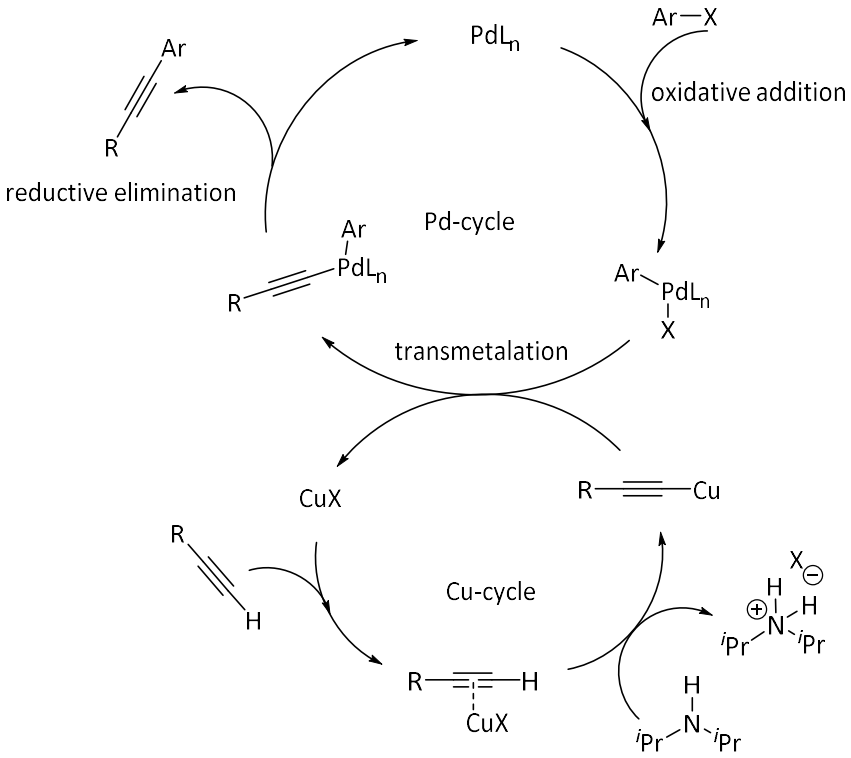

Scheme 9. *Mechanism of a Sonogashira coupling. The illustrated diisopropylamine (DIPA) in the Cu-cycle represents the used base for the system in this project. Generally, other bases can also be used.*

In order to verify the chemical uniformity of the film, the coupling efficiency in the frameworks of the carbon- and the boron-COF was evaluated. In consequence, the occurrence of unreacted triple bonds was reviewed for both films using FT-IR as well as Raman spectroscopy. A comparison of the COF film spectra with the spectra for the individual building blocks confirmed that no terminal triple bonds could be identified in the framework samples. Accordingly the produced frameworks have a high degree of polymerization. If not many unreacted terminal triple bonds exist in the framework structure, the amount of iodine atoms should be low as well, because for each linkage formation one carbon-iodine bond is cleaved (see **Scheme 9**). To confirm this hypothesis, XPS spectra from different surface positions of the carbon-COF film were measured. Since the spectra showed also prominent gold signals, it was concluded that the x-ray beam penetrated through the entire film depth and thus, the spectra shows the average elemental composition of the film. The results displayed a very low iodine ratio, around 0.1 atomic %. The measured carbon-iodine ratio is 71:0.1, which equals in average one iodine atom for every 17th TIPM in the network. Since probably most of the detected iodine atoms origin from the free binding sites of the film surface, the XPS measurement confirmed the high degree of polymerization in the framework.

If the two synthesized films are crystalline, due to the unity of their monomer size, they should have very similar lattice parameters and therefore their x-ray diffraction patterns should be comparable. The theoretical diffraction peaks were simulated and compared with the measured GIWAXS spectra

as shown in **Figure 22**. The first simulated peak is not observable in the measured spectrum, due to observation limitations for low-Q scattering signals of the used machine. However, the second simulated peak at 0.77 $Å^{-1}$ could be found. The degree of interpenetration could not be defined because of the limiting amount of scattering data. The detected peak positions for the refracted x-ray beam are the same for both frameworks. Moreover, they are consistent with the refraction peaks from the film synthesized from TBPM in project one. The data showed that both films are polycrystalline and to some extend anisotropic. The anisotropy is indicated by the increase of scattering intensity of the half circles towards lower Q_z values. Additionally, as expected have both films the same lattice parameters. The size of the unit cell for both was calculated to 15.2 Å. Since both crystalline frameworks have compatible unit cell dimensions, it should be possible to not just stack them on each other, but also to connect the different frameworks with covalent bonds on their interlayers.

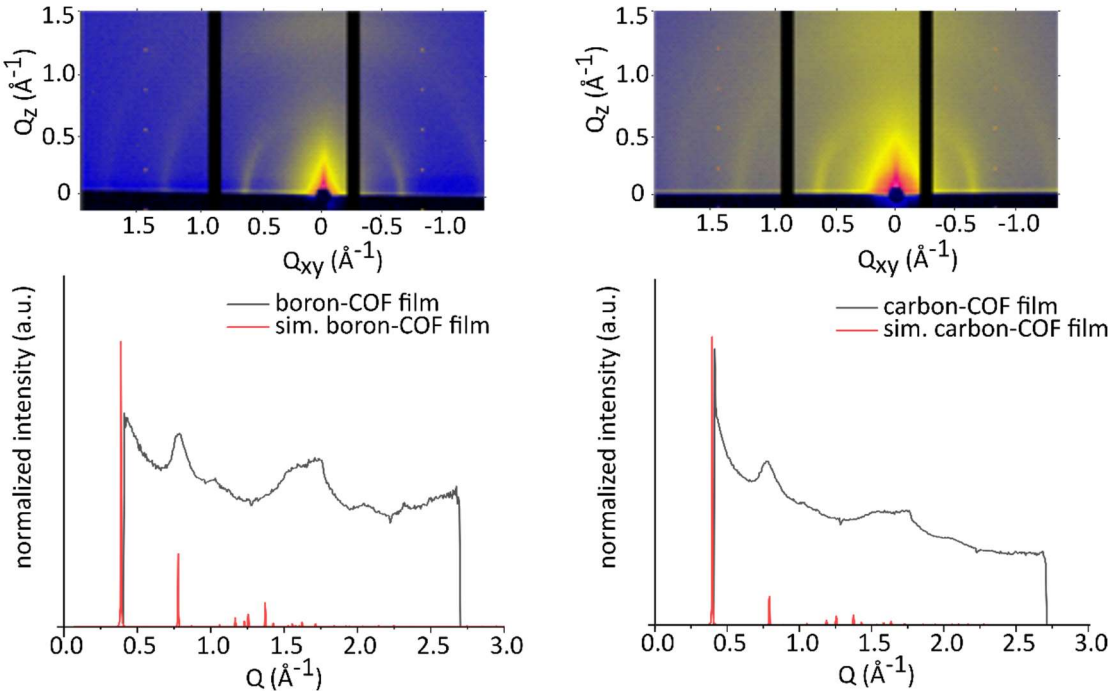

Figure 22. *Measured (top) and simulated (bottom, red) X-ray diffraction pattern (GIWAXS) for the boron- (left) and carbon-COF (right).*

4.7. The boron-carbon sandwich

The structural results for the boron- and the carbon-COF confirmed the initial hypothesis that both frameworks are suitable candidates to make layered films, since they have very similar crystal lattice parameters. Before the first experiments for sandwich-like materials could be done, one more property of the carbon- and the boron-COF had to be investigated. Knowledge about the surface

roughness for the individual layers is crucial in order to produce later on continuous layered films. The average surface roughness of each layer must be lower than the thickness. If not, the layer is not complete, and one cannot guarantee uniformity when building layers. From this perspective, the surface roughness can be seen as the lower limit for the thickness of every individual layer. One of the most common techniques to determine a materials surface roughness is AFM. AFM measurements performed on the COF film surface gave an average surface roughness of 10.8 nm for a 55 nm thick carbon-COF film and 12.9 nm for a 110 nm thick boron-COF film over an area of 4 μm^2. The frequency to thickness relationship of the films was studied by scratching the polymer surface and measuring the depth of the resulting scratches using a profilometer. This resulted in a correlation of 0.04 $nm \cdot Hz^{-1}$ for the boron- and the carbon-COF film for the used reaction. Attempts to grow smoother COF films with a lower monomer concentration were not successful.

After gaining the information about the lower thickness limit per layer, flow experiments to grow layered structures were performed. Every of the three building blocks (TIPM, LTIPB and alkyne **7**) and the catalyst were dissolved and stored in an individual syringe, mounted in a syringe pump. The fifth syringe contained only solvent for the washing periods. The sandwich film contained in the end four different layers, two of each framework. Each layer was grown for four hours and ended with a washing period for one hour, in which just solvents were flown over the surface. The shift of the resonance frequency over time and an illustration of the layered sandwich structure can be seen in **Figure 23**. The uniformity of the mass deposition on the QCM sensor (shown by the steady slope of

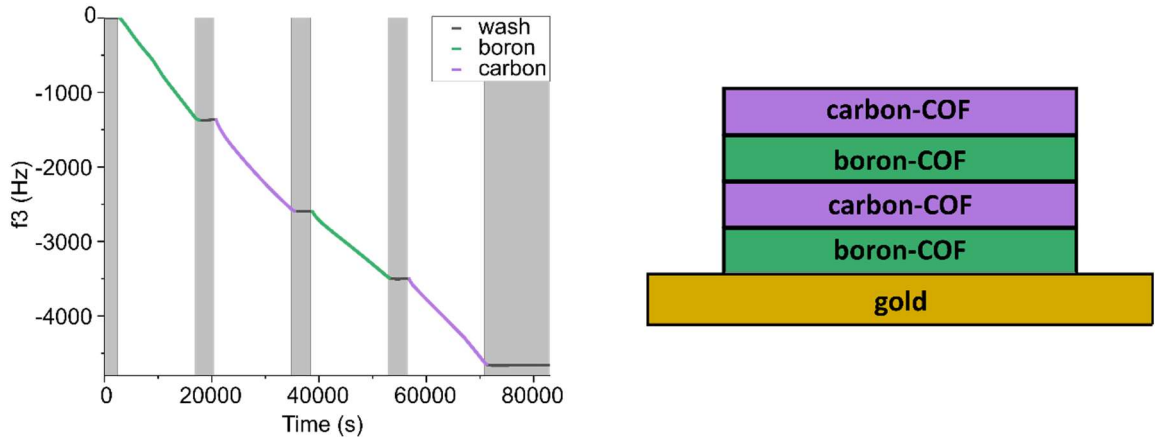

Figure 23. *Example for a resonance frequency decrease during the growth of a layered film (left) and an illustration of the corresponding layer order (right).*

the frequency shift over time) for each layer especially in the beginning indicates that they grow on each other via the formation of covalent bonds. If they would grow from aggregates in an island formation mechanism, it could be expected that the slope of the frequency shift over time would increase during the growth of each layer. As shown in project one, films, which are not covalently connected to their underlying layer, tend to form cracks. Those cracks couldn't be observed on optical

microscopy images nor SEM images of the carbon-COF, boron-COF or the layered film surfaces. If the layers don't grow covalently connected on each other, it can be also assumed that this would increase the surface roughness of the layered film significantly compared to the homo-structured films. Instead, the measured average surface roughness of a layered film was specified to 13.5 nm on a 4 μm^2 on a roughly 140 nm thick film. Thus the layered film has a similar average surface roughness than the previously described homo-structured films. By applying the determined frequency to thickness relationship of 0.04 $nm \cdot Hz^{-1}$, each layer has a thickness of 35-55 nm, which is larger than the average surface roughness. Hence, the individual layers are expected to be continuous and covalently connected.

The crystallinity of the resulting layered film was investigated using GIWAXS. As shown in **Figure 24**, the obtained diffraction peaks and their positions are complimentary to the diffraction spectra of the boron and the carbon-COF. That confirms the initial claim that it is possible to grow epitaxial chemically different COF films in a layered matter on each other without any loss in crystallinity.

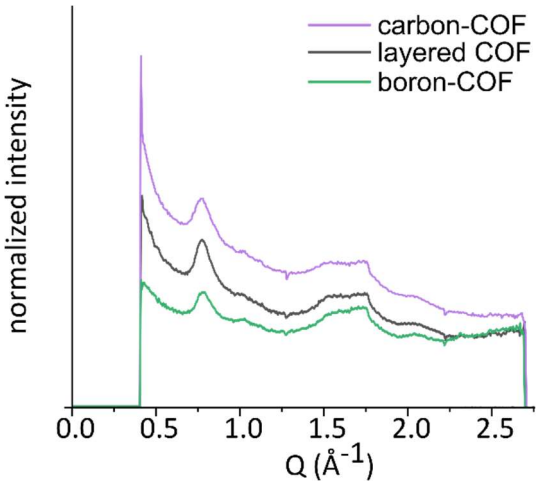

Figure 24. *1D GIWAXS spectra of the carbon-, layered and the boron-COF film.*

To confirm the layered nature of the material ToF-SIMS measurements of the layered samples were performed. It was expected to see an alternating amount of B and Li throughout the depth of the film. Local maxima in their concentration should indicate the existence of a boron-COF layer and local minima should represent the carbon-COF layers. Boron couldn't be detected because it did not ionize, which was observed before using this setup. However, the expected change in the lithium concentration could get detected, even though it only confirms the 2 bottom layers and indicates the third layer. The fourth and top carbon-layer could not get confirmed as shown in **Figure 25**. A reason for those findings could be that the surface of the film material is, due to its porosity, more sensitive to the ion gun bombardment. That means that in the beginning the etching might be too fast and

engraves during the first cycle already through the entire first layer. The detected distribution of gold and carbon also matches with the expectations, as the carbon signal decreases right before the gold

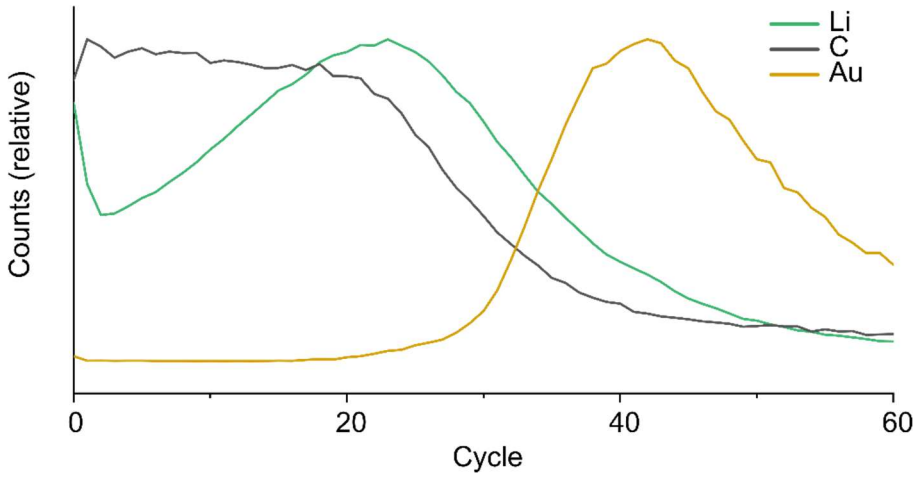

Figure 25. *ToF-SIMS measurement for the layered film.*

signal rises. It was tried to repeat the ToF-SIMS measurement with a sample which contained thicker individual layers and another which had a thicker top layer. During those measurements no lithium could be detected, but the copper concentration alternated to some extend and suggested the existence of four layers. However, the results were not totally conclusive. Copper could probably perform an ion exchange with lithium and therefore also indicate the existence of the different layers. Nonetheless, this exchange was not observed during the first measurements, which are shown in **Figure 25**. Summarized, it can be stated that some evidence for the existence of the layered structure could be found, but it cannot be absolutely confirmed.

4.8. Increased control – molecular single layers?

An additional question which was attempted to answer was, if it is possible to grow the individual carbon- or boron-COF stepwise and with control, single molecular layer by single molecular layer. This could promote the formation of the thermodynamic product and therefore increase the crystallinity. This method was also expected to lead to an increased smoothness of the films. Additionally it was tried to show that it is possible to monitor a single layer by single layer growth of the framework. The idea was to not flow like before both building blocks for each framework simultaneously over the surface, rather alternating. During the initial experiments of the first project it was concluded, that a SAM formation can be observed with a QCM. That is why, it was expected to be possible to monitor the formation of each single layer. During the first experiments to grow the COFs single layer by single, it was noticed that the oxidative addition of the Pd-catalyst into the carbon-bromine bond of the 4-

bromothiophenol could be detected by the QCM. But as soon as diethynylbenzene was flown together with the catalyst over the surface the resonance frequency did not stop to decline as shown in **Figure 26A**. The origin for the mass deposition on the sensor is most likely a homo-coupling of the diethynylbenzene in the presence of copper and oxygen, more generally described as Glaser–Hay coupling reaction.[299] To exclude the possibility that this side reaction has any influence on the formation the boron- and the carbon COF, a kinetic study, as shown in **Figure 26B**, was performed.

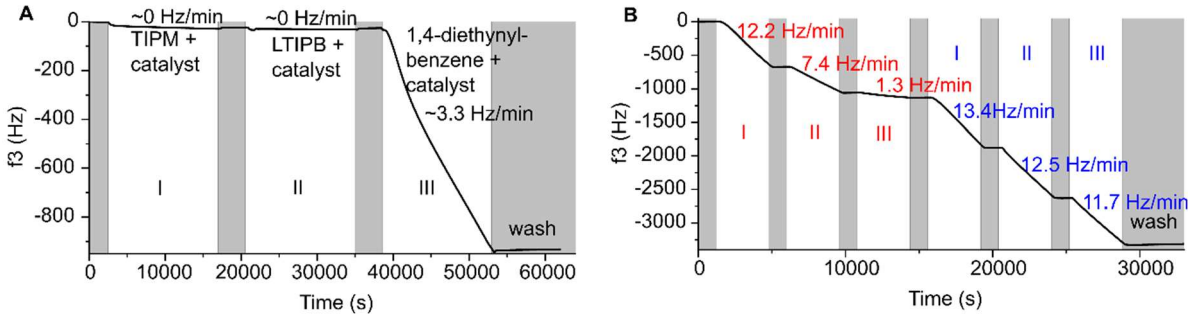

Figure 26. *Kinetic study of the COF formation. A: Control experiment showing that only the existence of TIPM and catalyst; (black I) or catalyst and LTIPB (black II) doesn't lead to any film growth. On the contrary, when the diethynylalkyne molecules are in contact with the catalyst (black III) a mass adsorption on the sensor surface is detectable. B: The catalyst concentration was kept constant during the reaction times. In the first area (red I-III) the concentration of the alkyne was kept constant and the concentration of the TIPM was stepwise reduced. In the second period (blue I-III) the concentration of the TIPM was kept constant and the amount of the alkyne was reduced.*

The obtained data showed that the reaction rate remains almost steady, if the alkyne concentration is decreased (see **Figure 26B**, I-III). If the Glaser–Hay reaction would have an impact in the framework formation, the rate would not stay constant while changing the alkyne concentration. However, the reaction rate declines distinctively if the TIPM concentration is decreased (see **Figure 26B**, I-III). That is in unison with the general opinion that the oxidative addition is the rate limiting step in Sonogashira couplings. Additionally, the reaction rate drops at low TIPM concentrations even under the observed reaction of the alkyne homo-coupling (see **Figure 26A**, III). With all those indications, it could be ruled out that the Glaser–Hay reaction has an influence on the framework formation, as long as both building blocks are mixed together during the reaction. With this limitation, it was concluded that the framework growth single layer by single layer was not feasible with the so far used catalytic system.

The reaction conditions were changed, to a copper-free Sonogashira coupling, since the presence of oxygen could not be entirely prevented in the used flow setup. The synthesis of the homogenous boron and carbon films under copper-free catalysis resulted in materials similar to the copper-catalyzed conditions. This can be seen as another confirmation that the Glaser-Hay coupling does not affect the framework assembly. Nevertheless, their investigation was not further continued, because the boron- and the carbon-COF synthesis require different solvents, which causes monitoring issues using the QCM when making layered structures.

4.9. Conclusions from **Paper II**

While using a Sonogashira hetero-coupling and the previously developed flow system, two new COF films, boron- and carbon-COF, could be synthesized. Both frameworks have a high degree of polymerization, which could be supported via via IR, Raman and XPS measurements. GIWAXS measurements confirmed the crystallinity of the films, making them to one of the first examples of carbon-carbon linked COFs. Thus, it could be confirmed that it is possible to synthesize COFs even using non-reversible linkage formation reactions, such as C-C cross couplings. This will enable the synthesis of more rigid and stable COF materials in the future and therefore broaden the application range for this class of materials.

The lattice parameters of both synthesized networks are the same, enabling their use in layered materials, in which the layers are covalently connected with each other on their interlayers. Both films have a low average surface roughness, which promotes their possible use also in thin, layered continuous films. Furthermore, sandwich-like structures based on alternating boron- and carbon-COF layers could be synthesized while containing their crystallinity and their lattice parameters. All three materials (boron-, carbon-COF and the layered film) showed a continuous and defect free surface while investigating them with an optical microscope and SEM. Even though no conclusive confirmation for all expected layers could be found, evidence for the existence of the bottom layers could be detected using ToF-SIMS depth measurements. Those findings confirm for the first time the successful assembly of a covalently connected layered 3D COF. This will enable the future synthesis of COF materials with different defined local functionalities. Those materials would be useful to catalyze for example cascade reactions.

The controlled single layer by single layer growth of a carbon-COF could not be established, due to a homo-coupling side reaction of the alkyne building block. Consequently a kinetic study was performed, which could rule out the possibility that this side reaction effects the framework assembly of the carbon- and boron-COF, as long as both building blocks are mixed together. In order to investigate the framework growth single layer by single layer in the future a different catalytic system and different starting materials have to be found, which are not prone to homo-coupling side reactions. One possible example could be a Suzuki-coupling if the diethynylbenzene gets exchanged to *p*-benzenediboronic acid.

5. Concluding remarks and outlook

Most of the previously explored procedures to synthesize porous organic materials lead to powdery materials. Furthermore, most of the few explored approaches, which can be used to obtain thin films lack a real time control of their thickness.

Therefore, the work presented in this thesis intended to develop a versatile method to grow smooth porous 3D linked organic films in a continuous flow setup. Furthermore, it was attempted to build a hetero-structured film, containing layers of different frameworks. The emphasis of the synthesis approach lies on the involvement of a QCM, which allows the real time monitoring of the framework growth and its film thickness on a nanometer scale. A correlation between the frequency shift of the QCM sensor and the film thickness could be found. The described strategy is versatile and enables the assembly of a variety of different amorphous and crystalline 3D films. Three of them, PAF-1, carbon and boron-COF, were synthesized and characterized in detail during this work. The development of boron- and carbon-COF are one of the first examples for COFs based on robust non-reversible C-C linkages. It could be shown that via a control of the used monomer concentration the surface reaction could be kinetically promoted over the bulk reaction, leading to an increased film smoothness. Moreover, it could be demonstrated that the developed strategy allows the formation of layered structures. To the best of our knowledge the presented layered film is the first example for a layered 3D COF on COF framework. The possibility to introduce a certain functionality only locally into a framework will certainly broaden the application range for porous films in the future.

The resulting opportunities for future development are numerous. To mention a few:

- The idea to use a SAM-templated substrate to grow rigid 3D structures would theoretically allow the production of films with different topologies. Therefore, the design of new flow cells, which can hold substrates of different shapes seems encouraging. This could lead to a direct synthesis approach for porous electrodes, if the films are grown on a conducting substrate of the desired shape.
- The crystallinity of the assembled C-C linked COF films could probably be increased with the described single layer by single layer approach. To confirm this hypothesis a different catalytic system, not prone to homo-coupling side reactions, has to be found. If it works to build up the film single layer by single layer, it would increase the control over the film growth even further. (Layered) materials with not only a specific thickness, but with a tailored amount of single layers could be made.

- The use of the ionic building block LTIPB results in frameworks with incorporated counter ions. It could be beneficial to try if those counter ions could be exchanged directly during or after the synthesis using the continuous flow set up. This would lead to a very practical strategy for framework modification. It would be also interesting to investigate, if the initial choice of a sterically demanding counter ion, suppresses the interpenetration of the framework, which later on can be exchanged to a smaller one. This could be an option to increase the surface area of the material and control the often unwanted network interpenetration.
- Another objective could be to assess the possibility to make thicker films (in µm range). If those films are self-standing and can be detached from the substrate, the here developed method would give access to freestanding membranes. Those membranes with a designable pore size could for example be used in filter applications.

6. Acknowledgments

Looking back at my PhD journey and comparing it with my long distance hiking trips, I have to admit that both have more in common as one might think. As in the mountains my PhD time had also a quite tough elevation profile with a lot of up and downs, when I look back. Sometimes it was steeper, sometimes more flat. There were periods, where it was constantly raining, slippery, annoying, bothered by bugs and heat, with a 20 Kg backpack on the shoulders, that it felt like there is no progress. But in the end, every step brought me closer to last summit. Despite that, there were also those sections, which felt more like a walk with amazing views and perfect weather conditions. And regardless of the conditions, one always has to be careful to not come in too close contact with one of those numerous toxic species along the way.

Like with every bigger thruhike, also my PhD time wouldn't have been possible without certain people helping me. Those trail angels, friends and colleagues, who shared parts or even the entire trail with me, I want to thank here.

There is almost no long journey without a sponsor and navigator. Thank you **Karl** for offering the possibility of taking this path, for financing my hike and the needed equipment. I know that we didn't always agree on which trail the right one to pick is. But in the end, I made it to the last summit, that wouldn't have been possible without you. Thanks you for your patience, your support and for your advices, when I needed them. I also want to thank **Prof. Arne Thomas** for accepting being my opponent and going the last mile with me to the final peak. Who would have assumed that 10 years ago, when you initially introduced me to porous materials, while I was a student in Berlin? Ett stort tack as well to the committee members **Dr. Alesia Tietze, Professor Lars Öhrström**, **Professor Martin Andersson** and **Dr. Kasper Pedersen** for their time and accepting to be part of the jury.

One true thruhiker and trail angel are you, **Alica** (I know, you prefer devils ;-). You actually went almost all the way with me and we shared shelter for 2 years. Thank you for the moral support in and outside of chemistry. Our friendship (and Sunday drinks) had a huge impact on me arriving on the terminus. You made the hike often feeling like slackpacking.

I also want to thank my hiking colleagues **Alex**, **Clara** and **Yizhou**. You supported me with advices for difficulties, which I struggled with and you helped me when it was foggy and I didn't see the right direction. **Yizhou**, specifically thanks for your help with the experiments. Without them our articles wouldn't have reached such a high impact, I am sure. The same counts for **Austin**. Thank you for your constant help, answers, corrections and experiments, making our articles a success. I am super glad that we met in the middle of nowhere in New Hampshire. **A^3**(**Alex**, **Alica** and **Andrew**), thanks for your

time while proof reading this final trail guide. **Peter** for the often fun time in the office and your help, regarding chemistry and life. Sorry, that I just followed 2 of your 3 advices. So far…never say never ;-) **Laura**, **Sara**, **Hanna**, **Emma**, **Julia** & **Ida** for helping me with my QCM runs through all the nights!

There are even more people off trail, trail angels, who helped me making it all the way.

Meine **Eltern** und meine **restliche Familie** daheim: Danke für die immerwährende Unterstützung durch meine insgesamt 13 jährige Unizeit. Eine so lange Reise wäre ohne euch nicht möglich gewesen.

Alfred, my twin: jag ska alltid uppskata och påminna din vänskap, hjälp, aktiviteter, CS historier, gym och våra andra vardagsrum. Jag saknar dig här i Göteborg. Tack för allt!

Fysiken (representerad i form av alla mina fantastiska kollegor och deltagare): för att ni ger mig möjligheten att utforska en helt annan sida av mig och för att stöda mig alltid med glädje och tacksamhet när det behövdes mest under alla regniga dagar på leden.

Dr. Louis & Nevita: For all the board games nights and evenings and the feeling that I have a second apartment on my floor.

Meine trail angels zu Hause in Berlin: Danke unter anderem **Anja** & **Ludwig**, **Patrick**, **Anne** & **Fabi** und **Felix,** dass es sich bei jedem Besuch so anfühlte, als ob ich nie weg gewesen wäre.

And all the other Mäuschens here in outside from Gothenburg: **Babsi**, **Berith, Björk, Carlos²**, **Chiara**, **Emma**, **Felix**, **Gabi**, **Hanna**, **Lubo**, **Luca**, **Ludwig**, **Maciek**, **Raffi** and **Sandra** for all the lunches, evenings, saunas, partys, movie evenings and trips…. For the constant support and amazing 8.5 years here in Gothenburg. Ett stort tack!

And as in the end of any hike, there is just one question left:

Which journey is the next one?

7. References

1. Davis, M. E., Ordered porous materials for emerging applications. *Nature* **2002,** *417* (6891), 813-821.
2. Everett, D. H., Manual of Symbols and Terminology for Physicochemical Quantities and Units, Appendix II: Definitions, Terminology and Symbols in Colloid and Surface Chemistry. *Pure Appl. Chem.* **1972,** *31* (4), 577-638.
3. Soldatov, D. V.; Ripmeester, J. A., Organic zeolites. In *Stud. Surf. Sci. Catal.*, Sayari, A.; Jaroniec, M., Eds. Elsevier: 2005; Vol. 156, pp 37-54.
4. Abdullahi, T.; Harun, Z.; Othman, M. H. D., A review on sustainable synthesis of zeolite from kaolinite resources via hydrothermal process. *Adv. Powder Technol.* **2017,** *28* (8), 1827-1840.
5. Freund, R.; Canossa, S.; Cohen, S. M.; Yan, W.; Deng, H.; Guillerm, V.; Eddaoudi, M.; Madden, D. G.; Fairen-Jimenez, D.; Lyu, H.; Macreadie, L. K.; Ji, Z.; Zhang, Y.; Wang, B.; Haase, F.; Wöll, C.; Zaremba, O.; Andreo, J.; Wuttke, S.; Diercks, C. S., 25 Years of Reticular Chemistry. *Angew. Chem. Int. Ed.* **2021,** *60* (45), 23946-23974.
6. Yaghi, O. M.; Li, G., Mutually Interpenetrating Sheets and Channels in the Extended Structure of [Cu(4,4'-bpy)Cl]. *Angewandte Chemie International Edition in English* **1995,** *34* (2), 207-209.
7. Hoffmann, R., How Should Chemists Think? *Scientific American* **1993,** *February*, 66-73.
8. Wang, Q.; Astruc, D., State of the Art and Prospects in Metal–Organic Framework (MOF)-Based and MOF-Derived Nanocatalysis. *Chemical Reviews* **2020,** *120* (2), 1438-1511.
9. Silva, P.; Vilela, S. M. F.; Tomé, J. P. C.; Almeida Paz, F. A., Multifunctional metal–organic frameworks: from academia to industrial applications. *Chem. Soc. Rev.* **2015,** *44* (19), 6774-6803.
10. Furukawa, H.; Cordova, K. E.; O'Keeffe, M.; Yaghi, O. M., The Chemistry and Applications of Metal-Organic Frameworks. *Science* **2013,** *341* (6149), 1230444.
11. Kitagawa, S.; Kitaura, R.; Noro, S.-i., Functional Porous Coordination Polymers. *Angew. Chem. Int. Ed.* **2004,** *43* (18), 2334-2375.
12. Dang, S.; Zhu, Q.-L.; Xu, Q., Nanomaterials derived from metal–organic frameworks. *Nature Reviews Materials* **2017,** *3* (1), 17075.
13. Furukawa, H.; Ko, N.; Go, Y. B.; Aratani, N.; Choi, S. B.; Choi, E.; Yazaydin, A. Ö.; Snurr, R. Q.; O'Keeffe, M.; Kim, J.; Yaghi, O. M., Ultrahigh Porosity in Metal-Organic Frameworks. *Science* **2010,** *329* (5990), 424-428.
14. Chui, S. S.-Y.; Lo, S. M.-F.; Charmant, J. P. H.; Orpen, A. G.; Williams, I. D., A Chemically Functionalizable Nanoporous Material [Cu₃(TMA)₂(H₂O)₃]_n. *Science* **1999,** *283* (5405), 1148-1150.
15. Czaja, A. U.; Trukhan, N.; Müller, U., Industrial applications of metal–organic frameworks. *Chem. Soc. Rev.* **2009,** *38* (5), 1284-1293.
16. Loiseau, T.; Serre, C.; Huguenard, C.; Fink, G.; Taulelle, F.; Henry, M.; Bataille, T.; Férey, G., A Rationale for the Large Breathing of the Porous Aluminum Terephthalate (MIL-53) Upon Hydration. *Chem. Eur. J.* **2004,** *10* (6), 1373-1382.
17. Rosi, N. L.; Eckert, J.; Eddaoudi, M.; Vodak, D. T.; Kim, J.; O'Keeffe, M.; Yaghi, O. M., Hydrogen Storage in Microporous Metal-Organic Frameworks. *Science* **2003,** *300* (5622), 1127-1129.
18. Basnayake, S. A.; Su, J.; Zou, X.; Balkus, K. J., Carbonate-Based Zeolitic Imidazolate Framework for Highly Selective CO2 Capture. *Inorg. Chem.* **2015,** *54* (4), 1816-1821.
19. Park, K. S.; Ni, Z.; Côté, A. P.; Choi, J. Y.; Huang, R.; Uribe-Romo, F. J.; Chae, H. K.; O'Keeffe, M.; Yaghi, O. M., Exceptional chemical and thermal stability of zeolitic imidazolate frameworks. *Proceedings of the National Academy of Sciences* **2006,** *103* (27), 10186-10191.

20. Chen, B.; Yang, Z.; Zhu, Y.; Xia, Y., Zeolitic imidazolate framework materials: recent progress in synthesis and applications. *Journal of Materials Chemistry A* **2014,** *2* (40), 16811-16831.
21. Moggach, S. A.; Bennett, T. D.; Cheetham, A. K., The Effect of Pressure on ZIF-8: Increasing Pore Size with Pressure and the Formation of a High-Pressure Phase at 1.47 GPa. *Angew. Chem. Int. Ed.* **2009,** *48* (38), 7087-7089.
22. Fairen-Jimenez, D.; Moggach, S. A.; Wharmby, M. T.; Wright, P. A.; Parsons, S.; Düren, T., Opening the Gate: Framework Flexibility in ZIF-8 Explored by Experiments and Simulations. *J. Am. Chem. Soc.* **2011,** *133* (23), 8900-8902.
23. Bergaoui, M.; Khalfaoui, M.; Awadallah-F, A.; Al-Muhtaseb, S., A review of the features and applications of ZIF-8 and its derivatives for separating CO2 and isomers of C3- and C4-hydrocarbons. *Journal of Natural Gas Science and Engineering* **2021,** *96*, 104289.
24. Aceituno Melgar, V. M.; Kim, J.; Othman, M. R., Zeolitic imidazolate framework membranes for gas separation: A review of synthesis methods and gas separation performance. *Journal of Industrial and Engineering Chemistry* **2015,** *28*, 1-15.
25. Phan, A.; Doonan, C. J.; Uribe-Romo, F. J.; Knobler, C. B.; O'Keeffe, M.; Yaghi, O. M., Synthesis, Structure, and Carbon Dioxide Capture Properties of Zeolitic Imidazolate Frameworks. *Accounts of Chemical Research* **2010,** *43* (1), 58-67.
26. Nguyen, L. T. L.; Le, K. K. A.; Phan, N. T. S., A Zeolite Imidazolate Framework ZIF-8 Catalyst for Friedel-Crafts Acylation. *Chinese Journal of Catalysis* **2012,** *33* (4), 688-696.
27. Kalidindi, S. B.; Esken, D.; Fischer, R. A., B□N Chemistry@ZIF-8: Dehydrocoupling of Dimethylamine Borane at Room Temperature by Size-Confinement Effects. *Chem. Eur. J.* **2011,** *17* (24), 6594-6597.
28. Lu, G.; Hupp, J. T., Metal−Organic Frameworks as Sensors: A ZIF-8 Based Fabry−Pérot Device as a Selective Sensor for Chemical Vapors and Gases. *J. Am. Chem. Soc.* **2010,** *132* (23), 7832-7833.
29. Ma, W.; Jiang, Q.; Yu, P.; Yang, L.; Mao, L., Zeolitic Imidazolate Framework-Based Electrochemical Biosensor for in Vivo Electrochemical Measurements. *Anal. Chem.* **2013,** *85* (15), 7550-7557.
30. Hashim, M. I.; Hsu, C.-W.; Le, H. T. M.; Miljanić, O. Š., Organic Molecules with Porous Crystal Structures. *Synlett* **2016,** *27* (13), 1907-1918.
31. Tian, J.; Thallapally, P. K.; McGrail, B. P., Porous organic molecular materials. *CrystEngComm* **2012,** *14* (6), 1909-1919.
32. McKeown, N. B., Nanoporous molecular crystals. *J. Mater. Chem.* **2010,** *20* (47), 10588-10597.
33. Yamagishi, H.; Nakajima, S.; Yoo, J.; Okazaki, M.; Takeda, Y.; Minakata, S.; Albrecht, K.; Yamamoto, K.; Badía-Domínguez, I.; Oliva, M. M.; Delgado, M. C. R.; Ikemoto, Y.; Sato, H.; Imoto, K.; Nakagawa, K.; Tokoro, H.; Ohkoshi, S.-i.; Yamamoto, Y., Sigmoidally hydrochromic molecular porous crystal with rotatable dendrons. *Commun. Chem.* **2020,** *3* (1), 118.
34. Jones, J. T. A.; Holden, D.; Mitra, T.; Hasell, T.; Adams, D. J.; Jelfs, K. E.; Trewin, A.; Willock, D. J.; Day, G. M.; Bacsa, J.; Steiner, A.; Cooper, A. I., On–Off Porosity Switching in a Molecular Organic Solid. *Angew. Chem. Int. Ed.* **2011,** *50* (3), 749-753.
35. Holst, J. R.; Trewin, A.; Cooper, A. I., *Nat. Chem.* **2010,** *2*, 915.
36. Hisaki, I.; Xin, C.; Takahashi, K.; Nakamura, T., Designing Hydrogen-Bonded Organic Frameworks (HOFs) with Permanent Porosity. *Angew. Chem. Int. Ed.* **2019,** *58* (33), 11160-11170.
37. Lin, R.-B.; He, Y.; Li, P.; Wang, H.; Zhou, W.; Chen, B., Multifunctional porous hydrogen-bonded organic framework materials. *Chem. Soc. Rev.* **2019,** *48* (5), 1362-1389.
38. Li, P.; Ryder, M. R.; Stoddart, J. F., Hydrogen-Bonded Organic Frameworks: A Rising Class of Porous Molecular Materials. *Accounts of Materials Research* **2020,** *1* (1), 77-87.
39. He, Y.; Xiang, S.; Chen, B., A Microporous Hydrogen-Bonded Organic Framework for Highly Selective C2H2/C2H4 Separation at Ambient Temperature. *J. Am. Chem. Soc.* **2011,** *133* (37), 14570-14573.

40. Lenz, A.; Ojamäe, L., Structures of the I-, II- and H-Methane Clathrates and the Ice−Methane Clathrate Phase Transition from Quantum-Chemical Modeling with Force-Field Thermal Corrections. *The Journal of Physical Chemistry A* **2011,** *115* (23), 6169-6176.
41. Yang, W.; Greenaway, A.; Lin, X.; Matsuda, R.; Blake, A. J.; Wilson, C.; Lewis, W.; Hubberstey, P.; Kitagawa, S.; Champness, N. R.; Schröder, M., Exceptional Thermal Stability in a Supramolecular Organic Framework: Porosity and Gas Storage. *J. Am. Chem. Soc.* **2010,** *132* (41), 14457-14469.
42. Luo, X.-Z.; Jia, X.-J.; Deng, J.-H.; Zhong, J.-L.; Liu, H.-J.; Wang, K.-J.; Zhong, D.-C., A Microporous Hydrogen-Bonded Organic Framework: Exceptional Stability and Highly Selective Adsorption of Gas and Liquid. *J. Am. Chem. Soc.* **2013,** *135* (32), 11684-11687.
43. Nandi, S.; Chakraborty, D.; Vaidhyanathan, R., A permanently porous single molecule H-bonded organic framework for selective CO2 capture. *Chem. Commun.* **2016,** *52* (45), 7249-7252.
44. Yang, W.; Wang, J.; Wang, H.; Bao, Z.; Zhao, J. C.-G.; Chen, B., Highly Interpenetrated Robust Microporous Hydrogen-Bonded Organic Framework for Gas Separation. *Crystal Growth & Design* **2017,** *17* (11), 6132-6137.
45. Hu, F.; Liu, C.; Wu, M.; Pang, J.; Jiang, F.; Yuan, D.; Hong, M., An Ultrastable and Easily Regenerated Hydrogen-Bonded Organic Molecular Framework with Permanent Porosity. *Angew. Chem. Int. Ed.* **2017,** *56* (8), 2101-2104.
46. Li, P.; He, Y.; Zhao, Y.; Weng, L.; Wang, H.; Krishna, R.; Wu, H.; Zhou, W.; O'Keeffe, M.; Han, Y.; Chen, B., A Rod-Packing Microporous Hydrogen-Bonded Organic Framework for Highly Selective Separation of C2H2/CO2 at Room Temperature. *Angew. Chem. Int. Ed.* **2015,** *54* (2), 574-577.
47. Sarkar, C.; Shit, S. C.; Das, N.; Mondal, J., Presenting porous–organic–polymers as next-generation invigorating materials for nanoreactors. *Chem. Commun.* **2021,** *57* (69), 8550-8567.
48. Zhang, Y.; Riduan, S. N., Functional porous organic polymers for heterogeneous catalysis. *Chem. Soc. Rev.* **2012,** *41* (6), 2083-2094.
49. Modak, A.; Nandi, M.; Mondal, J.; Bhaumik, A., Porphyrin based porous organic polymers: novel synthetic strategy and exceptionally high CO2 adsorption capacity. *Chem. Commun.* **2012,** *48* (2), 248-250.
50. Paul, R.; Sarkar, C.; Yan, Y.; Trinh, Q. T.; Rao, B. S.; Pao, C.-W.; Lee, J.-F.; Liu, W.; Mondal, J., Porous-Organic-Polymer-Triggered Advancement of Sustainable Magnetic Efficient Catalyst for Chemoselective Hydrogenation of Cinnamaldehyde. *ChemCatChem* **2020,** *12* (14), 3687-3704.
51. Paul, R.; Shit, S. C.; Fovanna, T.; Ferri, D.; Srinivasa Rao, B.; Gunasooriya, G. T. K. K.; Dao, D. Q.; Le, Q. V.; Shown, I.; Sherburne, M. P.; Trinh, Q. T.; Mondal, J., Realizing Catalytic Acetophenone Hydrodeoxygenation with Palladium-Equipped Porous Organic Polymers. *Appl. Mater. Interfaces* **2020,** *12* (45), 50550-50565.
52. Kim, K.; Kim, S.; Talapaneni, S. N.; Buyukcakir, O.; Almutawa, A. M. I.; Polychronopoulou, K.; Coskun, A., Transition metal complex directed synthesis of porous cationic polymers for efficient CO2 capture and conversion. *Polymer* **2017,** *126*, 296-302.
53. Kundu, S. K.; Bhaumik, A., Pyrene-Based Porous Organic Polymers as Efficient Catalytic Support for the Synthesis of Biodiesels at Room Temperature. *ACS Sustainable Chemistry & Engineering* **2015,** *3* (8), 1715-1723.
54. Chen, Q.; Luo, M.; Hammershøj, P.; Zhou, D.; Han, Y.; Laursen, B. W.; Yan, C.-G.; Han, B.-H., Microporous Polycarbazole with High Specific Surface Area for Gas Storage and Separation. *J. Am. Chem. Soc.* **2012,** *134* (14), 6084-6087.
55. Jin, T.; Xiong, Y.; Zhu, X.; Tian, Z.; Tao, D.-J.; Hu, J.; Jiang, D.-e.; Wang, H.; Liu, H.; Dai, S., Rational design and synthesis of a porous, task-specific polycarbazole for efficient CO2 capture. *Chem. Commun.* **2016,** *52* (24), 4454-4457.
56. Wang, J.; Huang, J.; Wu, X.; Yuan, B.; Sun, Y.; Zeng, Z.; Deng, S., Effect of nitrogen group on selective separation of CO2/N2 in porous polystyrene. *Chem. Eng. J.* **2014,** *256*, 390-397.

57. Chen, J.; Li, H.; Zhong, M.; Yang, Q., Hierarchical mesoporous organic polymer with an intercalated metal complex for the efficient synthesis of cyclic carbonates from flue gas. *Green Chemistry* **2016,** *18* (24), 6493-6500.
58. Bildirir, H.; Gregoriou, V. G.; Avgeropoulos, A.; Scherf, U.; Chochos, C. L., Porous organic polymers as emerging new materials for organic photovoltaic applications: current status and future challenges. *Materials Horizons* **2017,** *4* (4), 546-556.
59. Wood, C. D.; Tan, B.; Trewin, A.; Niu, H.; Bradshaw, D.; Rosseinsky, M. J.; Khimyak, Y. Z.; Campbell, N. L.; Kirk, R.; Stöckel, E.; Cooper, A. I., Hydrogen Storage in Microporous Hypercrosslinked Organic Polymer Networks. *Chem. Mater.* **2007,** *19* (8), 2034-2048.
60. Ahn, J.-H.; Jang, J.-E.; Oh, C.-G.; Ihm, S.-K.; Cortez, J.; Sherrington, D. C., Rapid Generation and Control of Microporosity, Bimodal Pore Size Distribution, and Surface Area in Davankov-Type Hyper-Cross-Linked Resins. *Macromolecules* **2006,** *39* (2), 627-632.
61. Lee, J.-Y.; Wood, C. D.; Bradshaw, D.; Rosseinsky, M. J.; Cooper, A. I., Hydrogen adsorption in microporous hypercrosslinked polymers. *Chem. Commun.* **2006,** (25), 2670-2672.
62. Jiang, J.-X.; Su, F.; Trewin, A.; Wood, C. D.; Campbell, N. L.; Niu, H.; Dickinson, C.; Ganin, A. Y.; Rosseinsky, M. J.; Khimyak, Y. Z.; Cooper, A. I., Conjugated Microporous Poly(aryleneethynylene) Networks. *Angew. Chem. Int. Ed.* **2007,** *46* (45), 8574-8578.
63. Sprick, R. S.; Jiang, J.-X.; Bonillo, B.; Ren, S.; Ratvijitvech, T.; Guiglion, P.; Zwijnenburg, M. A.; Adams, D. J.; Cooper, A. I., Tunable Organic Photocatalysts for Visible-Light-Driven Hydrogen Evolution. *J. Am. Chem. Soc.* **2015,** *137* (9), 3265-3270.
64. Ben, T.; Ren, H.; Ma, S. Q.; Cao, D. P.; Lan, J. H.; Jing, X. F.; Wang, W. C.; Xu, J.; Deng, F.; Simmons, J. M.; Qiu, S. L.; Zhu, G. S., Targeted Synthesis of a Porous Aromatic Framework with High Stability and Exceptionally High Surface Area. *Angew. Chem. Int. Ed.* **2009,** *48* (50), 9457-9460.
65. Jing, X.; Sun, F.; Ren, H.; Tian, Y.; Guo, M.; Li, L.; Zhu, G., Targeted synthesis of micro–mesoporous hybrid material derived from octaphenylsilsesquioxane building units. *Microporous Mesoporous Mater.* **2013,** *165*, 92-98.
66. Li, M.; Ren, H.; Sun, F.; Tian, Y.; Zhu, Y.; Li, J.; Mu, X.; Xu, J.; Deng, F.; Zhu, G., Construction of Porous Aromatic Frameworks with Exceptional Porosity via Building Unit Engineering. *Adv. Mater.* **2018,** *30* (43), 1804169.
67. Rose, M.; Klein, N.; Böhlmann, W.; Böhringer, B.; Fichtner, S.; Kaskel, S., New element organic frameworks viaSuzuki coupling with high adsorption capacity for hydrophobic molecules. *Soft Matter* **2010,** *6* (16), 3918-3923.
68. Ren, H.; Ben, T.; Wang, E.; Jing, X.; Xue, M.; Liu, B.; Cui, Y.; Qiu, S.; Zhu, G., Targeted synthesis of a 3D porous aromatic framework for selective sorption of benzene. *Chem. Commun.* **2010,** *46* (2), 291-293.
69. Meng, S.; Ma, H.; Jiang, L.; Ren, H.; Zhu, G., A facile approach to prepare porphyrinic porous aromatic frameworks for small hydrocarbon separation. *Journal of Materials Chemistry A* **2014,** *2* (35), 14536-14541.
70. Yan, Z.; Ren, H.; Ma, H.; Yuan, R.; Yuan, Y.; Zou, X.; Sun, F.; Zhu, G., Construction and sorption properties of pyrene-based porous aromatic frameworks. *Microporous Mesoporous Mater.* **2013,** *173*, 92-98.
71. Wang, L.; Jia, J.; Faheem, M.; Tian, Y.; Zhu, G., Fabrication of triazine-based Porous Aromatic Framework (PAF) membrane with structural flexibility for gas mixtures separation. *Journal of Industrial and Engineering Chemistry* **2018,** *67*, 373-379.
72. Zhang, L.; Sun, J.-S.; Sun, F.; Chen, P.; Liu, J.; Zhu, G., Facile Synthesis of Ultrastable Porous Aromatic Frameworks by Suzuki–Miyaura Coupling Reaction for Adsorption Removal of Organic Dyes. *Chem. Eur. J.* **2019,** *25* (15), 3903-3908.
73. Ben, T.; Pei, C.; Zhang, D.; Xu, J.; Deng, F.; Jing, X.; Qiu, S., Gas storage in porous aromatic frameworks (PAFs). *Energy & Environmental Science* **2011,** *4* (10), 3991-3999.
74. Yuan, D.; Lu, W.; Zhao, D.; Zhou, H.-C., Highly Stable Porous Polymer Networks with Exceptionally High Gas-Uptake Capacities. *Adv. Mater.* **2011,** *23* (32), 3723-3725.

75. Fischer, S.; Schmidt, J.; Strauch, P.; Thomas, A., An Anionic Microporous Polymer Network Prepared by the Polymerization of Weakly Coordinating Anions. *Angew. Chem. Int. Ed.* **2013,** *52* (46), 12174-12178.
76. Yan, Z.; Yuan, Y.; Tian, Y.; Zhang, D.; Zhu, G., Highly Efficient Enrichment of Volatile Iodine by Charged Porous Aromatic Frameworks with Three Sorption Sites. *Angew. Chem. Int. Ed.* **2015,** *54* (43), 12733-12737.
77. Fischer, S.; Schimanowitz, A.; Dawson, R.; Senkovska, I.; Kaskel, S.; Thomas, A., Cationic microporous polymer networks by polymerisation of weakly coordinating cations with CO2-storage ability. *Journal of Materials Chemistry A* **2014,** *2* (30), 11825-11829.
78. Lan, J.; Cao, D.; Wang, W.; Ben, T.; Zhu, G., High-Capacity Hydrogen Storage in Porous Aromatic Frameworks with Diamond-like Structure. *The Journal of Physical Chemistry Letters* **2010,** *1* (6), 978-981.
79. Lukose, B.; Wahiduzzaman, M.; Kuc, A.; Heine, T., Mechanical, Electronic, and Adsorption Properties of Porous Aromatic Frameworks. *The Journal of Physical Chemistry C* **2012,** *116* (43), 22878-22884.
80. Lu, W.; Yuan, D.; Zhao, D.; Schilling, C. I.; Plietzsch, O.; Muller, T.; Bräse, S.; Guenther, J.; Blümel, J.; Krishna, R.; Li, Z.; Zhou, H.-C., Porous Polymer Networks: Synthesis, Porosity, and Applications in Gas Storage/Separation. *Chem. Mater.* **2010,** *22* (21), 5964-5972.
81. Totten, R. K.; Olenick, L. L.; Kim, Y.-S.; Chakraborty, S.; Weston, M. H.; Farha, O. K.; Hupp, J. T.; Nguyen, S. T., A dual approach to tuning the porosity of porous organic polymers: controlling the porogen size and supercritical CO2 processing. *Chemical Science* **2014,** *5* (2), 782-787.
82. Bunz, U. H. F., Poly(aryleneethynylene)s: Syntheses, Properties, Structures, and Applications. *Chemical Reviews* **2000,** *100* (4), 1605-1644.
83. Sun, L.; Liang, Z.; Yu, J.; Xu, R., Luminescent microporous organic polymers containing the 1,3,5-tri(4-ethenylphenyl)benzene unit constructed by Heck coupling reaction. *Polymer Chemistry* **2013,** *4* (6), 1932-1938.
84. Yuan, Y.; Yang, Y.; Faheem, M.; Zou, X.; Ma, X.; Wang, Z.; Meng, Q.; Wang, L.; Zhao, S.; Zhu, G., Molecularly Imprinted Porous Aromatic Frameworks Serving as Porous Artificial Enzymes. *Adv. Mater.* **2018,** *30* (27), 1800069.
85. Wang, L.; Wan, Y.; Ding, Y.; Wu, S.; Zhang, Y.; Zhang, X.; Zhang, G.; Xiong, Y.; Wu, X.; Yang, J.; Xu, H., Conjugated Microporous Polymer Nanosheets for Overall Water Splitting Using Visible Light. *Adv. Mater.* **2017,** *29* (38), 1702428.
86. Zhao, H.; Jin, Z.; Su, H.; Jing, X.; Sun, F.; Zhu, G., Targeted synthesis of a 2D ordered porous organic framework for drug release. *Chem. Commun.* **2011,** *47* (22), 6389-6391.
87. Zhao, H.; Jin, Z.; Su, H.; Zhang, J.; Yao, X.; Zhao, H.; Zhu, G., Target synthesis of a novel porous aromatic framework and its highly selective separation of CO2/CH4. *Chem. Commun.* **2013,** *49* (27), 2780-2782.
88. Patel, H. A.; Je, S. H.; Park, J.; Jung, Y.; Coskun, A.; Yavuz, C. T., Directing the Structural Features of N2-Phobic Nanoporous Covalent Organic Polymers for CO2 Capture and Separation. *Chem. Eur. J.* **2014,** *20* (3), 772-780.
89. Patel, H. A.; Hyun Je, S.; Park, J.; Chen, D. P.; Jung, Y.; Yavuz, C. T.; Coskun, A., Unprecedented high-temperature CO2 selectivity in N2-phobic nanoporous covalent organic polymers. *Nat. Commun.* **2013,** *4* (1), 1357.
90. Li, L.; Zhao, H.; Wang, R., Tailorable Synthesis of Porous Organic Polymers Decorating Ultrafine Palladium Nanoparticles for Hydrogenation of Olefins. *ACS Catalysis* **2015,** *5* (2), 948-955.
91. Pandey, P.; Farha, O. K.; Spokoyny, A. M.; Mirkin, C. A.; Kanatzidis, M. G.; Hupp, J. T.; Nguyen, S. T., A “click-based” porous organic polymer from tetrahedral building blocks. *J. Mater. Chem.* **2011,** *21* (6), 1700-1703.
92. Jing, X.; Zou, D.; Cui, P.; Ren, H.; Zhu, G., Facile synthesis of cost-effective porous aromatic materials with enhanced carbon dioxide uptake. *Journal of Materials Chemistry A* **2013,** *1* (44), 13926-13931.

93. Li, L.; Ren, H.; Yuan, Y.; Yu, G.; Zhu, G., Construction and adsorption properties of porous aromatic frameworks via AlCl3-triggered coupling polymerization. *Journal of Materials Chemistry A* **2014,** *2* (29), 11091-11098.
94. Ma, H.; Ren, H.; Zou, X.; Sun, F.; Yan, Z.; Cai, K.; Wang, D.; Zhu, G., Novel lithium-loaded porous aromatic framework for efficient CO2 and H2 uptake. *Journal of Materials Chemistry A* **2013,** *1* (3), 752-758.
95. Yuan, R.; Ren, H.; Yan, Z.; Wang, A.; Zhu, G., Robust tri(4-ethynylphenyl)amine-based porous aromatic frameworks for carbon dioxide capture. *Polymer Chemistry* **2014,** *5* (7), 2266-2272.
96. Ma, H.; Ren, H.; Zou, X.; Meng, S.; Sun, F.; Zhu, G., Post-metalation of porous aromatic frameworks for highly efficient carbon capture from CO2 + N2 and CH4 + N2 mixtures. *Polymer Chemistry* **2014,** *5* (1), 144-152.
97. Hei, Z.-H.; Huang, M.-H.; Luo, Y.; Wang, Y., A well-defined nitro-functionalized aromatic framework (NO2-PAF-1) with high CO2 adsorption: synthesis via the copper-mediated Ullmann homo-coupling polymerization of a nitro-containing monomer. *Polymer Chemistry* **2016,** *7* (4), 770-774.
98. Lu, W.; Yuan, D.; Sculley, J.; Zhao, D.; Krishna, R.; Zhou, H.-C., Sulfonate-Grafted Porous Polymer Networks for Preferential CO2 Adsorption at Low Pressure. *J. Am. Chem. Soc.* **2011,** *133* (45), 18126-18129.
99. Merino, E.; Verde-Sesto, E.; Maya, E. M.; Iglesias, M.; Sánchez, F.; Corma, A., Synthesis of Structured Porous Polymers with Acid and Basic Sites and Their Catalytic Application in Cascade-Type Reactions. *Chem. Mater.* **2013,** *25* (6), 981-988.
100. Islamoglu, T.; Kim, T.; Kahveci, Z.; El-Kadri, O. M.; El-Kaderi, H. M., Systematic Postsynthetic Modification of Nanoporous Organic Frameworks for Enhanced CO2 Capture from Flue Gas and Landfill Gas. *The Journal of Physical Chemistry C* **2016,** *120* (5), 2592-2599.
101. Li, B.; Sun, Q.; Zhang, Y.; Abney, C. W.; Aguila, B.; Lin, W.; Ma, S., Functionalized Porous Aromatic Framework for Efficient Uranium Adsorption from Aqueous Solutions. *Appl. Mater. Interfaces* **2017,** *9* (14), 12511-12517.
102. Rangel-Rangel, E.; Verde-Sesto, E.; Rasero-Almansa, A. M.; Iglesias, M.; Sánchez, F., Porous aromatic frameworks (PAFs) as efficient supports for N-heterocyclic carbene catalysts. *Catal. Sci. Technol.* **2016,** *6* (15), 6037-6045.
103. Lu, W. G.; Yuan, D. Q.; Zhao, D.; Schilling, C. I.; Plietzsch, O.; Muller, T.; Brase, S.; Guenther, J.; Blumel, J.; Krishna, R.; Li, Z.; Zhou, H. C., Porous Polymer Networks: Synthesis, Porosity, and Applications in Gas Storage/Separation. *Chem. Mater.* **2010,** *22* (21), 5964-5972.
104. Pei, C.; Ben, T.; Li, Y.; Qiu, S., Synthesis of copolymerized porous organic frameworks with high gas storage capabilities at both high and low pressures. *Chem. Commun.* **2014,** *50* (46), 6134-6136.
105. Wang, W.; Ren, H.; Sun, F.; Cai, K.; Ma, H.; Du, J.; Zhao, H.; Zhu, G., Synthesis of porous aromatic framework with tuning porosity via ionothermal reaction. *Dalton Transactions* **2012,** *41* (14), 3933-3936.
106. Jiang, L.; Tian, Y.; Sun, T.; Zhu, Y.; Ren, H.; Zou, X.; Ma, Y.; Meihaus, K. R.; Long, J. R.; Zhu, G., A Crystalline Polyimide Porous Organic Framework for Selective Adsorption of Acetylene over Ethylene. *J. Am. Chem. Soc.* **2018,** *140* (46), 15724-15730.
107. Li, B.; Zhang, Y.; Krishna, R.; Yao, K.; Han, Y.; Wu, Z.; Ma, D.; Shi, Z.; Pham, T.; Space, B.; Liu, J.; Thallapally, P. K.; Liu, J.; Chrzanowski, M.; Ma, S., Introduction of π-Complexation into Porous Aromatic Framework for Highly Selective Adsorption of Ethylene over Ethane. *J. Am. Chem. Soc.* **2014,** *136* (24), 8654-8660.
108. Xu, S.; Roy, S.; Ben, T.; Pei, C.; Qiu, S., Enhanced recognition of a nitrogen containing organic compound by adjusting the acidity of the porous organic frameworks base (JUC-Z2). *Journal of Materials Chemistry A* **2015,** *3* (6), 2628-2633.

109. Yuan, Y.; Sun, F.; Ren, H.; Jing, X.; Wang, W.; Ma, H.; Zhao, H.; Zhu, G., Targeted synthesis of a porous aromatic framework with a high adsorption capacity for organic molecules. *J. Mater. Chem.* **2011,** *21* (35), 13498-13502.
110. Shen, X.; Faheem, M.; Matsuo, Y.; Aziz, S.; Zhang, X.; Li, Y.; Song, J.; Tian, Y.; Zhu, G., Polarity engineering of porous aromatic frameworks for specific water contaminant capture. *Journal of Materials Chemistry A* **2019,** *7* (6), 2507-2512.
111. Li, B.; Zhang, Y.; Ma, D.; Shi, Z.; Ma, S., Mercury nano-trap for effective and efficient removal of mercury(II) from aqueous solution. *Nat. Commun.* **2014,** *5* (1), 5537.
112. Yang, Y.; Yan, Z.; Wang, L.; Meng, Q.; Yuan, Y.; Zhu, G., Constructing synergistic groups in porous aromatic frameworks for the selective removal and recovery of lead(ii) ions. *Journal of Materials Chemistry A* **2018,** *6* (12), 5202-5207.
113. Lee, S.; Barin, G.; Ackerman, C. M.; Muchenditsi, A.; Xu, J.; Reimer, J. A.; Lutsenko, S.; Long, J. R.; Chang, C. J., Copper Capture in a Thioether-Functionalized Porous Polymer Applied to the Detection of Wilson's Disease. *J. Am. Chem. Soc.* **2016,** *138* (24), 7603-7609.
114. Zhang, Y.; Li, B.; Ma, S., Dual functionalization of porous aromatic frameworks as a new platform for heterogeneous cascade catalysis. *Chem. Commun.* **2014,** *50* (62), 8507-8510.
115. Chen, P.; Sun, J.-S.; Zhang, L.; Ma, W.-Y.; Sun, F.; Zhu, G., Porous aromatic framework (PAF-1) as hyperstable platform for enantioselective organocatalysis. *Science China Materials* **2019,** *62* (2), 194-202.
116. Jiang, J.; Luo, R.; Zhou, X.; Chen, Y.; Ji, H., Photocatalytic Properties and Mechanistic Insights into Visible Light-Promoted Aerobic Oxidation of Sulfides to Sulfoxides via Tin Porphyrin-Based Porous Aromatic Frameworks. *Adv. Synth. Catal.* **2018,** *360* (22), 4402-4411.
117. Wang, X.-S.; Chrzanowski, M.; Yuan, D.; Sweeting, B. S.; Ma, S., Covalent Heme Framework as a Highly Active Heterogeneous Biomimetic Oxidation Catalyst. *Chem. Mater.* **2014,** *26* (4), 1639-1644.
118. Yuan, Y.; Ren, H.; Sun, F.; Jing, X.; Cai, K.; Zhao, X.; Wang, Y.; Wei, Y.; Zhu, G., Sensitive detection of hazardous explosives via highly fluorescent crystalline porous aromatic frameworks. *J. Mater. Chem.* **2012,** *22* (47), 24558-24562.
119. Ma, T.; Zhao, X.; Matsuo, Y.; Song, J.; Zhao, R.; Faheem, M.; Chen, M.; Zhang, Y.; Tian, Y.; Zhu, G., Fluorescein-based fluorescent porous aromatic framework for Fe3+ detection with high sensitivity. *Journal of Materials Chemistry C* **2019,** *7* (8), 2327-2332.
120. Pei, C.; Ben, T.; Xu, S.; Qiu, S., Ultrahigh iodine adsorption in porous organic frameworks. *Journal of Materials Chemistry A* **2014,** *2* (20), 7179-7187.
121. Comotti, A.; Bracco, S.; Mauri, M.; Mottadelli, S.; Ben, T.; Qiu, S.; Sozzani, P., Confined Polymerization in Porous Organic Frameworks with an Ultrahigh Surface Area. *Angew. Chem. Int. Ed.* **2012,** *51* (40), 10136-10140.
122. Peng, Y.; Ben, T.; Jia, Y.; Yang, D.; Zhao, H.; Qiu, S.; Yao, X., Dehydrogenation of Ammonia Borane Confined by Low-Density Porous Aromatic Framework. *The Journal of Physical Chemistry C* **2012,** *116* (49), 25694-25700.
123. Kundu, P. K.; Olsen, G. L.; Kiss, V.; Klajn, R., Nanoporous frameworks exhibiting multiple stimuli responsiveness. *Nat. Commun.* **2014,** *5* (1), 3588.
124. Yuan, R.; Ren, H.; He, H.; Jiang, L.; Zhu, G., Targeted synthesis of porous aromatic frameworks with stimuli-responsive adsorption properties. *Science China Materials* **2015,** *58* (1), 38-43.
125. Cote, A. P.; Benin, A. I.; Ockwig, N. W.; O'Keeffe, M.; Matzger, A. J.; Yaghi, O. M., Porous, crystalline, covalent organic frameworks. *Science* **2005,** *310* (5751), 1166-1170.
126. Yaghi, O. M., Kalmutzki M. J., Diercks C. S., *Introduction to Reticular Chemistry*. Wiley-VCH Verlag GmbH & Co. KGaA: Weinheim, Germany, 2019.
127. Feng, X.; Ding, X.; Jiang, D., Covalent organic frameworks. *Chem. Soc. Rev.* **2012,** *41* (18), 6010-6022.

128. Fang, Q.; Zhuang, Z.; Gu, S.; Kaspar, R. B.; Zheng, J.; Wang, J.; Qiu, S.; Yan, Y., Designed synthesis of large-pore crystalline polyimide covalent organic frameworks. *Nat. Commun.* **2014,** *5*, 4503.
129. Kuhn, P.; Antonietti, M.; Thomas, A., Porous, covalent triazine-based frameworks prepared by ionothermal synthesis. *Angew. Chem. Int. Ed.* **2008,** *47* (18), 3450-3453.
130. Kandambeth, S.; Shinde, D. B.; Panda, M. K.; Lukose, B.; Heine, T.; Banerjee, R., Enhancement of Chemical Stability and Crystallinity in Porphyrin-Containing Covalent Organic Frameworks by Intramolecular Hydrogen Bonds. *Angew. Chem. Int. Ed.* **2013,** *52* (49), 13052-13056.
131. Xu, H.; Gao, J.; Jiang, D., Stable, crystalline, porous, covalent organic frameworks as a platform for chiral organocatalysts. *Nature Chemistry* **2015,** *7* (11), 905-912.
132. Guo, J.; Xu, Y.; Jin, S.; Chen, L.; Kaji, T.; Honsho, Y.; Addicoat, M. A.; Kim, J.; Saeki, A.; Ihee, H.; Seki, S.; Irle, S.; Hiramoto, M.; Gao, J.; Jiang, D., Conjugated organic framework with three-dimensionally ordered stable structure and delocalized π clouds. *Nat. Commun.* **2013,** *4* (1), 2736.
133. Kandambeth, S.; Mallick, A.; Lukose, B.; Mane, M. V.; Heine, T.; Banerjee, R., Construction of Crystalline 2D Covalent Organic Frameworks with Remarkable Chemical (Acid/Base) Stability via a Combined Reversible and Irreversible Route. *J. Am. Chem. Soc.* **2012,** *134* (48), 19524-19527.
134. Campbell, N. L.; Clowes, R.; Ritchie, L. K.; Cooper, A. I., Rapid Microwave Synthesis and Purification of Porous Covalent Organic Frameworks. *Chem. Mater.* **2009,** *21* (2), 204-206.
135. Yang, S.-T.; Kim, J.; Cho, H.-Y.; Kim, S.; Ahn, W.-S., Facile synthesis of covalent organic frameworks COF-1 and COF-5 by sonochemical method. *RSC Advances* **2012,** *2* (27), 10179-10181.
136. Zhang, M.; Chen, J.; Zhang, S.; Zhou, X.; He, L.; Sheridan, M. V.; Yuan, M.; Zhang, M.; Chen, L.; Dai, X.; Ma, F.; Wang, J.; Hu, J.; Wu, G.; Kong, X.; Zhou, R.; Albrecht-Schmitt, T. E.; Chai, Z.; Wang, S., Electron Beam Irradiation as a General Approach for the Rapid Synthesis of Covalent Organic Frameworks under Ambient Conditions. *J. Am. Chem. Soc.* **2020,** *142* (20), 9169-9174.
137. Kim, S.; Park, C.; Lee, M.; Song, I.; Kim, J.; Lee, M.; Jung, J.; Kim, Y.; Lim, H.; Choi, H. C., Rapid Photochemical Synthesis of Sea-Urchin-Shaped Hierarchical Porous COF-5 and Its Lithography-Free Patterned Growth. *Adv. Funct. Mater.* **2017,** *27* (32), 1700925.
138. Kim, S.; Choi, H. C., Light-promoted synthesis of highly-conjugated crystalline covalent organic framework. *Commun. Chem.* **2019,** *2* (1), 60.
139. Biswal, B. P.; Chandra, S.; Kandambeth, S.; Lukose, B.; Heine, T.; Banerjee, R., Mechanochemical Synthesis of Chemically Stable Isoreticular Covalent Organic Frameworks. *J. Am. Chem. Soc.* **2013,** *135* (14), 5328-5331.
140. Shinde, D. B.; Aiyappa, H. B.; Bhadra, M.; Biswal, B. P.; Wadge, P.; Kandambeth, S.; Garai, B.; Kundu, T.; Kurungot, S.; Banerjee, R., A mechanochemically synthesized covalent organic framework as a proton-conducting solid electrolyte. *Journal of Materials Chemistry A* **2016,** *4* (7), 2682-2690.
141. Das, G.; Balaji Shinde, D.; Kandambeth, S.; Biswal, B. P.; Banerjee, R., Mechanosynthesis of imine, β-ketoenamine, and hydrogen-bonded imine-linked covalent organic frameworks using liquid-assisted grinding. *Chem. Commun.* **2014,** *50* (84), 12615-12618.
142. Li, Rebecca L.; Flanders, N. C.; Evans, A. M.; Ji, W.; Castano, I.; Chen, L. X.; Gianneschi, N. C.; Dichtel, W. R., Controlled growth of imine-linked two-dimensional covalent organic framework nanoparticles. *Chemical Science* **2019,** *10* (13), 3796-3801.
143. Matsumoto, M.; Dasari, R. R.; Ji, W.; Feriante, C. H.; Parker, T. C.; Marder, S. R.; Dichtel, W. R., Rapid, Low Temperature Formation of Imine-Linked Covalent Organic Frameworks Catalyzed by Metal Triflates. *J. Am. Chem. Soc.* **2017,** *139* (14), 4999-5002.
144. Huang, N.; Krishna, R.; Jiang, D., Tailor-Made Pore Surface Engineering in Covalent Organic Frameworks: Systematic Functionalization for Performance Screening. *J. Am. Chem. Soc.* **2015,** *137* (22), 7079-7082.

145. Xu, F.; Xu, H.; Chen, X.; Wu, D.; Wu, Y.; Liu, H.; Gu, C.; Fu, R.; Jiang, D., Radical Covalent Organic Frameworks: A General Strategy to Immobilize Open-Accessible Polyradicals for High-Performance Capacitive Energy Storage. *Angew. Chem. Int. Ed.* **2015,** *54* (23), 6814-6818.
146. Huang, N.; Chen, X.; Krishna, R.; Jiang, D., Two-Dimensional Covalent Organic Frameworks for Carbon Dioxide Capture through Channel-Wall Functionalization. *Angew. Chem. Int. Ed.* **2015,** *54* (10), 2986-2990.
147. Lohse, M. S.; Stassin, T.; Naudin, G.; Wuttke, S.; Ameloot, R.; De Vos, D.; Medina, D. D.; Bein, T., Sequential Pore Wall Modification in a Covalent Organic Framework for Application in Lactic Acid Adsorption. *Chem. Mater.* **2016,** *28* (2), 626-631.
148. Qian, C.; Qi, Q.-Y.; Jiang, G.-F.; Cui, F.-Z.; Tian, Y.; Zhao, X., Toward Covalent Organic Frameworks Bearing Three Different Kinds of Pores: The Strategy for Construction and COF-to-COF Transformation via Heterogeneous Linker Exchange. *J. Am. Chem. Soc.* **2017,** *139* (19), 6736-6743.
149. Waller, P. J.; AlFaraj, Y. S.; Diercks, C. S.; Jarenwattananon, N. N.; Yaghi, O. M., Conversion of Imine to Oxazole and Thiazole Linkages in Covalent Organic Frameworks. *J. Am. Chem. Soc.* **2018,** *140* (29), 9099-9103.
150. Waller, P. J.; Lyle, S. J.; Popp, T. M. O.; Diercks, C. S.; Reimer, J. A.; Yaghi, O. M., Chemical Conversion of Linkages in Covalent Organic Frameworks. *J. Am. Chem. Soc.* **2016,** *138* (48), 15519-15522.
151. Lin, S.; Diercks, C. S.; Zhang, Y.-B.; Kornienko, N.; Nichols, E. M.; Zhao, Y.; Paris, A. R.; Kim, D.; Yang, P.; Yaghi, O. M.; Chang, C. J., Covalent organic frameworks comprising cobalt porphyrins for catalytic CO₂ reduction in water. *Science* **2015,** *349* (6253), 1208-1213.
152. Diercks, C. S.; Lin, S.; Kornienko, N.; Kapustin, E. A.; Nichols, E. M.; Zhu, C.; Zhao, Y.; Chang, C. J.; Yaghi, O. M., Reticular Electronic Tuning of Porphyrin Active Sites in Covalent Organic Frameworks for Electrocatalytic Carbon Dioxide Reduction. *J. Am. Chem. Soc.* **2018,** *140* (3), 1116-1122.
153. Xu, H.; Tao, S.; Jiang, D., Proton conduction in crystalline and porous covalent organic frameworks. *Nature Materials* **2016,** *15* (7), 722-726.
154. Rodríguez-San-Miguel, D.; Yazdi, A.; Guillerm, V.; Pérez-Carvajal, J.; Puntes, V.; Maspoch, D.; Zamora, F., Confining Functional Nanoparticles into Colloidal Imine-Based COF Spheres by a Sequential Encapsulation–Crystallization Method. *Chem. Eur. J.* **2017,** *23* (36), 8623-8627.
155. Furukawa, H.; Yaghi, O. M., Storage of Hydrogen, Methane, and Carbon Dioxide in Highly Porous Covalent Organic Frameworks for Clean Energy Applications. *J. Am. Chem. Soc.* **2009,** *131* (25), 8875-8883.
156. Mendoza-Cortes, J. L.; Goddard, W. A.; Furukawa, H.; Yaghi, O. M., A Covalent Organic Framework that Exceeds the DOE 2015 Volumetric Target for H2 Uptake at 298 K. *The Journal of Physical Chemistry Letters* **2012,** *3* (18), 2671-2675.
157. Lan, J.; Cao, D.; Wang, W., High Uptakes of Methane in Li-Doped 3D Covalent Organic Frameworks. *Langmuir* **2010,** *26* (1), 220-226.
158. Stegbauer, L.; Hahn, M. W.; Jentys, A.; Savasci, G.; Ochsenfeld, C.; Lercher, J. A.; Lotsch, B. V., Tunable Water and CO2 Sorption Properties in Isostructural Azine-Based Covalent Organic Frameworks through Polarity Engineering. *Chem. Mater.* **2015,** *27* (23), 7874-7881.
159. Doonan, C. J.; Tranchemontagne, D. J.; Glover, T. G.; Hunt, J. R.; Yaghi, O. M., Exceptional ammonia uptake by a covalent organic framework. *Nature Chemistry* **2010,** *2* (3), 235-238.
160. Yang, Y.; Faheem, M.; Wang, L.; Meng, Q.; Sha, H.; Yang, N.; Yuan, Y.; Zhu, G., Surface Pore Engineering of Covalent Organic Frameworks for Ammonia Capture through Synergistic Multivariate and Open Metal Site Approaches. *ACS Central Science* **2018,** *4* (6), 748-754.
161. Gao, C.; Li, J.; Yin, S.; Lin, G.; Ma, T.; Meng, Y.; Sun, J.; Wang, C., Isostructural Three-Dimensional Covalent Organic Frameworks. *Angew. Chem. Int. Ed.* **2019,** *58* (29), 9770-9775.

162. Vyas, V. S.; Haase, F.; Stegbauer, L.; Savasci, G.; Podjaski, F.; Ochsenfeld, C.; Lotsch, B. V., A tunable azine covalent organic framework platform for visible light-induced hydrogen generation. *Nat. Commun.* **2015,** *6* (1), 8508.
163. Wei, P.-F.; Qi, M.-Z.; Wang, Z.-P.; Ding, S.-Y.; Yu, W.; Liu, Q.; Wang, L.-K.; Wang, H.-Z.; An, W.-K.; Wang, W., Benzoxazole-Linked Ultrastable Covalent Organic Frameworks for Photocatalysis. *J. Am. Chem. Soc.* **2018,** *140* (13), 4623-4631.
164. Zhi, Y.; Li, Z.; Feng, X.; Xia, H.; Zhang, Y.; Shi, Z.; Mu, Y.; Liu, X., Covalent organic frameworks as metal-free heterogeneous photocatalysts for organic transformations. *Journal of Materials Chemistry A* **2017,** *5* (44), 22933-22938.
165. Ma, W.; Yu, P.; Ohsaka, T.; Mao, L., An efficient electrocatalyst for oxygen reduction reaction derived from a Co-porphyrin-based covalent organic framework. *Electrochem. Commun.* **2015,** *52*, 53-57.
166. Nandi, S.; Singh, S. K.; Mullangi, D.; Illathvalappil, R.; George, L.; Vinod, C. P.; Kurungot, S.; Vaidhyanathan, R., Low Band Gap Benzimidazole COF Supported Ni3N as Highly Active OER Catalyst. *Advanced Energy Materials* **2016,** *6* (24), 1601189.
167. Sun, Q.; Aguila, B.; Ma, S., A bifunctional covalent organic framework as an efficient platform for cascade catalysis. *Materials Chemistry Frontiers* **2017,** *1* (7), 1310-1316.
168. Fang, Q. R.; Gu, S.; Zheng, J.; Zhuang, Z. B.; Qiu, S. L.; Yan, Y. S., 3D Microporous Base-Functionalized Covalent Organic Frameworks for Size-Selective Catalysis. *Angew. Chem. Int. Ed.* **2014,** *53* (11), 2878-2882.
169. Hou, Y.; Zhang, X.; Sun, J.; Lin, S.; Qi, D.; Hong, R.; Li, D.; Xiao, X.; Jiang, J., Good Suzuki-coupling reaction performance of Pd immobilized at the metal-free porphyrin-based covalent organic framework. *Microporous Mesoporous Mater.* **2015,** *214*, 108-114.
170. Ding, S.-Y.; Gao, J.; Wang, Q.; Zhang, Y.; Song, W.-G.; Su, C.-Y.; Wang, W., Construction of Covalent Organic Framework for Catalysis: Pd/COF-LZU1 in Suzuki–Miyaura Coupling Reaction. *J. Am. Chem. Soc.* **2011,** *133* (49), 19816-19822.
171. Mu, M.; Wang, Y.; Qin, Y.; Yan, X.; Li, Y.; Chen, L., Two-Dimensional Imine-Linked Covalent Organic Frameworks as a Platform for Selective Oxidation of Olefins. *Appl. Mater. Interfaces* **2017,** *9* (27), 22856-22863.
172. Pachfule, P.; Kandambeth, S.; Díaz Díaz, D.; Banerjee, R., Highly stable covalent organic framework–Au nanoparticles hybrids for enhanced activity for nitrophenol reduction. *Chem. Commun.* **2014,** *50* (24), 3169-3172.
173. Vardhan, H.; Hou, L.; Yee, E.; Nafady, A.; Al-Abdrabalnabi, M. A.; Al-Enizi, A. M.; Pan, Y.; Yang, Z.; Ma, S., Vanadium Docked Covalent-Organic Frameworks: An Effective Heterogeneous Catalyst for Modified Mannich-Type Reaction. *ACS Sustainable Chemistry & Engineering* **2019,** *7* (5), 4878-4888.
174. Lyu, H.; Diercks, C. S.; Zhu, C.; Yaghi, O. M., Porous Crystalline Olefin-Linked Covalent Organic Frameworks. *J. Am. Chem. Soc.* **2019,** *141* (17), 6848-6852.
175. Yang, Y.; Börjesson, K., Electroactive covalent organic frameworks: a new choice for organic electronics. *Trends in Chemistry* **2021**.
176. Yang, Y.; Mallick, S.; Izquierdo-Ruiz, F.; Schäfer, C.; Xing, X.; Rahm, M.; Börjesson, K., A Highly Conductive All-Carbon Linked 3D Covalent Organic Framework Film. *Small* **2021,** *17* (40), 2103152.
177. Feng, X.; Liu, L.; Honsho, Y.; Saeki, A.; Seki, S.; Irle, S.; Dong, Y.; Nagai, A.; Jiang, D., High-Rate Charge-Carrier Transport in Porphyrin Covalent Organic Frameworks: Switching from Hole to Electron to Ambipolar Conduction. *Angew. Chem. Int. Ed.* **2012,** *51* (11), 2618-2622.
178. Ding, X.; Guo, J.; Feng, X.; Honsho, Y.; Guo, J.; Seki, S.; Maitarad, P.; Saeki, A.; Nagase, S.; Jiang, D., Synthesis of Metallophthalocyanine Covalent Organic Frameworks That Exhibit High Carrier Mobility and Photoconductivity. *Angew. Chem. Int. Ed.* **2011,** *50* (6), 1289-1293.
179. Fernandes, S. P. S.; Romero, V.; Espiña, B.; Salonen, L. M., Tailoring Covalent Organic Frameworks To Capture Water Contaminants. *Chem. Eur. J.* **2019,** *25* (26), 6461- 6473.

180. Li, Z.; Zhang, Y.; Xia, H.; Mu, Y.; Liu, X., A robust and luminescent covalent organic framework as a highly sensitive and selective sensor for the detection of Cu2+ ions. *Chem. Commun.* **2016,** *52* (39), 6613-6616.
181. Ding, S.-Y.; Dong, M.; Wang, Y.-W.; Chen, Y.-T.; Wang, H.-Z.; Su, C.-Y.; Wang, W., Thioether-Based Fluorescent Covalent Organic Framework for Selective Detection and Facile Removal of Mercury(II). *J. Am. Chem. Soc.* **2016,** *138* (9), 3031-3037.
182. Zhang, W.; Qiu, L.-G.; Yuan, Y.-P.; Xie, A.-J.; Shen, Y.-H.; Zhu, J.-F., Microwave-assisted synthesis of highly fluorescent nanoparticles of a melamine-based porous covalent organic framework for trace-level detection of nitroaromatic explosives. *J. Hazard. Mater.* **2012,** *221-222*, 147-154.
183. Fang, Q.; Wang, J.; Gu, S.; Kaspar, R. B.; Zhuang, Z.; Zheng, J.; Guo, H.; Qiu, S.; Yan, Y., 3D Porous Crystalline Polyimide Covalent Organic Frameworks for Drug Delivery. *J. Am. Chem. Soc.* **2015,** *137* (26), 8352-8355.
184. Akyuz, L., An imine based COF as a smart carrier for targeted drug delivery: From synthesis to computational studies. *Microporous Mesoporous Mater.* **2020,** *294*, 109850.
185. Kandambeth, S.; Venkatesh, V.; Shinde, D. B.; Kumari, S.; Halder, A.; Verma, S.; Banerjee, R., Self-templated chemically stable hollow spherical covalent organic framework. *Nat. Commun.* **2015,** *6* (1), 6786.
186. Kalidindi, S. B.; Oh, H.; Hirscher, M.; Esken, D.; Wiktor, C.; Turner, S.; Van Tendeloo, G.; Fischer, R. A., Metal@COFs: Covalent Organic Frameworks as Templates for Pd Nanoparticles and Hydrogen Storage Properties of Pd@COF-102 Hybrid Material. *Chem. Eur. J.* **2012,** *18* (35), 10848-10856.
187. Zhang, W.; Jiang, P.; Wang, Y.; Zhang, J.; Gao, Y.; Zhang, P., Bottom-up approach to engineer a molybdenum-doped covalent-organic framework catalyst for selective oxidation reaction. *RSC Advances* **2014,** *4* (93), 51544-51547.
188. Chen, X.; Huang, N.; Gao, J.; Xu, H.; Xu, F.; Jiang, D., Towards covalent organic frameworks with predesignable and aligned open docking sites. *Chem. Commun.* **2014,** *50* (46), 6161-6163.
189. Baldwin, L. A.; Crowe, J. W.; Pyles, D. A.; McGrier, P. L., Metalation of a Mesoporous Three-Dimensional Covalent Organic Framework. *J. Am. Chem. Soc.* **2016,** *138* (46), 15134-15137.
190. Liu, Y.; Ma, Y.; Zhao, Y.; Sun, X.; Gándara, F.; Furukawa, H.; Liu, Z.; Zhu, H.; Zhu, C.; Suenaga, K.; Oleynikov, P.; Alshammari, A. S.; Zhang, X.; Terasaki, O.; Yaghi, O. M., Weaving of organic threads into a crystalline covalent organic framework. *Science* **2016,** *351* (6271), 365-369.
191. Zhao, Y.; Guo, L.; Gándara, F.; Ma, Y.; Liu, Z.; Zhu, C.; Lyu, H.; Trickett, C. A.; Kapustin, E. A.; Terasaki, O.; Yaghi, O. M., A Synthetic Route for Crystals of Woven Structures, Uniform Nanocrystals, and Thin Films of Imine Covalent Organic Frameworks. *J. Am. Chem. Soc.* **2017,** *139* (37), 13166-13172.
192. Liu, Y.; Ma, Y.; Yang, J.; Diercks, C. S.; Tamura, N.; Jin, F.; Yaghi, O. M., Molecular Weaving of Covalent Organic Frameworks for Adaptive Guest Inclusion. *J. Am. Chem. Soc.* **2018,** *140* (47), 16015-16019.
193. Diercks, C. S.; Yaghi, O. M., The atom, the molecule, and the covalent organic framework. *Science* **2017,** *355* (6328), eaal1585.
194. Smith, B. J.; Dichtel, W. R., Mechanistic Studies of Two-Dimensional Covalent Organic Frameworks Rapidly Polymerized from Initially Homogenous Conditions. *J. Am. Chem. Soc.* **2014,** *136* (24), 8783-8789.
195. Smith, B. J.; Hwang, N.; Chavez, A. D.; Novotney, J. L.; Dichtel, W. R., Growth rates and water stability of 2D boronate ester covalent organic frameworks. *Chem. Commun.* **2015,** *51* (35), 7532-7535.
196. Smith, B. J.; Overholts, A. C.; Hwang, N.; Dichtel, W. R., Insight into the crystallization of amorphous imine-linked polymer networks to 2D covalent organic frameworks. *Chem. Commun.* **2016,** *52* (18), 3690-3693.

197. Evans, A. M.; Parent, L. R.; Flanders, N. C.; Bisbey, R. P.; Vitaku, E.; Kirschner, M. S.; Schaller, R. D.; Chen, L. X.; Gianneschi, N. C.; Dichtel, W. R., Seeded growth of single-crystal two-dimensional covalent organic frameworks. *Science* **2018,** *361* (6397), 52-57.
198. Liu, M.; Guo, L.; Jin, S.; Tan, B., Covalent triazine frameworks: synthesis and applications. *Journal of Materials Chemistry A* **2019,** *7* (10), 5153-5172.
199. Zhu, X.; Tian, C.; Mahurin, S. M.; Chai, S.-H.; Wang, C.; Brown, S.; Veith, G. M.; Luo, H.; Liu, H.; Dai, S., A Superacid-Catalyzed Synthesis of Porous Membranes Based on Triazine Frameworks for CO2 Separation. *J. Am. Chem. Soc.* **2012,** *134* (25), 10478-10484.
200. Liebl, M. R.; Senker, J., Microporous Functionalized Triazine-Based Polyimides with High CO2 Capture Capacity. *Chem. Mater.* **2013,** *25* (6), 970-980.
201. Hug, S.; Stegbauer, L.; Oh, H.; Hirscher, M.; Lotsch, B. V., Nitrogen-Rich Covalent Triazine Frameworks as High-Performance Platforms for Selective Carbon Capture and Storage. *Chem. Mater.* **2015,** *27* (23), 8001-8010.
202. Bi, J.; Fang, W.; Li, L.; Wang, J.; Liang, S.; He, Y.; Liu, M.; Wu, L., Covalent Triazine-Based Frameworks as Visible Light Photocatalysts for the Splitting of Water. *Macromol. Rapid Commun.* **2015,** *36* (20), 1799-1805.
203. Guo, L.; Niu, Y.; Xu, H.; Li, Q.; Razzaque, S.; Huang, Q.; Jin, S.; Tan, B., Engineering heteroatoms with atomic precision in donor–acceptor covalent triazine frameworks to boost photocatalytic hydrogen production. *Journal of Materials Chemistry A* **2018,** *6* (40), 19775-19781.
204. Xie, J.; Shevlin, S. A.; Ruan, Q.; Moniz, S. J. A.; Liu, Y.; Liu, X.; Li, Y.; Lau, C. C.; Guo, Z. X.; Tang, J., Efficient visible light-driven water oxidation and proton reduction by an ordered covalent triazine-based framework. *Energy & Environmental Science* **2018,** *11* (6), 1617-1624.
205. Hao, L.; Ning, J.; Luo, B.; Wang, B.; Zhang, Y.; Tang, Z.; Yang, J.; Thomas, A.; Zhi, L., Structural Evolution of 2D Microporous Covalent Triazine-Based Framework toward the Study of High-Performance Supercapacitors. *J. Am. Chem. Soc.* **2015,** *137* (1), 219-225.
206. Talapaneni, S. N.; Hwang, T. H.; Je, S. H.; Buyukcakir, O.; Choi, J. W.; Coskun, A., Elemental-Sulfur-Mediated Facile Synthesis of a Covalent Triazine Framework for High-Performance Lithium–Sulfur Batteries. *Angew. Chem. Int. Ed.* **2016,** *55* (9), 3106-3111.
207. Liu, J.; Lyu, P.; Zhang, Y.; Nachtigall, P.; Xu, Y., New Layered Triazine Framework/Exfoliated 2D Polymer with Superior Sodium-Storage Properties. *Adv. Mater.* **2018,** *30* (11), 1705401.
208. Zhu, G.; Shi, S.; Liu, M.; Zhao, L.; Wang, M.; Zheng, X.; Gao, J.; Xu, J., Formation of Strong Basicity on Covalent Triazine Frameworks as Catalysts for the Oxidation of Methylene Compounds. *Appl. Mater. Interfaces* **2018,** *10* (15), 12612-12617.
209. Palkovits, R.; Antonietti, M.; Kuhn, P.; Thomas, A.; Schüth, F., Solid Catalysts for the Selective Low-Temperature Oxidation of Methane to Methanol. *Angew. Chem. Int. Ed.* **2009,** *48* (37), 6909-6912.
210. Puthiaraj, P.; Lee, Y.-R.; Zhang, S.; Ahn, W.-S., Triazine-based covalent organic polymers: design, synthesis and applications in heterogeneous catalysis. *Journal of Materials Chemistry A* **2016,** *4* (42), 16288-16311.
211. Bisbey, R. P.; Dichtel, W. R., Covalent Organic Frameworks as a Platform for Multidimensional Polymerization. *ACS Central Science* **2017,** *3* (6), 533-543.
212. Spitler, E. L.; Koo, B. T.; Novotney, J. L.; Colson, J. W.; Uribe-Romo, F. J.; Gutierrez, G. D.; Clancy, P.; Dichtel, W. R., A 2D Covalent Organic Framework with 4.7-nm Pores and Insight into Its Interlayer Stacking. *J. Am. Chem. Soc.* **2011,** *133* (48), 19416-19421.
213. Lukose, B.; Kuc, A.; Heine, T., The Structure of Layered Covalent-Organic Frameworks. *Chem. Eur. J.* **2011,** *17* (8), 2388-2392.
214. Koo, B. T.; Dichtel, W. R.; Clancy, P., A classification scheme for the stacking of two-dimensional boronate ester-linked covalent organic frameworks. *J. Mater. Chem.* **2012,** *22* (34), 17460-17469.

215. Ascherl, L.; Sick, T.; Margraf, J. T.; Lapidus, S. H.; Calik, M.; Hettstedt, C.; Karaghiosoff, K.; Döblinger, M.; Clark, T.; Chapman, K. W.; Auras, F.; Bein, T., Molecular docking sites designed for the generation of highly crystalline covalent organic frameworks. *Nature Chemistry* **2016,** *8* (4), 310-316.
216. El-Kaderi, H. M.; Hunt, J. R.; Mendoza-Cortes, J. L.; Cote, A. P.; Taylor, R. E.; O'Keeffe, M.; Yaghi, O. M., Designed synthesis of 3D covalent organic frameworks. *Science* **2007,** *316* (5822), 268-272.
217. Zhang, Y.; Duan, J.; Ma, D.; Li, P.; Li, S.; Li, H.; Zhou, J.; Ma, X.; Feng, X.; Wang, B., Three-Dimensional Anionic Cyclodextrin-Based Covalent Organic Frameworks. *Angew. Chem. Int. Ed.* **2017,** *56* (51), 16313-16317.
218. Yahiaoui, O.; Fitch, A. N.; Hoffmann, F.; Fröba, M.; Thomas, A.; Roeser, J., 3D Anionic Silicate Covalent Organic Framework with srs Topology. *J. Am. Chem. Soc.* **2018,** *140* (16), 5330-5333.
219. Lan, Y.; Han, X.; Tong, M.; Huang, H.; Yang, Q.; Liu, D.; Zhao, X.; Zhong, C., Materials genomics methods for high-throughput construction of COFs and targeted synthesis. *Nat. Commun.* **2018,** *9* (1), 5274.
220. Ma, T.; Kapustin, E. A.; Yin, S. X.; Liang, L.; Zhou, Z.; Niu, J.; Li, L.-H.; Wang, Y.; Su, J.; Li, J.; Wang, X.; Wang, W. D.; Wang, W.; Sun, J.; Yaghi, O. M., Single-crystal x-ray diffraction structures of covalent organic frameworks. *Science* **2018,** *361* (6397), 48-52.
221. Xie, Y.; Li, J.; Lin, C.; Gui, B.; Ji, C.; Yuan, D.; Sun, J.; Wang, C., Tuning the Topology of Three-Dimensional Covalent Organic Frameworks via Steric Control: From pts to Unprecedented Ijh. *J. Am. Chem. Soc.* **2021,** *143* (19), 7279-7284.
222. Li, Z.; Sheng, L.; Wang, H.; Wang, X.; Li, M.; Xu, Y.; Cui, H.; Zhang, H.; Liang, H.; Xu, H.; He, X., Three-Dimensional Covalent Organic Framework with ceq Topology. *J. Am. Chem. Soc.* **2021,** *143* (1), 92-96.
223. Li, H.; Ding, J.; Guan, X.; Chen, F.; Li, C.; Zhu, L.; Xue, M.; Yuan, D.; Valtchev, V.; Yan, Y.; Qiu, S.; Fang, Q., Three-Dimensional Large-Pore Covalent Organic Framework with stp Topology. *J. Am. Chem. Soc.* **2020,** *142* (31), 13334-13338.
224. Zhu, Q.; Wang, X.; Clowes, R.; Cui, P.; Chen, L.; Little, M. A.; Cooper, A. I., 3D Cage COFs: A Dynamic Three-Dimensional Covalent Organic Framework with High-Connectivity Organic Cage Nodes. *J. Am. Chem. Soc.* **2020,** *142* (39), 16842-16848.
225. Kang, X.; Han, X.; Yuan, C.; Cheng, C.; Liu, Y.; Cui, Y., Reticular Synthesis of tbo Topology Covalent Organic Frameworks. *J. Am. Chem. Soc.* **2020,** *142* (38), 16346-16356.
226. Nguyen, H. L.; Gropp, C.; Ma, Y.; Zhu, C.; Yaghi, O. M., 3D Covalent Organic Frameworks Selectively Crystallized through Conformational Design. *J. Am. Chem. Soc.* **2020,** *142* (48), 20335-20339.
227. Gropp, C.; Ma, T.; Hanikel, N.; Yaghi, O. M., Design of higher valency in covalent organic frameworks. *Science* **2020,** *370* (6515), eabd6406.
228. O'Keeffe, M. www.rcsr.net (accessed 03.02.2022).
229. Beaudoin, D.; Maris, T.; Wuest, J. D., Constructing monocrystalline covalent organic networks by polymerization. *Nature Chemistry* **2013,** *5* (10), 830-834.
230. Zhang, Y. B.; Su, J.; Furukawa, H.; Yun, Y. F.; Gandara, F.; Duong, A.; Zou, X. D.; Yaghi, O. M., Single-Crystal Structure of a Covalent Organic Framework. *J. Am. Chem. Soc.* **2013,** *135* (44), 16336-16339.
231. Hunt, J. R.; Doonan, C. J.; LeVangie, J. D.; Côté, A. P.; Yaghi, O. M., Reticular Synthesis of Covalent Organic Borosilicate Frameworks. *J. Am. Chem. Soc.* **2008,** *130* (36), 11872-11873.
232. Stewart, D.; Antypov, D.; Dyer, M. S.; Pitcher, M. J.; Katsoulidis, A. P.; Chater, P. A.; Blanc, F.; Rosseinsky, M. J., Stable and ordered amide frameworks synthesised under reversible conditions which facilitate error checking. *Nat. Commun.* **2017,** *8* (1), 1102.
233. Guan, X.; Chen, F.; Fang, Q.; Qiu, S., Design and applications of three dimensional covalent organic frameworks. *Chem. Soc. Rev.* **2020,** *49* (5), 1357-1384.

234. Berlanga, I.; Ruiz-González, M. L.; González-Calbet, J. M.; Fierro, J. L. G.; Mas-Ballesté, R.; Zamora, F., Delamination of Layered Covalent Organic Frameworks. *Small* **2011,** *7* (9), 1207-1211.
235. Bunck, D. N.; Dichtel, W. R., Bulk Synthesis of Exfoliated Two-Dimensional Polymers Using Hydrazone-Linked Covalent Organic Frameworks. *J. Am. Chem. Soc.* **2013,** *135* (40), 14952-14955.
236. Chandra, S.; Kandambeth, S.; Biswal, B. P.; Lukose, B.; Kunjir, S. M.; Chaudhary, M.; Babarao, R.; Heine, T.; Banerjee, R., Chemically Stable Multilayered Covalent Organic Nanosheets from Covalent Organic Frameworks via Mechanical Delamination. *J. Am. Chem. Soc.* **2013,** *135* (47), 17853-17861.
237. Khayum, M. A.; Kandambeth, S.; Mitra, S.; Nair, S. B.; Das, A.; Nagane, S. S.; Mukherjee, R.; Banerjee, R., Chemically Delaminated Free-Standing Ultrathin Covalent Organic Nanosheets. *Angew. Chem. Int. Ed.* **2016,** *55* (50), 15604-15608.
238. Mitra, S.; Kandambeth, S.; Biswal, B. P.; Khayum M, A.; Choudhury, C. K.; Mehta, M.; Kaur, G.; Banerjee, S.; Prabhune, A.; Verma, S.; Roy, S.; Kharul, U. K.; Banerjee, R., Self-Exfoliated Guanidinium-Based Ionic Covalent Organic Nanosheets (iCONs). *J. Am. Chem. Soc.* **2016,** *138* (8), 2823-2828.
239. Colson, J. W.; Woll, A. R.; Mukherjee, A.; Levendorf, M. P.; Spitler, E. L.; Shields, V. B.; Spencer, M. G.; Park, J.; Dichtel, W. R., Oriented 2D Covalent Organic Framework Thin Films on Single-Layer Graphene. *Science* **2011,** *332* (6026), 228-231.
240. Medina, D. D.; Rotter, J. M.; Hu, Y.; Dogru, M.; Werner, V.; Auras, F.; Markiewicz, J. T.; Knochel, P.; Bein, T., Room Temperature Synthesis of Covalent–Organic Framework Films through Vapor-Assisted Conversion. *J. Am. Chem. Soc.* **2015,** *137* (3), 1016-1019.
241. Matsumoto, M.; Valentino, L.; Stiehl, G. M.; Balch, H. B.; Corcos, A. R.; Wang, F.; Ralph, D. C.; Mariñas, B. J.; Dichtel, W. R., Lewis-Acid-Catalyzed Interfacial Polymerization of Covalent Organic Framework Films. *Chem* **2018,** *4* (2), 308-317.
242. Dey, K.; Pal, M.; Rout, K. C.; Kunjattu H, S.; Das, A.; Mukherjee, R.; Kharul, U. K.; Banerjee, R., Selective Molecular Separation by Interfacially Crystallized Covalent Organic Framework Thin Films. *J. Am. Chem. Soc.* **2017,** *139* (37), 13083-13091.
243. Liu, X.-H.; Guan, C.-Z.; Ding, S.-Y.; Wang, W.; Yan, H.-J.; Wang, D.; Wan, L.-J., On-Surface Synthesis of Single-Layered Two-Dimensional Covalent Organic Frameworks via Solid–Vapor Interface Reactions. *J. Am. Chem. Soc.* **2013,** *135* (28), 10470-10474.
244. Rotter, J. M.; Weinberger, S.; Kampmann, J.; Sick, T.; Shalom, M.; Bein, T.; Medina, D. D., Covalent Organic Framework Films through Electrophoretic Deposition—Creating Efficient Morphologies for Catalysis. *Chem. Mater.* **2019**.
245. Kandambeth, S.; Biswal, B. P.; Chaudhari, H. D.; Rout, K. C.; Kunjattu, H. S.; Mitra, S.; Karak, S.; Das, A.; Mukherjee, R.; Kharul, U. K.; Banerjee, R., Selective Molecular Sieving in Self-Standing Porous Covalent-Organic-Framework Membranes. *Adv. Mater.* **2017,** *29* (2).
246. Bisbey, R. P.; DeBlase, C. R.; Smith, B. J.; Dichtel, W. R., Two-dimensional Covalent Organic Framework Thin Films Grown in Flow. *J. Am. Chem. Soc.* **2016,** *138* (36), 11433-11436.
247. Fan, C.; Geng, H.; Wu, H.; Peng, Q.; Wang, X.; Shi, B.; Kong, Y.; Yin, Z.; Liu, Y.; Jiang, Z., Three-dimensional covalent organic framework membrane for efficient proton conduction. *Journal of Materials Chemistry A* **2021,** *9* (33), 17720-17723.
248. Das, S.; Ben, T., A [COF-300]-[UiO-66] composite membrane with remarkably high permeability and H2/CO2 separation selectivity. *Dalton Transactions* **2018,** *47* (21), 7206-7212.
249. Wang, Z.; Si, Z.; Cai, D.; Shufeng Li, G. L.; Qin, P., Synthesis of stable COF-300 nanofiltration membrane via in-situ growth with ultrahigh flux for selective dye separation. *J. Membrane Sci.* **2020,** *615*, 118466.
250. Li, W., Metal–organic framework membranes: Production, modification, and applications. *Prog. Mater Sci.* **2019,** *100*, 21-63.
251. Zacher, D.; Shekhah, O.; Wöll, C.; Fischer, R. A., Thin films of metal–organic frameworks. *Chem. Soc. Rev.* **2009,** *38* (5), 1418-1429.

252. Li, W.; Mukerjee, S.; Ren, B.; Cao, R.; Fischer, R. A., Open Framework Material Based Thin Films: Electrochemical Catalysis and State-of-the-art Technologies. *Advanced Energy Materials* **2022,** *12* (4), 2003499.
253. Ikigaki, K.; Okada, K.; Tokudome, Y.; Toyao, T.; Falcaro, P.; Doonan, C. J.; Takahashi, M., MOF-on-MOF: Oriented Growth of Multiple Layered Thin Films of Metal–Organic Frameworks. *Angew. Chem. Int. Ed.* **2019,** *58* (21), 6886-6890.
254. Niu, Q.; Jin, M.; Liu, G.; Lv, Z.; Si, C.; Han, H., Bilayer MOF@MOF and MoOx species functionalization to access prominent stability and selectivity in cascade-selective biphase catalysis. *Molecular Catalysis* **2021,** *513*, 111818.
255. Wang, Z.; Liu, J.; Lukose, B.; Gu, Z.; Weidler, P. G.; Gliemann, H.; Heine, T.; Wöll, C., Nanoporous Designer Solids with Huge Lattice Constant Gradients: Multiheteroepitaxy of Metal–Organic Frameworks. *Nano Lett.* **2014,** *14* (3), 1526-1529.
256. Choi, S.; Kim, T.; Ji, H.; Lee, H. J.; Oh, M., Isotropic and Anisotropic Growth of Metal–Organic Framework (MOF) on MOF: Logical Inference on MOF Structure Based on Growth Behavior and Morphological Feature. *J. Am. Chem. Soc.* **2016,** *138* (43), 14434-14440.
257. Fu, J.; Das, S.; Xing, G.; Ben, T.; Valtchev, V.; Qiu, S., Fabrication of COF-MOF Composite Membranes and Their Highly Selective Separation of H2/CO2. *J. Am. Chem. Soc.* **2016,** *138* (24), 7673-7680.
258. Garzón-Tovar, L.; Pérez-Carvajal, J.; Yazdi, A.; Hernández-Muñoz, J.; Tarazona, P.; Imaz, I.; Zamora, F.; Maspoch, D., A MOF@COF Composite with Enhanced Uptake through Interfacial Pore Generation. *Angew. Chem. Int. Ed.* **2019,** *58* (28), 9512-9516.
259. Peng, H.; Huang, S.; Tranca, D.; Richard, F.; Baaziz, W.; Zhuang, X.; Samorì, P.; Ciesielski, A., Quantum Capacitance through Molecular Infiltration of 7,7,8,8-Tetracyanoquinodimethane in Metal–Organic Framework/Covalent Organic Framework Hybrids. *ACS Nano* **2021,** *15* (11), 18580-18589.
260. Sauerbrey, G., Verwendung von Schwingquarzen zur Wägung dünner Schichten und zur Mikrowägung. *Zeitschrift für Physik* **1959,** *155* (2), 206-222.
261. Nomura, T.; Minemura, A., Behavior of a Piezoelectric Quartz Crystal in an Aqueous the Application to the Determination of Minute Aniotint Solution and of Cyanide. *NIPPON KAGAKU KAISHI* **1980,** *1980* (10), 1621-1625.
262. Janshoff, A.; Galla, H.-J.; Steinem, C., Piezoelectric Mass-Sensing Devices as Biosensors—An Alternative to Optical Biosensors? *Angew. Chem. Int. Ed.* **2000,** *39* (22), 4004-4032.
263. Bassett, C. A. L., Biologic significance of piezoelectricity. *Calcified Tissue Research* **1967,** *1* (1), 252-272.
264. Fathizadeh, S.; Behnia, S., Control of a DNA Based Piezoelectric Biosensor. *J. Phys. Soc. Jpn.* **2020,** *89* (2), 024004.
265. Scientific, B. Available sensors. https://www.biolinscientific.com/qsense/sensors (accessed 06.01.2022).
266. Tanzi, M. C.; Farè, S.; Candiani, G., Chapter 2 - Mechanical Properties of Materials. In *Foundations of Biomaterials Engineering*, Tanzi, M. C.; Farè, S.; Candiani, G., Eds. Academic Press: 2019; pp 105-136.
267. Rodahl, M.; Höök, F.; Krozer, A.; Brzezinski, P.; Kasemo, B., Quartz crystal microbalance setup for frequency and Q-factor measurements in gaseous and liquid environments. *Rev. Sci. Instrum.* **1995,** *66* (7), 3924-3930.
268. Scientific, B. why are overtones important in qcm. https://www.biolinscientific.com/blog/why-are-overtones-important-in-qcm (accessed 06.01.2022).
269. Easley, A. D.; Ma, T.; Eneh, C. I.; Yun, J.; Thakur, R. M.; Lutkenhaus, J. L., A practical guide to quartz crystal microbalance with dissipation monitoring of thin polymer films. *Journal of Polymer Science n/a* (n/a).

270. Liu, Y.; Jaiswal, A.; Poggi, M. A.; Wilson, W. D., Surface Plasmon Resonance and Quartz Crystal Microbalance Methods for Detection of Molecular Interactions. In *Chemosensors*, 2011; pp 329-344.
271. Becker, B.; Cooper, M. A., A survey of the 2006–2009 quartz crystal microbalance biosensor literature. *Journal of Molecular Recognition* **2011,** *24* (5), 754-787.
272. Tonda-Turo, C.; Carmagnola, I.; Ciardelli, G., Quartz Crystal Microbalance With Dissipation Monitoring: A Powerful Method to Predict the in vivo Behavior of Bioengineered Surfaces. *Frontiers in Bioengineering and Biotechnology* **2018,** *6* (158).
273. Binnig, G.; Quate, C. F.; Gerber, C., Atomic Force Microscope. *Phys. Rev. Lett.* **1986,** *56* (9), 930-933.
274. Kim, S.; Shafiei, F.; Ratchford, D.; Li, X., Controlled AFM manipulation of small nanoparticles and assembly of hybrid nanostructures. *Nanotechnology* **2011,** *22* (11), 115301.
275. Giessibl, F. J., Atomic Resolution of the Silicon (111)-(7×7) Surface by Atomic Force Microscopy. *Science* **1995,** *267* (5194), 68-71.
276. Hinterdorfer, P.; Dufrêne, Y. F., Detection and localization of single molecular recognition events using atomic force microscopy. *Nature Methods* **2006,** *3* (5), 347-355.
277. Vigneswaran, N.; Samsuri, F.; Ranganathan, B.; Padmapriya, Recent Advances in Nano Patterning and Nano Imprint Lithography for Biological Applications. *Procedia Engineering* **2014,** *97*, 1387-1398.
278. Stevie, F. A.; Donley, C. L., Introduction to x-ray photoelectron spectroscopy. *Journal of Vacuum Science & Technology A* **2020,** *38* (6), 063204.
279. Hertz, H., Ueber einen Einfluss des ultravioletten Lichtes auf die electrische Entladung. *Annalen der Physik* **1887,** *267* (8), 983-1000.
280. Einstein, A., Über einen die Erzeugung und Verwandlung des Lichtes betreffenden heuristischen Gesichtspunkt. *Annalen der Physik* **1905,** *322* (6), 132-148.
281. Nordling, C.; Sokolowski, E.; Siegbahn, K., Precision Method for Obtaining Absolute Values of Atomic Binding Energies. *Physical Review* **1957,** *105* (5), 1676-1677.
282. Schnablegger, H.; Singh, Y., *The SAXS Guide*. 3 ed.; Anton Paar GmbH: Austria, 2013.
283. Holý, V.; Kuběna, J.; Ohlídal, I.; Lischka, K.; Plotz, W., X-ray reflection from rough layered systems. *Physical Review B* **1993,** *47* (23), 15896-15903.
284. Gary D. Christian, J. E. O. R., *Instrumental Analysis*. Allyn and Bacon. Inc.: United States of America, 1990.
285. Graham, L. J. B. S. H. F. L. D. A. C. R., *Organic structural spectroscopy*. Prentice-Hall, Inc: Upper Saddle River, New Jersey, 2001.
286. Maitland Jones, J., *Organic Chemistry*. W. W. Norton & Company, Inc.,: USA, 2000.
287. Ben, T.; Qiu, S. L., Porous aromatic frameworks: Synthesis, structure and functions. *Crystengcomm* **2013,** *15* (1), 17-26.
288. Wang, X.; Lu, S.-m.; Li, J.; Liu, Y.; Li, C., Conjugated microporous polymers with chiral BINAP ligand built-in as efficient catalysts for asymmetric hydrogenation. *Catal. Sci. Technol.* **2015,** *5* (5), 2585-2589.
289. Medina, D. D.; Werner, V.; Auras, F.; Tautz, R.; Dogru, M.; Schuster, J.; Linke, S.; Döblinger, M.; Feldmann, J.; Knochel, P.; Bein, T., Oriented Thin Films of a Benzodithiophene Covalent Organic Framework. *ACS Nano* **2014,** *8* (4), 4042-4052.
290. Ma, M.; Lu, L.; Li, H.; Xiong, Y.; Dong, F., Functional Metal Organic Framework/SiO2 Nanocomposites: From Versatile Synthesis to Advanced Applications. *Polymers* **2019,** *11* (11), 1823.
291. Wang, K.; Hui, K. N.; San Hui, K.; Peng, S.; Xu, Y., Recent progress in metal–organic framework/graphene-derived materials for energy storage and conversion: design, preparation, and application. *Chemical Science* **2021,** *12* (16), 5737-5766.
292. Becker, D.; Heidary, N.; Horch, M.; Gernert, U.; Zebger, I.; Schmidt, J.; Fischer, A.; Thomas, A., Microporous polymer network films covalently bound to gold electrodes. *Chem. Commun.* **2015,** *51* (20), 4283-4286.

293. Vericat, C.; Vela, M. E.; Benitez, G.; Carro, P.; Salvarezza, R. C., Self-assembled monolayers of thiols and dithiols on gold: new challenges for a well-known system. *Chem. Soc. Rev.* **2010,** *39* (5), 1805-1834.
294. Stranick, S. J.; Parikh, A. N.; Allara, D. L.; Weiss, P. S., A New Mechanism for Surface Diffusion: Motion of a Substrate-Adsorbate Complex. *The Journal of Physical Chemistry* **1994,** *98* (43), 11136-11142.
295. Erb, R. A., Wettability of gold. *The Journal of Physical Chemistry* **1968,** *72* (7), 2412-2417.
296. Tian, Y.; Zhu, G., Porous Aromatic Frameworks (PAFs). *Chemical Reviews* **2020,** *120* (16), 8934-8986.
297. Thomas, J. M. H.; Trewin, A., Amorphous PAF-1: Guiding the Rational Design of Ultraporous Materials. *The Journal of Physical Chemistry C* **2014,** *118* (34), 19712-19722.
298. Trunk, M.; Herrmann, A.; Bildirir, H.; Yassin, A.; Schmidt, J.; Thomas, A., Copper-Free Sonogashira Coupling for High-Surface-Area Conjugated Microporous Poly(aryleneethynylene) Networks. *Chem. Eur. J.* **2016,** *22* (21), 7179-7183.
299. Akhtar, R.; Zahoor, A. F., Transition metal catalyzed Glaser and Glaser-Hay coupling reactions: Scope, classical/green methodologies and synthetic applications. *Synth. Commun.* **2020,** *50* (22), 3337-3368.

8. Appendices